Design and Implementation of Fast Ambulatory System for Cardiac Patients Using GSM Network and ECG Signal

Ass. Prof. Dr. Majid S. Naghmash

Head of Information Technology Department

Dijlah University College

E-Mail: majid.salal@duc.edu.iq

Lecturer Dr. Abass F. Humadi

Middel Technical UniversityCollege of Electrical and Electronic EngineeringTechniqueE-Mail: drabbas1962@gmail.com

Ass. Prof. Dr. Mousa K. Wali

Middel Technical UniversityCollege of Electrical and Electronic EngineeringTechniqueE-Mail: musawali@yahoo.com

Abstract

This paper presents, the design and implementation of fast ambulatory system for cardiac patients by using global system mobile (GSM) network and Electrocardiography (ECG) signal. The early detecting of critical case in the heart performance gave enough time to help the patient with heart disease. Depending on the filter response and ECG band limited signal, the proposed system generate voice alarms to the monitor when the time band of the QRS complex wave in the ECG signal is exceeded the standards duration which indicate that the patients in dangerous condition and arrhythmia may be founded. The FIR filter response analyzed the distorted ECG signal and produce an alarm which will be send by GSM transmitter to the nurse or doctor mobile phone reciever at monitor center when the ECG frequency band jumb over natural frequency and high risk of cardiac patients. The low pass FIR filter performance using kaiser window permit to pass only the natural band otherwise send emergency alarms via GSM mobile phone. Results shows and efficient and hilight observation with each case recording by FDA tool in MATLAB.

Keywords-Fast Ambulatory, Cardiac Patients, ECG, GSM, MATLAB

تصميم وتنفيذ نظام الاسعاف الفوري لمرضى القلب باستخدام شبكة النظام العالمي للهاتف المحمول (جي إس أم) وإشارة جهاز تخطيط القلب الكهربائي (أي، سي،جي).

الملخص:
تعرض هذه الورقة، تصميم نظام فعال في حالات الطوارئ للمرضى الذين يعانون من أمراض القلب، استناداً إلى إشارات تخطيط القلب الكهربائية (ECG) باستخدام مرشح عامل تصفية الاستجابة (FIR) وشبكة النظام العالمي للهاتف المحمول (GSM). أنالكشف المبكر للحالة الحرجة في أداء القلب تساعد على تقديم المساعدة للمريض بمرض القلب في وقت مبكر اعتماداً على استجابةالمرشح وإشارة الحزمةالمحدودة لتخطيط القلب الكهربائي ، أن النظام المقترح يولد الإنذارات الصوتية إلى جهاز العرض عندما تتجاوز وقت الموجة المركبة في إشارة تخطيط القلب الكهربائي لاكثر من0.08من الثانية مما يشير إلى أن المريض في حالة خطيرة وعدم انتظام ضربات القلب. أن تحليل إشارة تخطيط القلب الكهربائي المضطربة باستخدام مرشح عامل تصفية الاستجابة (FIR)يولد إنذار الذي سيرسل عبر شبكة النظام العالمي للهاتف المحمول(GSM) الى متلقي الهاتف المحمول كالممرضة أو الطبيب عندما تتجاوز ترددات القلب عن التردد الطبيعي في تخطيط القلب الكهربائيوحدوث خطورة عالية لمريض القلب. باستخدام مرشح عامل تصفية الاستجابة (FIR) منخفض التمرير باستخدام نافذة كايزر تسمح لتمرير الحزم الطبيعية فقط وإلا سيتم إرسال إنذارات الطوارئ تحت تكنولوجيا البرمجيات الراديو عن طريق الشبكة الدولية للهاتف النقال GSM. النتائج تظهر كفاءة، وتسلط الضوء على المراقبة مع كل حالة تسجل عن طريق أداة تصميم الفلتر الرقمي (FDA tool) في MATLAB.

Introduction

The Electrocardiography machine records signals from the patients body and it is useful in identifying patients with coronary artery disease and dangerous arrhythmias or a portion of the heart has been damaged, the affected muscle cells will no longer conduct action potentials, so an ECG will reveal an abnormal pattern of impulse conduction[1,2]. In one-fourth of patients with coronary disease the sudden death may be the first clinical manifestation. In addition, 20% of patients with myocardial infarction will die before reaching a hospital. Most of these deaths are caused by ventricular fibrillation[3]. When ST segment depression of ECG exceeds 0.1 mV, is strongly suggestive for ischemia. The ECG changes in myocardial infarction with classic evolution is from peaked (hyperacute) T wave, to ST segment elevation, to Q wave development to T inversion. The evolution of new Q wave (> 30 ms in duration and 25% of the R wave amplitude) is diagnostic[4].

In recent years, the modern communication system is used in health care for many performing such as surgery and delivering assistance to the patients in the form of telemedicine and biotelemetry using local area network (LAN) and radio frequency(5). To establish these technology required more investment with slow return rate(6). The medical facilities not provide full extent in all over the word due to poor transportation with large distance. However, the current communication technology should be applied in home automation and networking. By using the GSM network, the heart patients data could be moved immediately to the doctor in charge and surveillance nurse(7). The trasmitter and reciever in GSM mobile system can be used to transmitte and receive the patients information instantly for early detectionof any emergency case after some signal processing like digital signal processing (DSP). The FIR filter is one of the signal processing part which used to pass an accurate band of interest and neglect the undesired band (8). The patient monitoring system is placed near patient bed and connected to the mobile phone by mean of wireless technology or interfacing with personal computer for more processing associated the physician room(9). The GSM network interfacing and analysis the ECG signal by FIR filtration with kaiser windowing techniques (10). The attractive characteristics in frequency domain of kaiser window will produce high efficiency and capability in the noise elimination than other windowing techniques (11). The ECG filtration by FIR filter performs earlier analysis to minimize the false detection rate and decrease the time spent by this processing (12). Consequently, the software defined radio (SDR) technology used in the FIR filter design minimize and optimize the power consumption to lowest level as well (13). The need of having modern tools like SDR technology and portable devices allow the biomedical signal recording to further study of the high prevalence of cardiovascular diseases (14). The use of SDR technology help the medical staff to capture process and store signals from the patients to perform succeeding analysis and comprehensive clinical studies in order to make more perfect decisions (15). The alarm message sending through mobile communication device via mobile phone could be reduce the emergency time to assist patients and staff in the telemedicine services (16). The selection of appropriate technology to develop a suitable design in the software and hardware side and perform good analysis detection assist the patients to move from

critical situation to stable case early (17). The development of bioengineering applications becomes more popular technology and wide used due to fast and accurate results of patients assistance (18). In this paper, the combination of digital signal processing (DSP) technology with ECG monitering device depend on the ECG duration is developed and investigated using FIR filter and SDR technology. Figure 1 shows the conventional designs of ECG transformation via GSM system depending on the heart beat per minuts (BPM) proposed by (19).

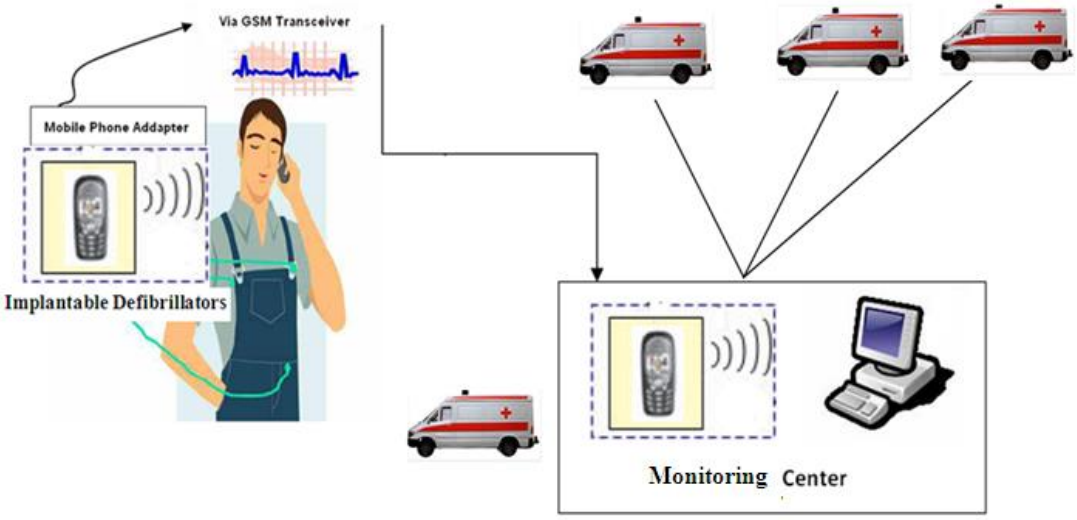

Figure 1: Proposed ECG trasfer system

The design method accessible can be basically comprehensive to FIR highpass (HP), bandpass (BP) and bandstop (BS) filters. Consider the case of BP filter is requied that would satisfy the specifications of heart signal band. The only differences in the design of BP filter are to use the more critical of the two trasition width for the design and the idealized frequency of BP filter for the determination of the initial impulse response.

I. Proposed System

The proposed system shown in Figure 2 represent the GSM transciever that performs ECG analysis and transformation by using the digital modem with FIR Kaise window technique. Decision whether the person is normal or abnormal is based on calculating the value of ECG interval and if any abnormality is detected, the system initiates an command to the inbuilt GSM Baseband Processor module, which sends an SMS to physician or caretaker mobile through the SIM module. Analysis of the ECG signal is done by performing the FIR decomposition

followed by upsampling filter to increase the modulated frequency from baseband to intermediate frequency (IF). The F0IR filter permit to pass only 0.12 secondband in an ECG signal. The stadards amplitude range of ECG signal is 1-10mV and its frequency range is 0.05 -100 Hz. Simulation performed in MATLAB environment using the FDATool.

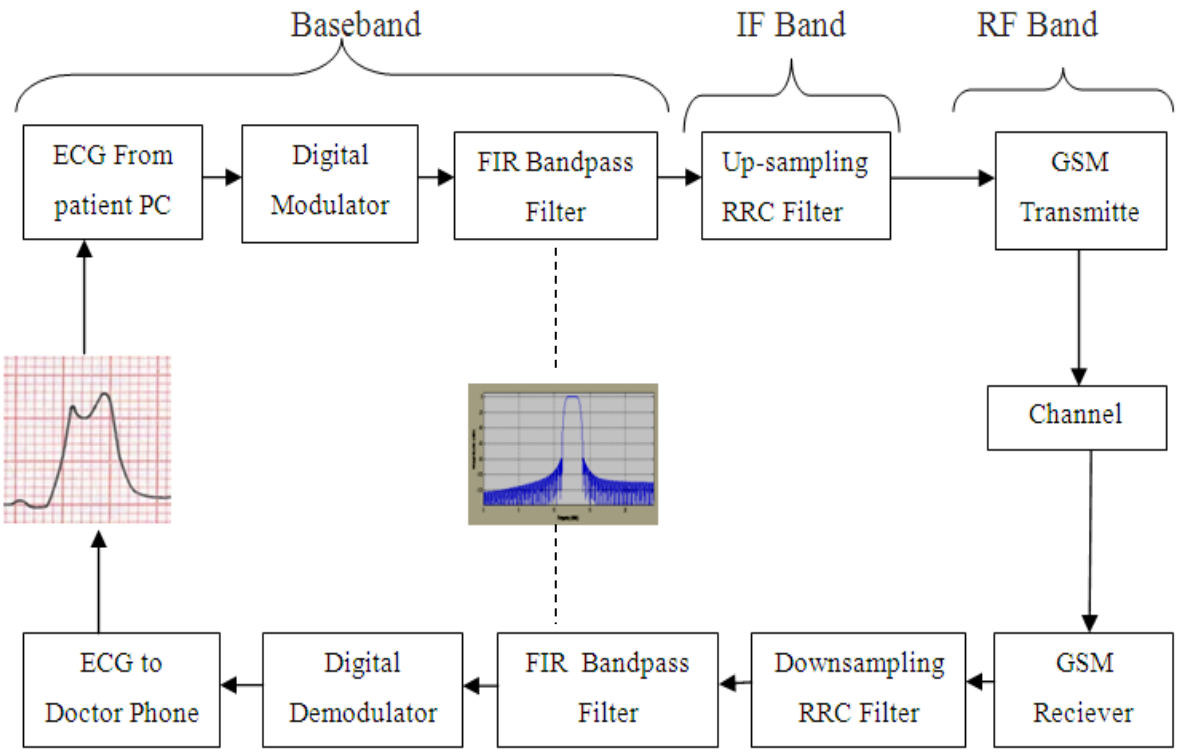

Figure 2: Proposed design for ECG transportation using GSM system and MATLAB

A. GSM Transciever Design

The transmitter and reciever path of GSM system is designed and simulated using MATLAB/SIMULINK with digital filter design tool (FDATool) as shown in Figure 3. In the transmitter path, the ECG signal is generated by using random integer generator block. The GSMK digital modulator is used to modulate the ECG signal and feed to the FIR band pass filter under specialspecifications. This FIR filter use to pass only the non-normal ECG signal. The filterd signal is then upsampled to IF band using RRC filter. The RF band from GSM tranmitter is send to the channel under 20dB SNR. In the reciever pathe, the down sampling RRC filter is used to decimate the incoming signal from RF to IF band and then

feed to the FIR banpass filter to recover and isolate the ECG signal. The recover ECG signal is demodulated by GMSK demodulator which will send to the doctor hand phand for investigation.

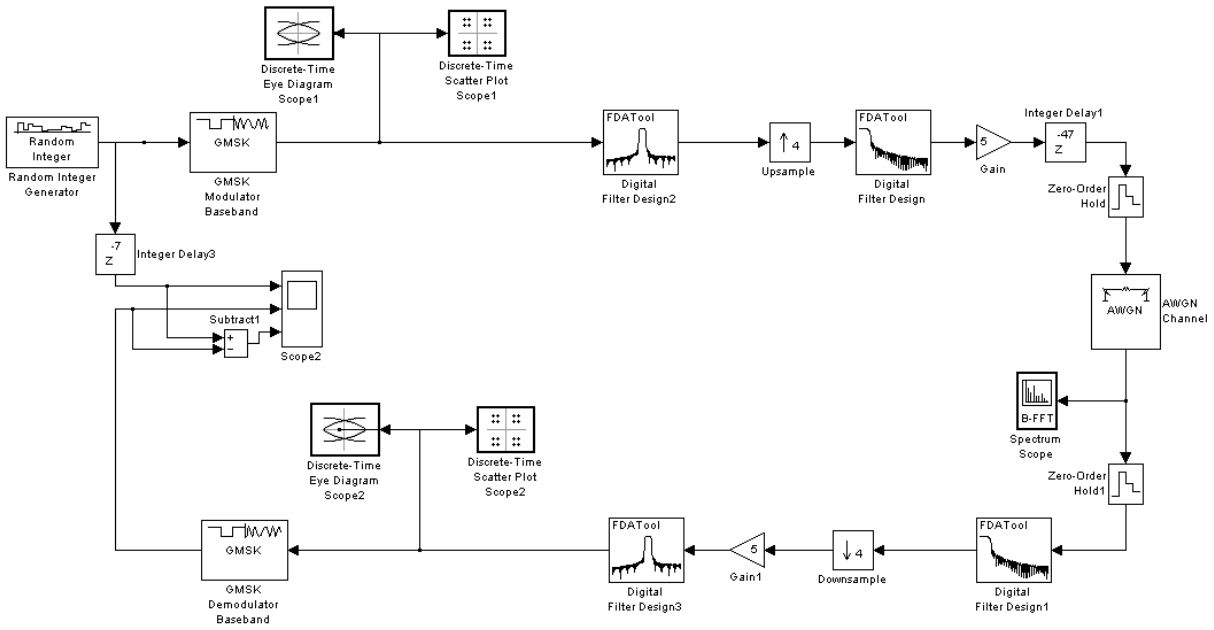

Figure 3: Proposed design of ECG transfer system using MATLAB and FDATool

B. Design of FIR Filter

The desirable characteristics of Kaiser window in the time and frequency domain assist to give time limited function in the ECG signals. The magnitude response of bandpass filter with Kaiser window is illustrated in Figure 4.The filter order is chosen to be 64 with the sampling frequency of 50Hz. The pass-stop band of the designed filter is selected to pass only the ECG signal band from 0.12- 15 second which represent the critical situation of patient. After the ECG signal passed through the FIR filter, the channel processor increase the signal frequency to intermediate frequency (IF) band by using of so called upsampling filter. The IF band of GSM system in this case is 69.333248 MHz. The FDATool in MATLAB is used to show the frequency and magnitude response of suggested filter. The filter information of all decomposition design provide a linear phase and high stability in the band of ECG signal.

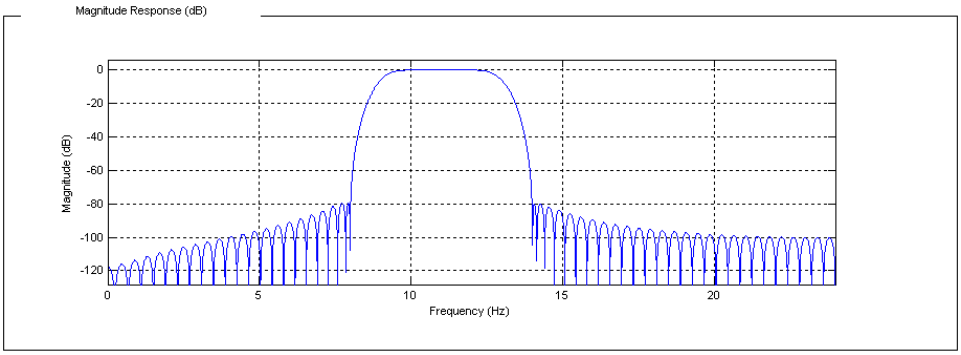

Figure 4: magnitude response of FIR RRC filter

The FDATool environment in MATLAB and the signal processing toolbox is used to provide a decmposition design for many advanced techniques assistance. The FIR filter specifications shown in Table 1 is recognized in this paper to work in the GSM transciever as pulse shaping filter after modulation process. The filter performance in term of impulse, magnitude and phase response of proposed filter shows a linear and constant response with respect to digital filter rols which is mean high stabilty in the band of interest as illustrated inFigure 5, Figure 6and Figure 7 respectively. The power spectrum of transmitted waveform is illustrated in Figure 8 as close as possible to ECG signal.

Table 1: FIR Filter specifications

Parameters	Specifications
Response Type	*Bandpass*
Design Method	*FIR Window*
Filter Order	*64*
Scale Passband	*Kaiser*
Sampling Frequency (Fs)	*48 Hz*
First stopband (Fstop 1)	*8 Hz*
First passband (Fpass 1)	*8.5 Hz*
Second stopband (Fstop 2)	*9 Hz*
Second passband (Fpass 2)	*9.5 Hz*
Filter stability	*Stable*
Linear phase	*Yes*

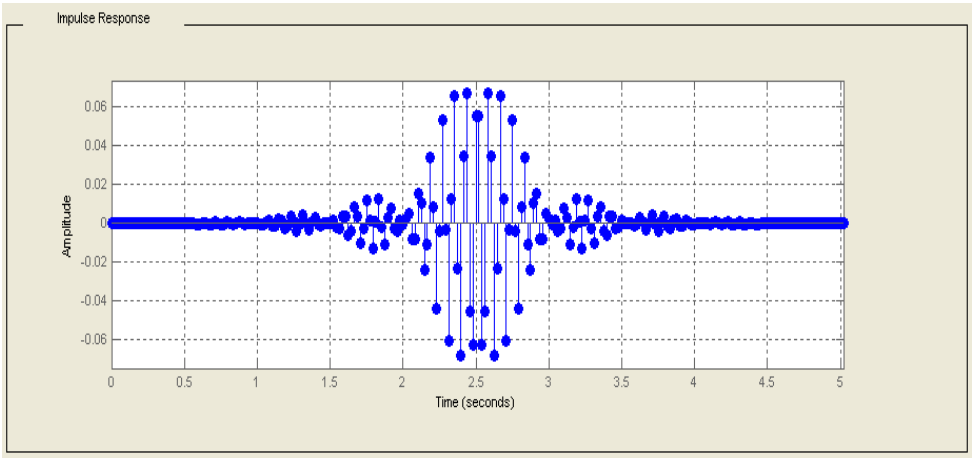

Figure 5: FIR Impulse response

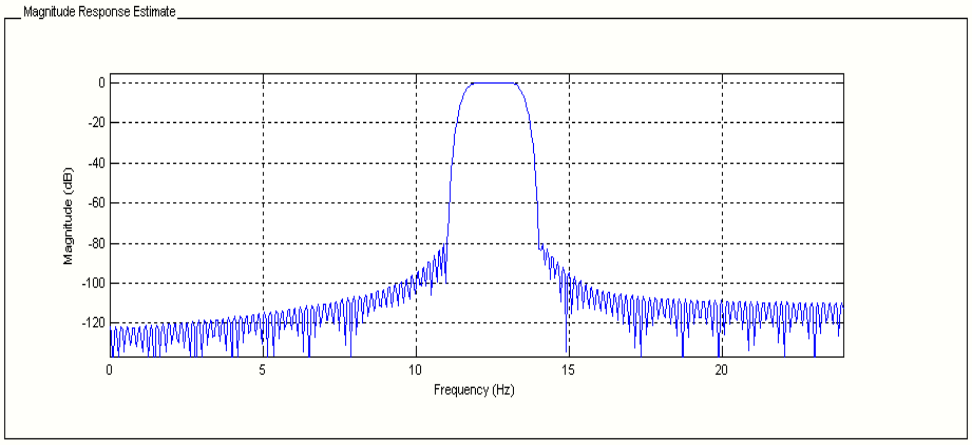

Figure 6: FIR Estimated magnitude response

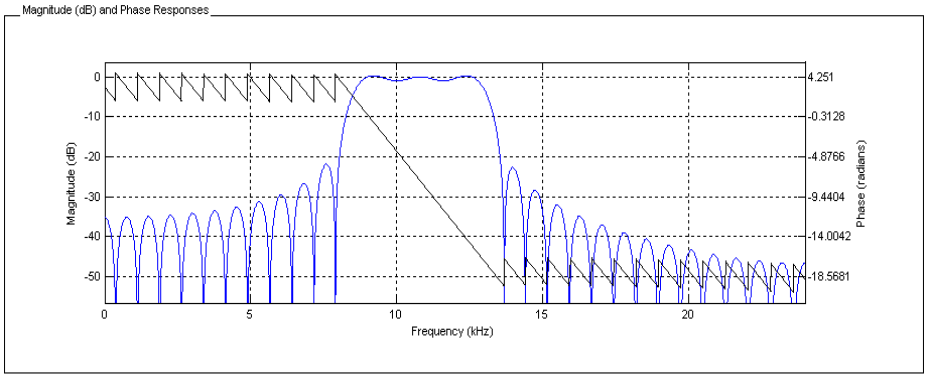

Figure 7: FIR magnitude and phase response

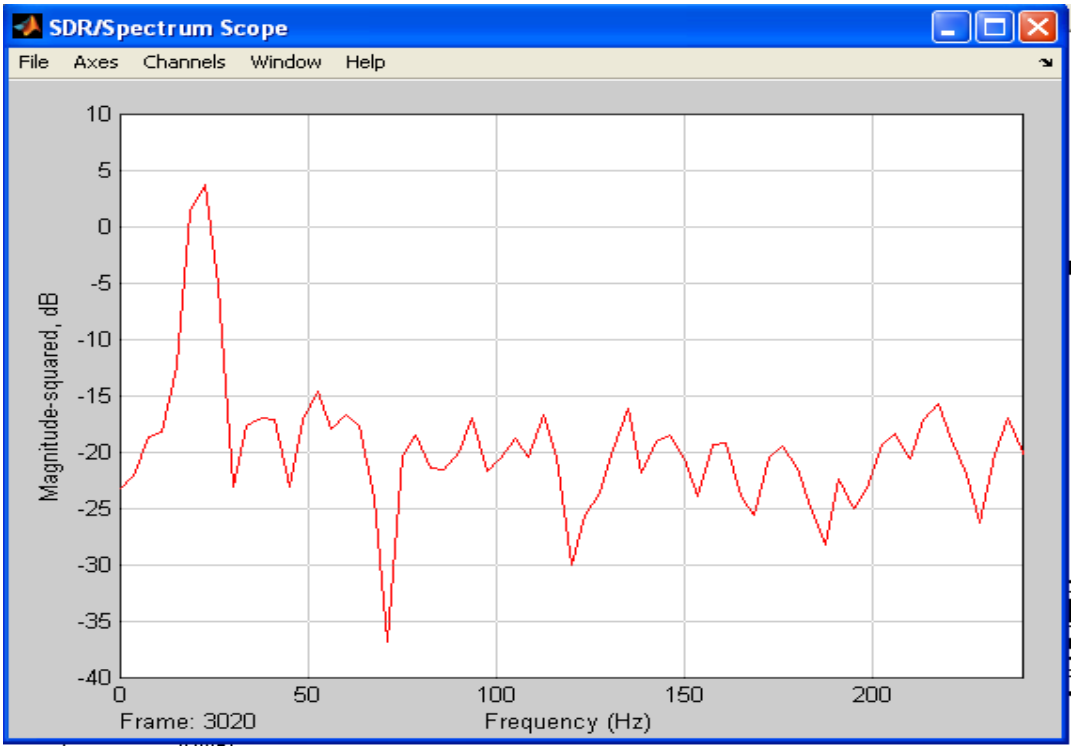

Figure 8: Power spectrum of transmitted signal

II. FPGA Implementation

The GSM transcievers with FIR filter is designed and implemented in FPGA Vertex-4 to verify the filter performance in real time. The implementation and useful confirmation of the proposed FIR filter is concluded by resolve the Xilinx system generator and ISE programs with FPGA virtex 4. The hardware description language (HDL) code is generated by using the ModelSim software and the synthesis step is done using simplify pro from simplicity. The implementation design flow illustrated in Figure 9[15] is used to satisfy the FPGA performance and requirements as well. The project design and synthesis using Xilinx supported schematic is implemented by HDL for text based entry. The HDL file is synthesis into EDIF file and NGC file. In this case, the logical design format in EDIF is converted into physical file format. The native circuit description file NCD for FPGA to generate the bitsteam file from these files in order to optionally program the PROM for following programing into Xilinx FPGA. To ensure the design meet a timing requirements and function properly, the gate level simulator is used for design verification.

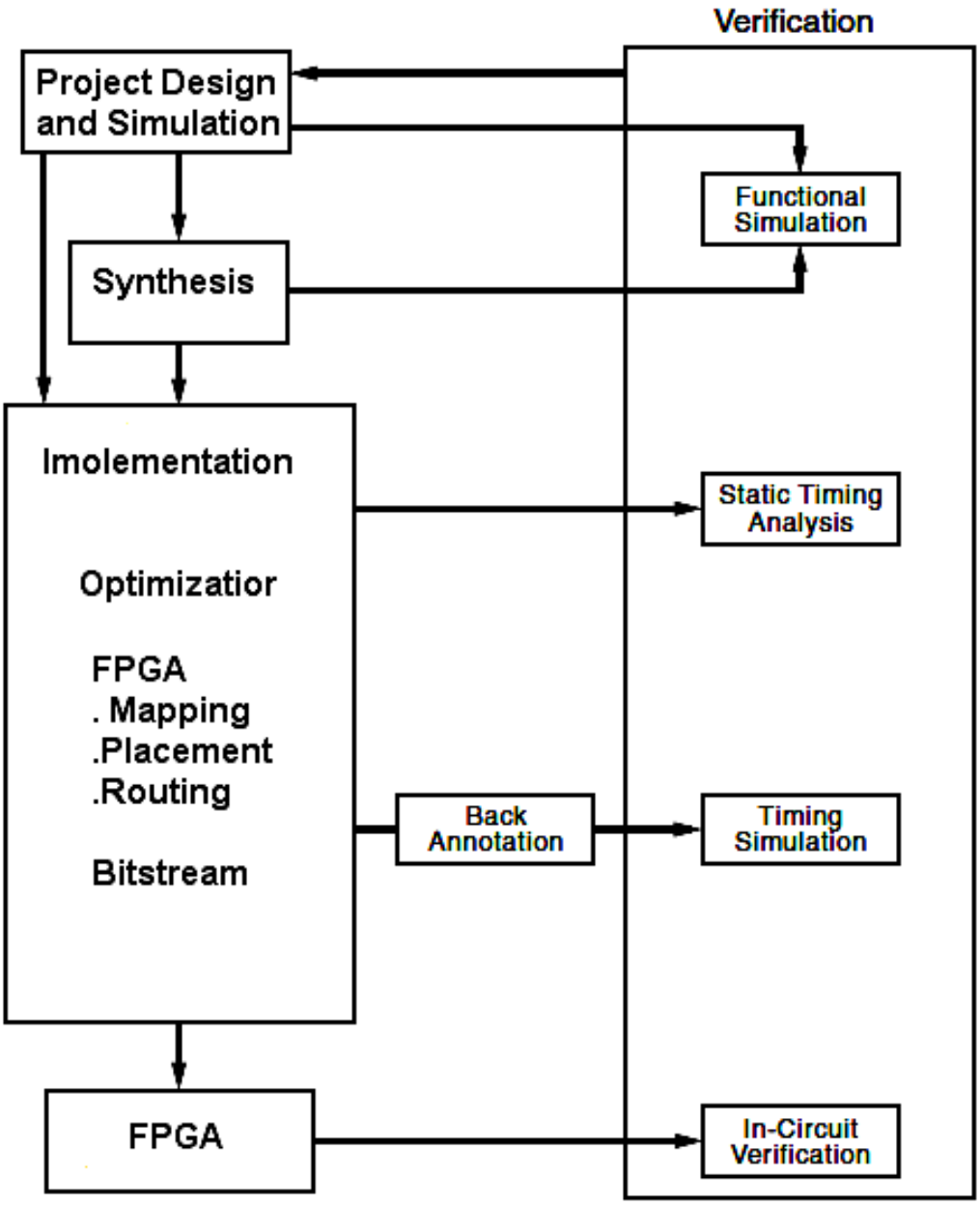

Figure 9: FPGA design flow [14]

Table 2 illustrate the devices summary that used in the proposed system given by ISE programs. The FPGA area consumption in term of slices and LUT in the project implementation shows an important reduction in the FPGA required area compared with current design. The consume elements of used logic number to the available logic elemnts could be calculated using the following formula:

Table2 : Device utilization summary

Device Utilization Summary				
Logic Utilization	**Used**	**Available**	**Utilization**	**Note(s)**
Number of Slice Flip Flops	890	30,720	3%	
Number of 4 input LUTs	745	30,720	2.5%	
Logic Distribution				
Number of occupied Slices	742	15,360	5%	
Number of Slices containing only related logic	710	332	21%	
Number of Slices containing unrelated logic	22	332	7%	
Total Number of 4 input LUTs	433	30,720	1%	
Number used as logic	731			
Number used as Shift registers	104			
Number of bonded IOBs	73	448	16%	
Number of BUFG/BUFGCTRLs	6	32	18%	
Number used as BUFGs	6			
Number used as BUFGCTRLs	0			
Number of FIFO16/RAMB16s	6	192	3%	
Number used as FIFO16s	0			
Number used as RAMB16s	6			
Number of DSP48s	6	192	3%	
Total equivalent gate count for design	275,160			
Additional JTAG gate count for IOBs	3,024			

Conclusions

This paper presents, the most important process to the critical situation of heart patients. The main advantage of the proposed system is the early detection of cardiac disorder of the patients for immediate treatment. When the time interval of ECG signal exceed the normal case, an alert of call or SMS is transmitted throught GSM system to the doctor or nurse hand phone to sought for saving the patient life by prompt medicines. Futhermore, new cellular access technology such as 4G provide much higher data transmission speed which will support the proposed system in terms of time and data size. Consequently, the implementation of ECG transciever using GUI on personal computer is successful with high resolution.

The implementation results provide an important utilization in the Slices and LUT via FPGA resources compared with conventional system design.

References

1. Mardino patients atlas, Cardiology patient atlas 2010-2011, Gold star medical publication SAL, P 2.
2. Frederic H Martini, Edwin F Bartholomew, William C. Ober, Claire W. Garrison, Kathleen Welch, & Ralf T Hutchings (2007), Essentials of Anatomy and Physiology, 14th edn, Pearson Education, San Francesco, USA.
3. Kannel WB, Capples LA, D'Agostino RB: Sudden death risk in overt coronary heart

disease: The Framingham Study. Am.Heart J 1987:113:799.

4. Steven A Schroeder, Marcus A Krupp, Lawrence M Tierney Jr, and Stephen J Mcphee (1989), Current Medical Diagnosis and treatment, a LANGE medical book, Middle East Edition, p 194.
5. Li N. qiang, et al. (2012). Application of distributed FIR filter based on FPGA in the analyzing of ECG signal. IEEE.
6. Prakash S and Venkatesh V. (2013). Real time monitoring of ECG signal using PIC and web server. Int J Appl Sci Eng Tech, 5 (2).
7. SwaroopThool. (2013). Implementation Of ARM7 Based Handheld ECG Unit Prototype For Remote Areas As Premedical Checkup At Home. Int. J. Eng. Res. Technol., 2 (7).
8. Mbachu C.B, et al. (2012). Processing ECG Signal with Kaiser Window- Based Fir Digital Filters, Int. J. Eng. Sci. Technol. 3 (8).
9. El Mimouni El Hassan and Karim Mohammed. (2012). Design and Implementation of an Embedded System for Ambulatory Cardiac Monitoring. J. Telecommunications and Information Technol.
10. Stojvanic R, Karadaglic D, Mirkovic M, Milosevic D. (2011). A FPGA system for QRS detection based on integer wavelet transform. Measurement Science Review.11(4).
11. Nian-qiang L, Si-Yu H, Shi-Yao C. Application of distributed FIR filter based on FPGA in the analyzing of ECG signal. IEEE; 2012.
12. Xuan-Thang Vu, et al., "16-QAM Transmitter and Receiver Design Based on FPGA", in the Proceedings of 5th IEEE International Symposium on Electronic Design, Test and Application (DELTA), 13-15, pp. 95-98, Vietnam, 2010
13. C Dick, et al., "Architecture and Simulation of Timing Synchronization Circuits for the FPGA Implementation of Narrowband Waveforms", Proceedings of Software Defined Radio Technical Conference and Product Exposition, 13-16 , pp. 1-6, IEEE explorer, USA, 2009
14. Popescu, S.O, et al., "Review of PSK and QAM – Digital modulation techniques on FPGA", in the Proceedings of International Joint Conference on Computational Cybernetics and Technical Informatics (ICCC-CONTI), 27-29, pp. 327-332, IEEE explorer, Romania , 2010
15. Rouphael, T. J. RF and Digital Signal Processing for Software-Defined Radio: A Multi-Standard Multi-Mode Approach. MA: Newness, Elsevier, 2009
16. Hatai, I. and Chakrabarti., "Parameter Controlled Reconfigurable Baseband Modulator for SDR Architecture", Proceedings of the 2nd International Conference on Mechanical and Electronics Engineering (ICMEE), vol. 1, 1-3, pp. 29-33, IEEE explorer ,Japan, 2010
17. Song, W., and Yao, Q., Design and Implement of QPSK Modem Based on FPGA, in the Proceedings of 3rd IEEE International Conference on Computer Science and Information Technology (ICCSIT), vol. 9, 9-11, pp. 599-601, China, 2010
18. Xilinx, Inc. ,Xtreme DSP for Virtex-4 FPGAs User Guide, version 2.7 [Online]. [Access 20th May 2009]. Available from World Wide Web, 2009
19. G. Kavya and V. Thulasibai, " VLSI Implementation of Telemonitoring System for High Risk Cardiac Patients, Indian Journal of Science and Technology, Vol 7(5), 571–576, May 2014

Histopathological changes induce by piroxicam administration in kidneys of adult male albino mice *Mus musculus*

Intidhar M. Mnati*
Bushra O. Maaroof**
* Biology Dept./ College of Education for Pure Science (Ibn Al-Haitham) /University of Baghdad
** Anatomy Dept./ College of Medicine / Al-Iraqia University
E-mail:Bushraalmaroof@gmail.com

Abstract
Piroxicam is one of non-steroidal anti-inflammatory drugs (NSAIDs) which is widely used in treating rheumatic disorders. The current study aimed to detect the deleterious effect of piroxicam pertaining to the chronic administration in male albino mice *Mus musculus*.A total number of (64) adult male albino mice were utilized in this study, they were randomly distributed into four main groups, the first three groups were orally treated with concentrations (50,100,150) mg/kg of piroxicam respectively, the forth group considered as control group were orally treated with distilled water for eight weeks, kidney samples were collected every two weeks for the histological study. This study recorded the presence of histopathological changes in the kidney of the treated mice with the concentration (50) mg/kg represented by hemorrhage, vascular congestion, calcium casts formation inside the lumens of renal tubules, while the groups treated with (100)mg/kg of the drug showed a fibrin deposition inside renal tubular lumens, infiltration of inflammatory cells, cytoplasmic vacuolation in the epithelial cells of the renal tubules and sloughing epithelium of renal tubules. The histological examination of mice kidneys treated with (150) mg/kg showed the appearance of hyalinization, shrinkage and complete loss of glomeruli, pyknosis of nuclei as well as the presence of oedema, in addition there were a remarkable decrease in the glycogen and protein contents of cells. The statistical results of the present study revealed a significant differences ($P<0.05$) in the mean diameters of renal glomeruli for all concentrations of the experiment for the period of eight weeks also there were significant decrease in the mean diameters of proximal convoluted tubules in the period of four weeks of the treated animals with concentrations (100 and 150) mg/kg as compared with control group. While the diameter of distal convoluted tubules showed a significant decrease with the concentrations (100 and 150)mg/kg for the periods six and eight weeks as compared with control group. It is clear from this study that piroxicam has drastic toxic effects on kidney tissue as represented by the observed histopathological changes.

Key words: Histopathological changes, Piroxicam, Kidney, Albino mice

التغيرات المرضية النسجية الناجمة عن التجريع بعقار البيروكسيكام في كلى ذكور الفئران البيض البالغة *Mus musculus*

انتظار محمد مناتي *
بشرى عمر احمد معروف **

* قسم علوم الحياة / كلية التربية للعلوم الصرفة (ابن الهيثم)/ جامعة بغداد
** فرع التشريح/ كلية الطب/ الجامعة العراقية

الخلاصة

يعد عقار البيروكسيكام احدالعقاقيرغيرالستيرويديةالمضادةللالتهابوالمستخدمةعلىنطاقواسعفيعلاجالاضطراباتالروماتيزمية. تهدف الدراسةالحالية الكشفعن التأثيرالضارلعقار البيروكسيكام نتيجة التجريعالمزمنفيذكورالفئرانالبيض *Mus musculus* .

استعمل في الدراسة الحالية (64) ذكرا بالغامن الفئران البيض، وزعت الحيوانات عشوائيا إلى أربع مجموعات رئيسية، تم تجريع المجاميع الثلاثة الأولى فمويابتركيز (50، 100، 150) ملغم / كغم من عقار البيروكسيكام على التوالي، واعتبرت المجموعة الرابعة كمجموعة سيطرة حيث جرعت بالماء المقطر لمدة ثمانية أسابيع، تم جمع العينات كل أسبوعين لاغراض الدراسة النسجية.

سجلت الدراسةوجود تغيرات نسجية في كلى الفئران المجرعة بتركيز (50) ملغم / كغم تمثلتبحدوث النزف، احتقان الأوعية الدموية، و تكون قوالب الكالسيوم داخل تجاويف النبيبات الكلوية، في حين أظهرت المجاميع المجرعة بتركيز (100) ملغم/ كغم من العقار ترسب مادة الليفين داخل تجاويف النبيبات الكلوية، ارتشاح الخلايا الالتهابية، تفجي الخلايا الظهارية في النبيبات الكلوية وانفصال ظهارة النبيبات الكلوية، واظهر الفحص النسجي لكلى الفئران المجرعة بتركيز (150) ملغم / كغمحدوثالتنكس الزجاجي، انكماش وفقدان تام للكبيبات، تغلظ النوى وكذلك حدوثا لوذمة، بالإضافة الى حصولانخفاض ملحوظ في محتويات الخلايا من الكلايكوجين والبروتين.

أوضحت النتائج المورفولوجية لهذه الدراسة حدوث فروق معنوية ($P < 0.05$)في معدلأقطارالكبيباتالكلويةلجميع تراكيز التجربةلمدة ثمانية أسابيعكمالوحظ حدوثانخفاض ملحوظ في معدلأقطار النبيبات الملتوية الدانيةفي المدةاربعةأسابيع للمجاميع المجرعة بتركيز(100، 150)ملغم/كغممقارنةمعمجموعةالسيطرة،في حينأظهرت النتائج المتعلقة بالنبيبات الملتوية القاصية حدوث انخفاض ملحوظفيالتراكيز(100،150)ملغم/ كغم لمدةستةوثمانية أسابيعمقارنةمعمجموعة السيطرة.

يتضح من خلال الدراسة الحالية ان لعقار البيروكسيكام تأثيرات سمية كبيرة في نسج الكلية والمتمثلة بالتغيرات المرضية النسجية الانفة الذكر.

الكلمات المفتاحية: التغيرات المرضية النسجية، بيروكسيكام، كلية ، فئران بيض*

Introduction

Piroxicam is one of the most popular non-steroidal anti-inflammatory drugs (NSAIDs) used for the treatment of inflammatory conditions and rheumatic disorders, it is useful in the management of ankylosing spondylitis, acute musculoskeletal disorders and dysmenorrhea [1]. It is belong to oxicam group, a group of non –steroidal anti-inflammatory, analgesic and antipyretic drugs, it is readily absorbed following oral administration and its long plasma half-life allows once daily dosing which is possible advantage in improving compliance [2].

The unwanted effect of NSAIDs is involved in the inhibition of cyclooxygenase enzyme (COX) pathway, inhibition prostaglandins which prevents ovulation in rat [3]. The recent studies showed that piroxicam has many side effects on intestinal, digestive system, represented by ulcers, gastritis [4].

NSAIDs also caused pregnant mice abortion and congenital anomalies in mice fetuses [5], furthermore there were side effects of piroxicam on the testes of male mice [6]. Ebaid *et. al.* [7] also found that injecting piroxicam caused a remarkable histopathological symptoms in the liver and kidney of male albino mice.

This study was done to evaluate the histological alterations in kidneys of adult male albino mice that induced by piroxicam.

Materials and Methods

Animals

A total number of (64) healthy adult male albino mice *Mus musculus* were utilized in this study they were collected from Iraqi national center for drug control and research, Baghdad, Iraq. weighing between (25-30) gm and age approximately (8-10) weeks old, They were randomly distributed into four main groups of five mice for each, they were housed in cages and were kept in the laboratory under constant conditions for at least one week before use, they were fed a standard commercial diet.

Experimental design

The drug used in this study was piroxicam in capsule form of (20) mg for each, concentrations (50, 100, 150) mg/kg were prepared daily and they were given orally using stomach cannula for the periods two, four, six and eight weeks three of the four groups were orally treated with the concentrations (50, 100, 150) mg/kg respectively, the forth group considered as control group were orally treated with 0.1 ml of distilled water for eight weeks.

Histological & Histochemical preparations

Animals from control and treated groups were sacrificed, dissected and small pieces of the kidney were quickly removed, then fixed in formalin fixative for 22 hours followed by changing the fluids with 70% alcohol after washing the specimens for many times, after washing, specimens were dehydrated, embedded and then sectioned to 5 µ thickness, for the histological examinations, sections were stained with haematoxylin and eosin [8].

In the histochemical study, sections were stained with periodic acid schiff's method to demonstrate carbohydrates [8] and with bromophenol blue to demonstrate total proteins [9].

Morphometric measurements

The morphometric measurements were done under light microscope using ocular micrometer stage after calibrating the ocular lenses with micrometer stage for each magnification power[10].

Statistical analysis

The statistical analysis were done by using the statistical analysis system (SAS) program to demonstrate the effect of drug concentration and period in different

standards, which was performed by comparing the significant differences of the control groups and the treated groups for each period with the Least significant differences (LSD) at the level ($P<0.05$) [11].

Results

Histological examination of kidney tissue

Control group

Histological sections of this group appeared with normal histological structure represented by a kidney surrounded by a capsule and it is differentiated into an outer region called cortex which contains renal corpuscles and sections of proximal and distal convoluted tubules, and an inner region called medulla which showed sections of thick and thin segments of Henle's loop as well as sections of the collecting ducts figures (1,2,3).

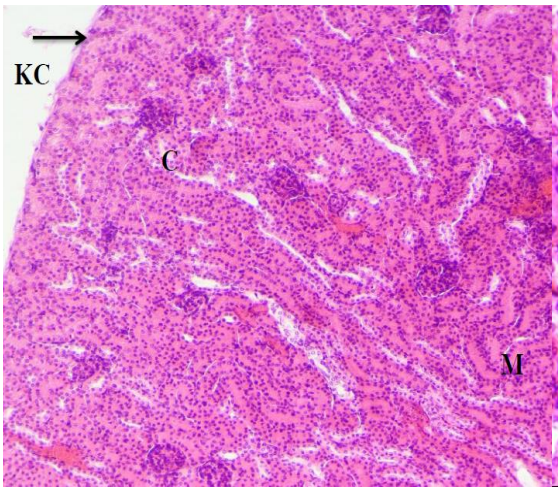

Fig(1): C.S in the kidney of control group showing Kidney capsule (KC), cortex (C) and medulla (M) (H&E, 100X).

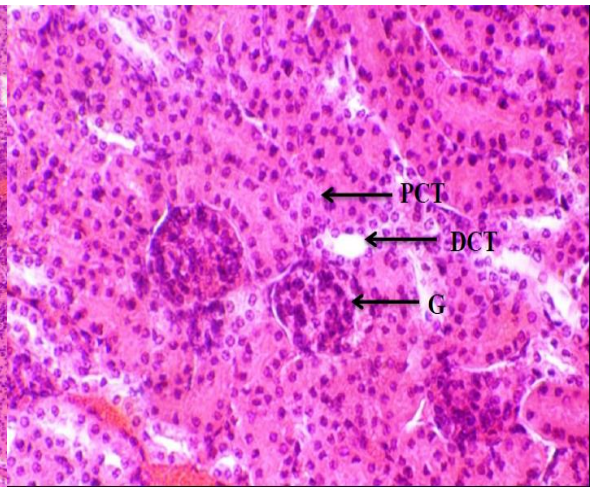

Fig(2):C.S in the kidney of control group showing Distal convoluted tubule (DCT), Glomerulus (G) and Proximal convoluted tubule (PCT)(H&E, 400X) .

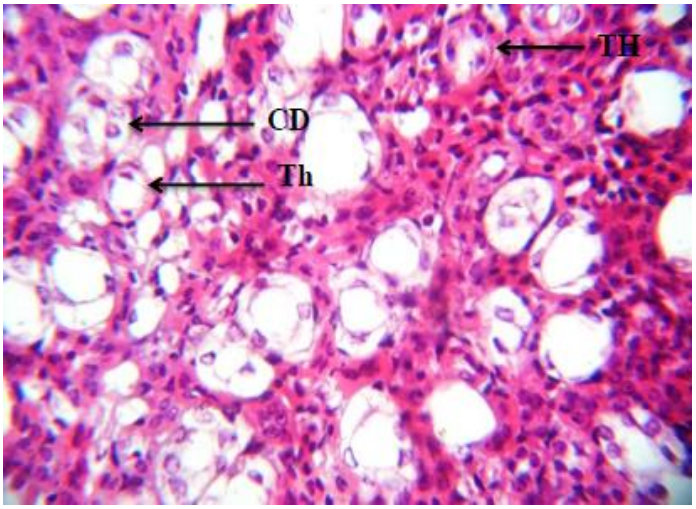

Fig(3): C.S in the kidney of control group showing sections of collecting ducts (CD), Thick segments (TH) and Thin segments (Th) of Henle's Loop(H&E, 400X).

Groups treated with (50) mg/kg of piroxicam

The examination of kidney sections of treated mice with (50) mg/kg of piroxicam for different periods revealed many pathological changes compared with control group. These changes are represented by vascular congestion and hemorrhage after 2 weeks, infiltration of leukocytes after 4 weeks of administration as well as the beginning of calcium casts formation after 6 and 8 weeks of administration figures (4,5,6,7).

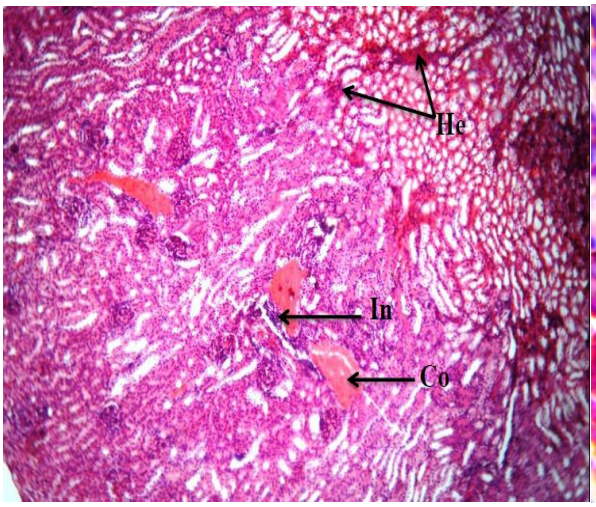

Fig(4):C.S in the kidney of group treated with (50)mg/kg for 2 weeks showing the congestion of blood vessels (Co), Hemorrhage (He) and Infiltration of leukocytes (In)(H&E, 100X)

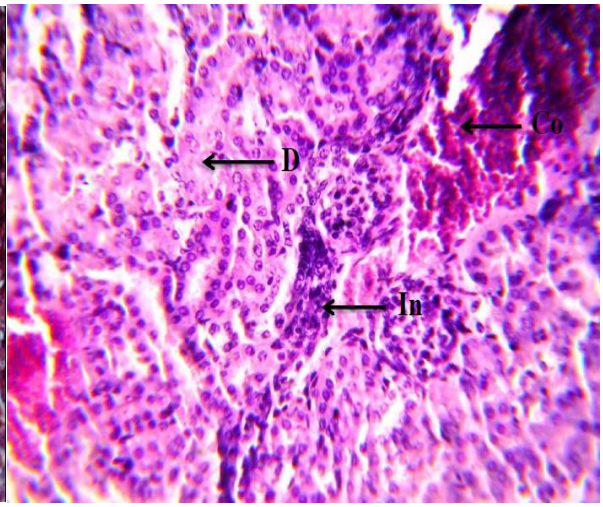

Fig(5): C.S in the kidney of group treated with (50) mg/kg for 4 weeks showing the congestion of blood vessels (Co), Degeneration of tubular epithelium (D) and Infiltration of leukocytes (In)(H&E, 400X)

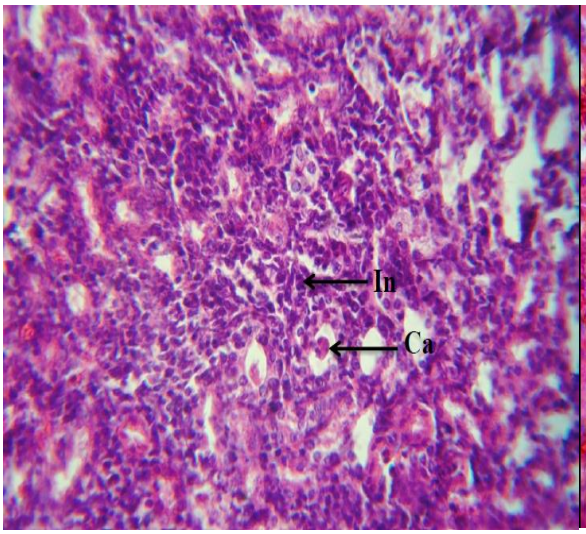

Fig(6): C.S in kidney of group treated with (50)mg/kg for 6 weeks showing the beginning of calcium

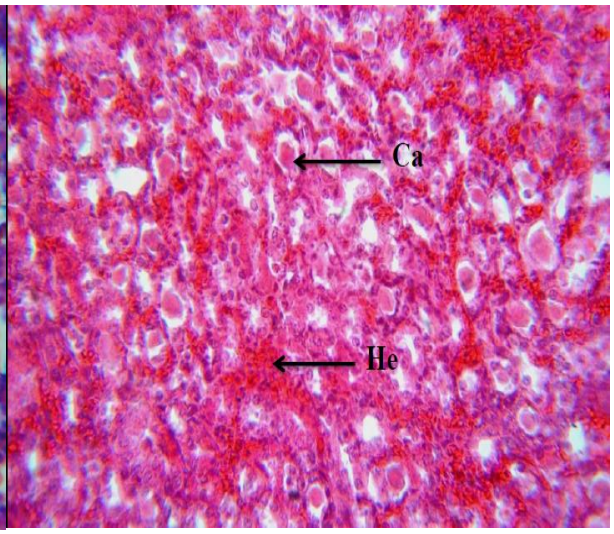

Fig(7): C.S in kidney of group treated with (50)mg/kg for 8 weeks showing the formation of calcium

casts formation (Ca) and the Infiltrationof casts (Ca) and the hemorrhage (He)(H&E, 400X)
leukocytes(In)(H&E, 400X)

Groups treated with (100) mg/kg of piroxicam

The results of microscopic examination showed many histopathological changes in the kidney of treated mice with (100)mg/kg of piroxicam for different periods of exposurethese changes included the increased thickness of kidney capsule, subcapsular hemorrhage, hypertrophy of epithelial cells and the Infiltration of leukocytes after 2 weeks of administration figure(8), the sloughing epithelium in renal tubules , fibrin deposition inside tubular lumens, atrophy of tubular epithelium and hemorrhage were shown after 4 and 6 weeks figures (9,10), while after 8 weeks of administration there was a shrinkage and loss of some glomeruli in the kidney sections figure(11).

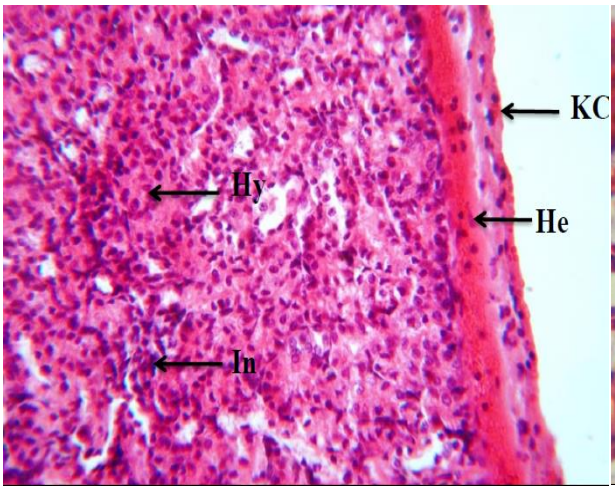

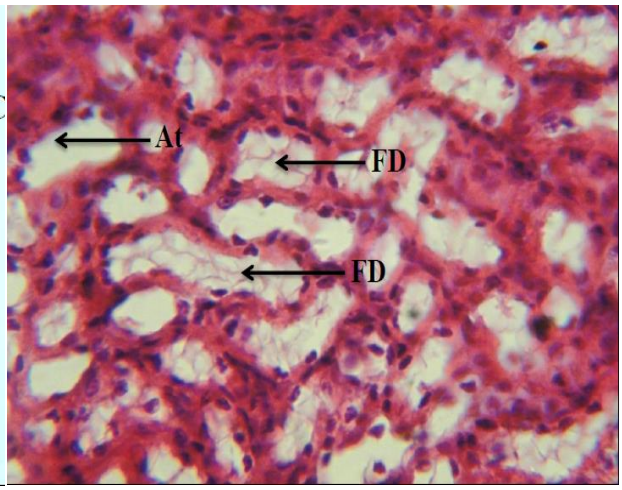

Fig(8): C.S in the kidney of group treated with (100) mg/kgFig(9): C.S in the kidney of group treated with (100) mg/kg
for 2weeks showing the subcapsular hemorrhage(He), for 4 weeks showing the Atrophyof tubular epithelium
hypertrophy(Hy) of epithelium and the Infiltration (At) and fibrin deposition (FD)(H&E, 400X)
of leukocytes (In), kidney capsule (KC).(H&E, 400X)

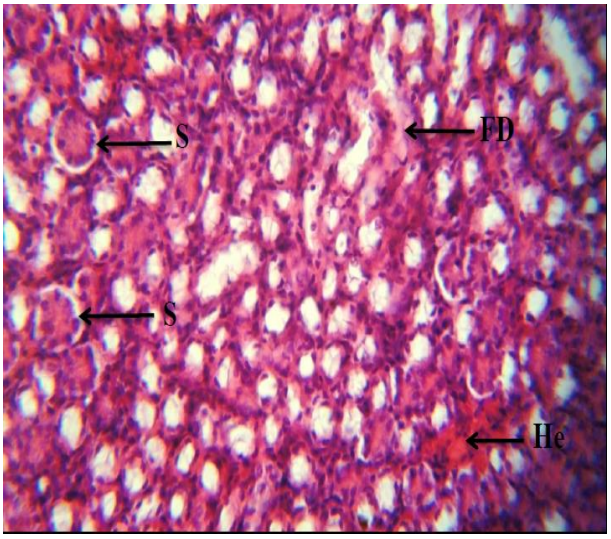

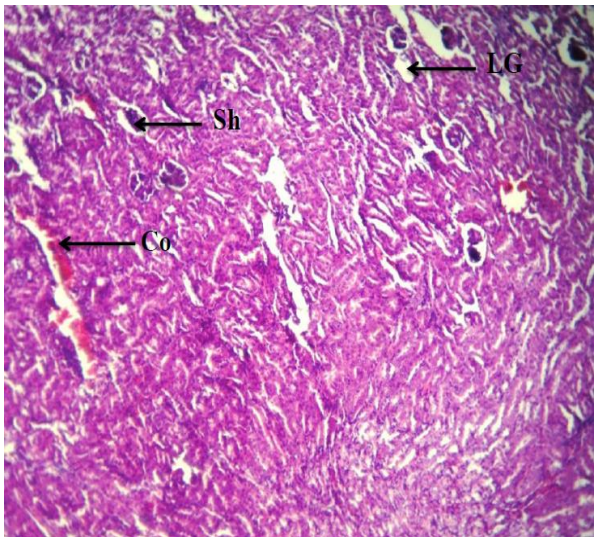

Fig(10): C.S in the kidney of group treated with (100)mg/kg for 6weeks showing the fibrin deposition (FD),sloughingepithelium (S)and hemorrhage(He)

Fig(11):C.S in the kidney of group treated with (100)mg/kg for 8weeks showing the congestion (Co), shrinkage(Sh) and completely loss of glomeruli (LG)(H&E, 100X). (H&E,400X).

Groups treated with (150) mg/kg of piroxicam

The examination of mice kidneys treated with (150) mg/kg of piroxicam showed severe changes that represented by pyknosis of nuclei, atrophy and sloughing of epithelium after 2weeks of administration figure(12).The appearance of hyalinization around the congested blood vessels was observed after 4 weeks figure(13), whereas after 6 and 8 weeks of administration the changes were vacuolation of tubular cytoplasm and atrophy of tubular epithelium as well as the presence of odema that occupied a large area of the kidney tissue figures (14,15).

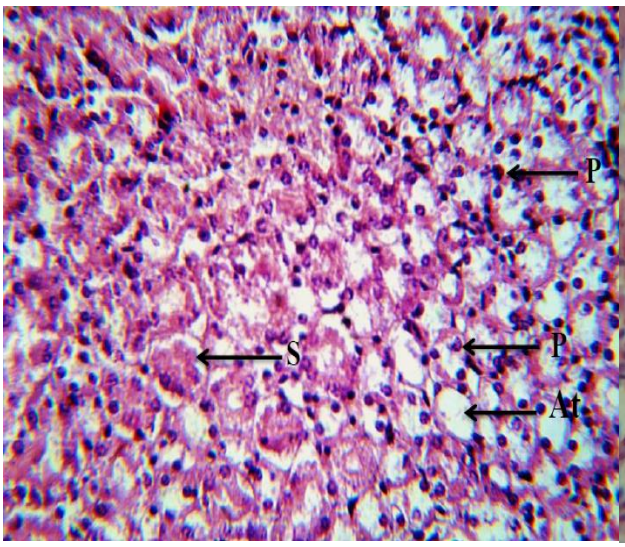

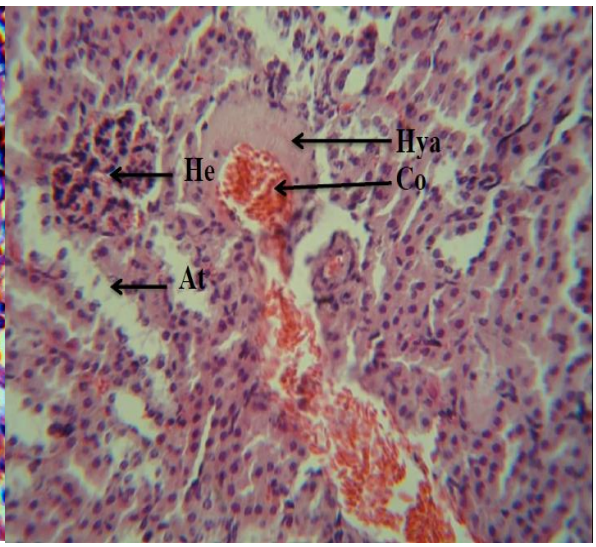

Fig(12):C.S in the kidney of group treated with (150)mg (150)mg/kg

Fig(13):C.S in the kidney of group treated with

/kg for 2weeks showing the atrophy of tubular for 4weeks showing the atrophy (At), congestion(Co), Epithelium(At),pyknosis (P)and sloughing epithelium hyalinization (Hya)and hemorrhage(He)(H&E,400X) (S)(H&E,400X).

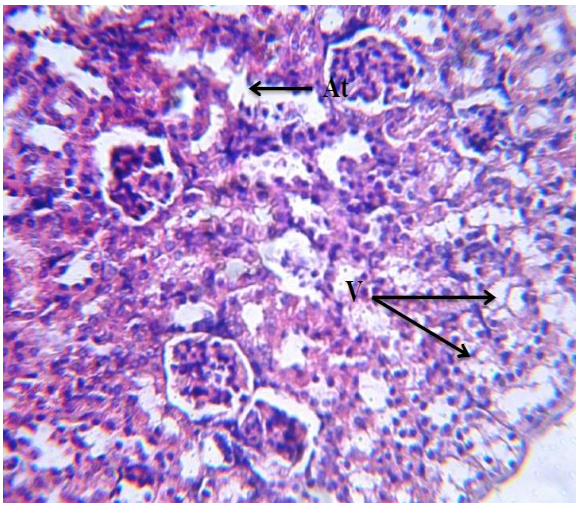

Fig(14): C.S in the kidney of group treated with (150)mg /kg for 6weeks showing the atrophy of epithelial cells (At) and vacuolation of tubular cytoplasm (V) (H&E,400X).

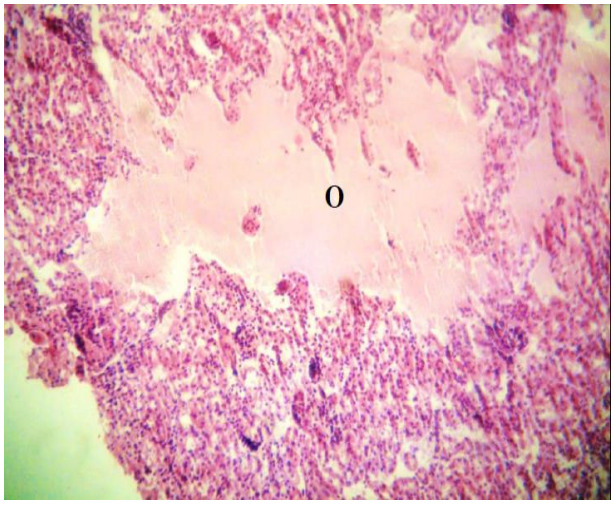

Fig(15): C.S in the kidney of group treated with (150)mg/kg for 8weeks showing the odema (O)(H&E,400X).

Histochemical changes in the kidney

Control kidney sections stained with periodic acid shiff's (PAS) showed a positive reaction to the stain as an indication for the existence of carbohydrates in the brush border of proximal convoluted tubules and the basement membrane of renal tubules figure (16).

Kidney tissue of treated mice with (50,100,150)mg/kg of piroxicam after 8 weeks of administration showed a depletion of carbohydrate content. The reduction increases with the increment of concentration and administration period figures (17,18,19).

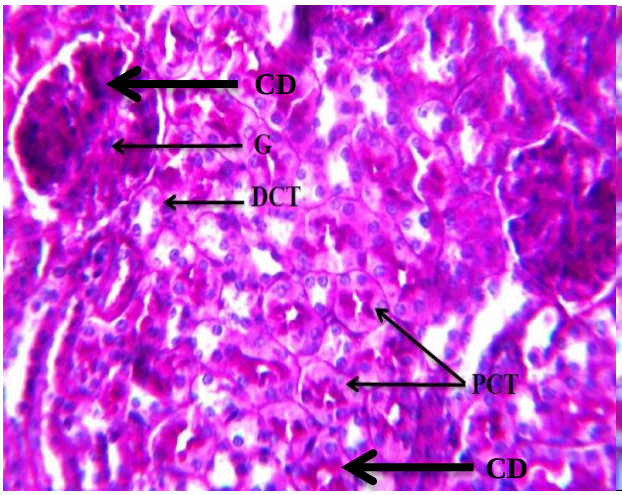

Fig(16):C.S in the kidney of control group showing

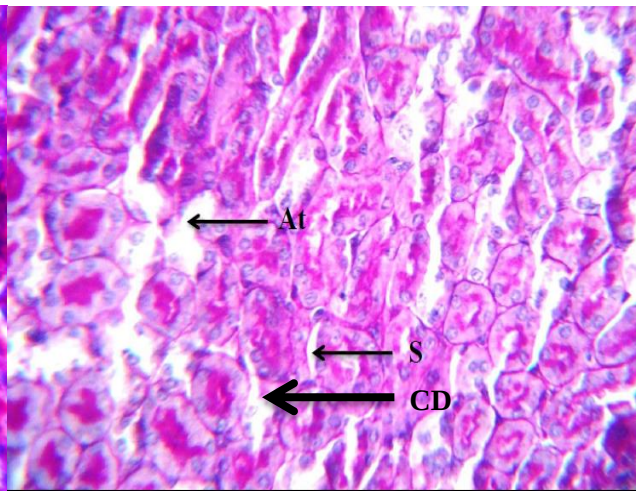

Fig(17):C.S in the kidney of group treated with(50) mg/kg

Carbohydrate deposition(CD),distal convoluted tubule for 8weeks showing atrophy (At) and carbohydrate
(DCT), glomerulus (G) and proximal convoluted tubuledeposition(CD) sloughing epithelium (S) (PAS,400X).
(PCT)(PAS, 400X).

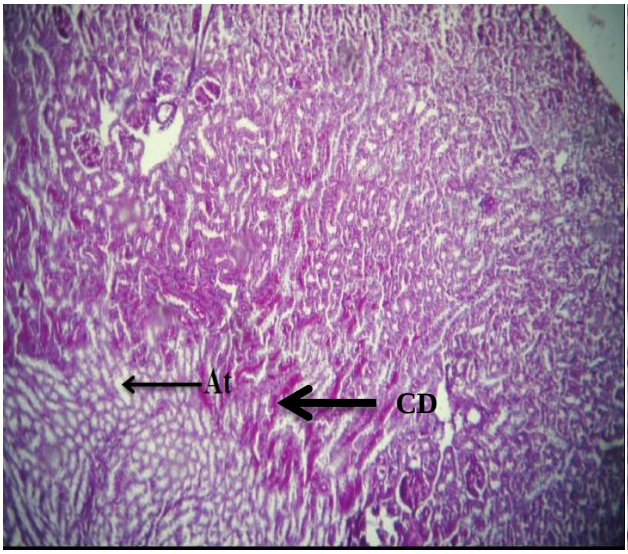

Fig(18):C.S in the kidney of group treated with (100) mg/kg for 8weeks showing atrophy (At), carbohydrate deposition(CD) (PAS,100X).

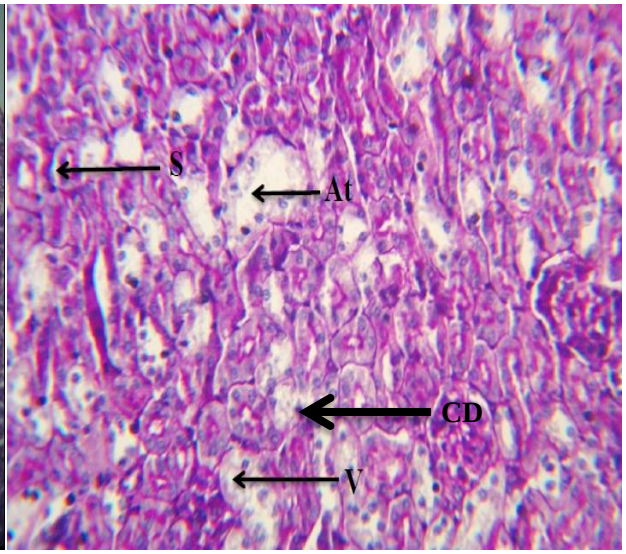

Fig(19):C.S in the kidney of group treated with (150) mg/kg for 8weeks showing atrophy (At),carbohydrate deposition (CD), sloughing epithelium (S) and Vacuolation (V) (PAS,400X).

The control sections stained with Bromophenol blue (Bpb) showed normal protein content which is equally distributed in glomeruli and renal tubules, while there were a reduction in protein content in the kidney tissue of treated mice with (50,100,150) after 8weeks of administration figures(20,21,22,23)

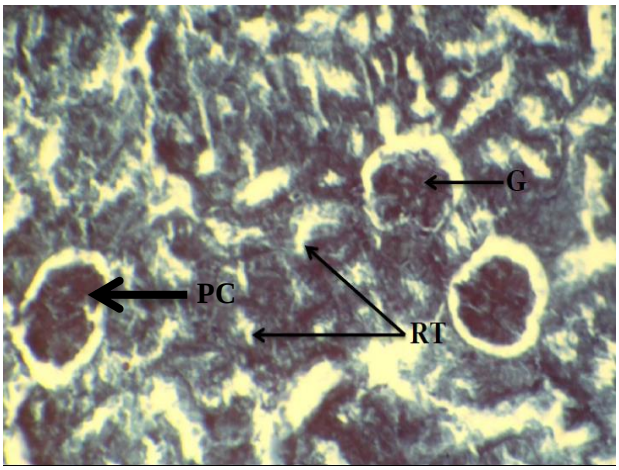

Fig(20):C.S in the kidney of control group showing the protein content (PC) in glomerulus (G),renal tubules (RT)(Bpb, 400X)

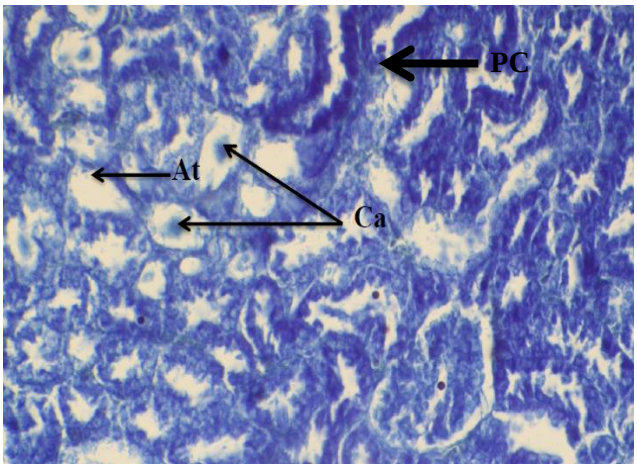

Fig(21):C.S in the kidney of group treated with (50) mg/kg for 8weeks showing atrophy (At) , calcium casts(Ca) and protein content (PC) (Bpb,400X).

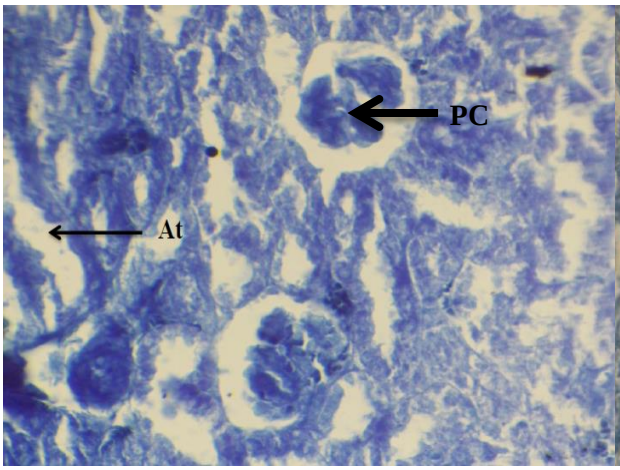

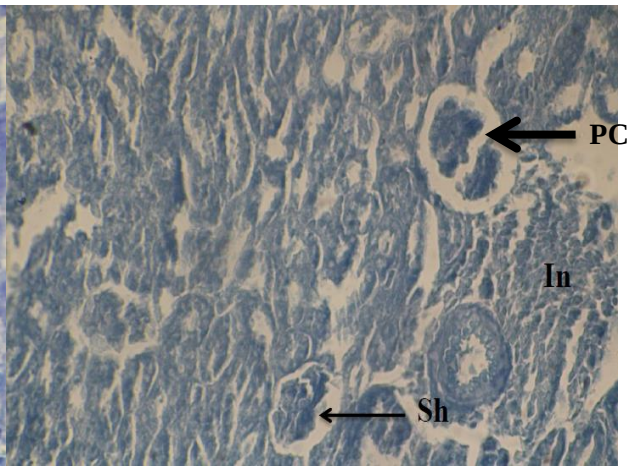

Fig(22):C.S in the kidney of group treated with (100) mg/kg for 8weeks showing Atrophy (At) and protein content (PC) (Bpb, 400X)shrinkage of glomerulus (Sh) and protein content (PC) (Bpb, 400X)

Fig(23):C.S in the kidney of group treated with (150) mg/kg for 8weeks showing infiltration of leukocytes (In) ,

Morphometric results

The morphometric results of the present study revealed significant differences ($P<0.05$) in the mean diameters of renal glomeruli for all concentrations of piroxicam for the period of eight weeks compared with control group, while the other periods did not show any significant differences (Table 1).Also there were non-significant decrease in the mean diameters of proximal convoluted tubules in the treated groups with concentration of (50,100,150) mg/kg in all periods except the period four weeks of the treated animals with concentrations (100,150) mg/kg that showed a significant decrease ($P<0.05$) in comparison with control group (Table 2). The results also clarified that there were significant differences ($P<0.05$) in the mean diameters of distal convoluted tubules of treated groups with concentration (100,150) mg/kg for six and eight weeks of administration, while the group treated with concentration (50)mg/kg of piroxicam did not show any significant differences over the whole administration period (Table 3).

Table(1): The effect of Piroxicam on the mean diameter of renal glomeruli (µm) of male mice compared with the control group

Mean diameter of renal glomeruli (µm) ± S.E

Drug concentration mg/kg	Periods (weeks)				L.S.D
	2	4	6	8	
Control (0)	50.5±1.9	49.8±1.5	48.5±1.6	50.5±1.9	NS 5.85
50	38.0±1.7	36.5±1.8	31.3±1.6	36.0±1.6	*7.88
100	39.0±3.1	41.0±1.7	33.0±3.0	32.0±1.3	*9.24
150	39.0±2.3	38.0±2.0	27.0±2.6	26.0±1.6	*7.94
L.S.D	NS 6.79	NS 5.93	NS 6.77	*4.70	----

NS: Non-significant, *(P<0.05)

Table (2): The effect of Piroxicam on the mean diameter of Proximal convoluted tubule (µm) of male mice compared with the control group

Drug	Mean diameter of proximal convoluted tubule (µm) ± S.E				
Concentration	Periods (weeks)				L.S.D
mg/kg	2	4	6	8	
Control (0)	28.2±1.1	28.0±1.0	28.0±1.1	28.5±1.2	NS 1.85
50	26.3±0.8	27.0±0.7	24.1±0.9	22.6±0.6	*4.87
100	26.5±1.1	23.5±0.6	23.5±0.7	22.0±0.6	*4.15
150	25.0±0.5	22.2±0.6	22.7±0.6	21.7±0.6	*3.59
L.S.D	NS 2.45	* 2.93	NS 2.35	NS 1.91	----

NS: Non-significant, *(P<0.05)

Table (3): The effect of Piroxicam on the mean diameter of Distal convoluted tubule (µm) of male mice compared with the control group

Drug concentration mg/kg	Mean diameter of distal convoluted tubule (µm) ± S.E				
	Periods (weeks)				L.S.D
	2	4	6	8	
Control (0)	25.6±0.6	24.5±0.9	25.2±0.5	25.8±0.8	NS 2.25
50	25.7±0.9	27.0±0.7	26.5±0.9	25.8±0.6	*4.06
100	25.5±0.8	26.2±0.6	23.5±0.7	21.2±0.4	*3.57
150	25.0±0.5	25.0±0.6	22.0±0.5	20.7±0.4	*3.74
L.S.D	NS 2.89	NS 2.29	*2.36	*1.69	----

NS: Non-significant, *(P<0.05)

Discussion

In this study, we tried to identify the effect of piroxicam in the kidneys of adult male albino mice. It was clear that its effect was time dependent, there were increased effects with prolonged time of dose administration this result is in agreement with[7].

The histological examination revealed that there were histopathological changes in the kidney of treated mice with the

concentrations (50, 100, 150)mg/kg of piroxicam and were more severe by using high concentrations (100, 150) mg/kg , the histopathological changes of groups treated with (50) mg/kg showed severe hemorrhage, congestion, formation of calcium casts, these findings in agreement with Baisakh *et. al.* foundation [12] , furthermore these changes were accompanied by invasion of inflammatory cells to the interlobular tissues in a trial to minimize the injury [13] .

There was also a remarkable histopathological changes in the most groups treated with piroxicam that represented by a vascular congestion that may be related to the use of drug that cause an acute inflammation this and led to change the blood flow inside blood vessels, this change may cause a relaxation and an extension in these blood vessels, thus the blood will accumulate into the vessels [14].

The hemorrhage observed in the present study may be caused by the continuous inflammation which is resulted from the effect of drug especially with high concentrations, and led to the shred of the endothelial cells that line the blood capillaries. These findings in agreement with [15].

Results also showed formation of calcium casts in the tubular lumen, this may attributed to the elevation of hydrogen peroxidase H_2O_2 that cause the nephrotoxicity which is responsible for changing the permeability of mitochondrial cellular membrane; Hence the amount of calcium taken by the mitochondria will increase and with the existence of oxygen, the mitochondria will break down and the calcium will be released in the kidney tissue [16].

The present study also showed the presence of histopathological symptoms in the groups treated with (100) mg/kg of piroxicam that represented by fibrin deposition inside the tubular lumens, these findings also observed by [17] who stated that fibrin deposition is attributed to the inhibition of cyclooxygenase-1 by NSAIDs which is responsible for prostaglandins production in different positions of kidney tissue.

The sloughing of tubular epithelium would happen in a trial to increase the distance, so that the drug will not reach the blood stream as much as possible to exclude its harmful effect [18].

The shrinkage and loss of some glomeruli that observed in this group, may be caused by the mesangial cell processes that retracted due to the contraction of their filaments [12].

Results also showed the appearance of hyalinization in the kidney of groups treated with 150 mg/kg of piroxicam after 8weeks of administration is probably caused by the accumulation of abnormal protein substances resulted from dissolution of amino acids especially the immunoglobulins and carbohydrates resulted from cell death [19].

Regarding the histochemical changes observed in this study under piroxicam administration, results showed a reduction in the polysaccharides and total proteins in the kidney tissue, The decrease in carbohydrate content could be attributed to the increased stress on organs, which lead to high energy consumption and allowed an equalized pressure to be exerted upon them [20,7] or

may be due to the depletion of mucopolysaccharide in tissue which is attributed to the turbulence of Golgi apparatus [21].

The decrease in protein content could be attributed to the depletion of ribosomal granules of the rough endoplasmic reticulum [21] or it may be caused by the disruption of lysosomal membrane under the effect of various toxicants leading to the liberation of their hydrolytic enzymes in the cytoplasm resulting in marked lysis and dissolution of the target materials [7].

The morphometric study regarding the measurements of glomerular diameters revealed a significant decrease in the mean diameters of glomeruli in groups treated with (50,100,150)mg/kg of piroxicam for the period 8 weeks, this findings are in agreement with the results of [17].Also measuring diameters of proximal convoluted tubules showed non-significant differences except the period of 4 weeks of treated groups with (100,150) mg/kg showed a significant decrease; while the results of distal convoluted tubules showed a significant decrease in the periods (6,8) weeks for the groups treated with (100,150)mg/kg. these results are consistent with many researchers included [22&23].

The main reason behind changing in the diameters of glomeruli, proximal and distal convoluted tubules is using NSAIDs that may reduce the collagen content in the tissue which probably has a big role in supporting the wall of renal tubules and ducts, therefore, the reduction of this material resulted in changing the tissue features [23].

Safari *et. al.*[24] suggested that using NSAIDs may cause free radicles releasing that is related with causing damages to renal tubules and glomeruli.

References

1. Starek,M.;Krzek,J.;Tarsa,M.&Zylewski,M.(2008). Determination of piroxicam and degradation products in drugs by TLC.Chromatographia,69: 351-356.
2. [2] Woolf,A.D.;Rogers,H.J.; Bradbrook,I.D. &Corless,D.(1983). Observations on piroxicam in young adult,middle aged and Elderly patients. Br.J. Clin. Pharmacol.,16:433-437.
3. Elivin,J.; Yang,C. & Matzak, M.(2000). Growth deferentiation factor-9 stimulates progesterone synthesis in granulosa cell via prostaglandin E2 receptor pathway. Proc. Nath. Acad. Sci. USA., 97: 10288-93.
4. Gattoegosandan, S.; Novalbos,J.; Rosado,A.;Gisber,J.; Galves,Mugica, M.; Garcia,A.; Pajares,J. & Francesco, A.(2004). Effect of Ibuprofen on cox and nitric oxide synthase of gastric mucosa; correlation with endoplasmic lesions and adverse reaction. Digestive Diseases and Sciences, 49: 1538-1544.
5. Burdan,F.(2004).Developmental toxicity of Ibuprofen and tolementin administration in triple daily doses to wistar rats. Birth. Defects. Res.,71: 321-330.
6. Obeys, A.K.&Mahood,A.K.(2013).Histological study of the effect of piroxicam on testis of albino mice Mus musculus.J.Anbar University for Pure Sciences,7(2):1-11

7. Ebaid,H.;Dkhil,M.A.;Danfour,M. ;Tohamy,A.&Gabry, M.S. (2007). Piroxicam induced hepatic and renal histopathological changes in mice. Libyan J.Med,13:56-61.
8. Bancroft,J.D.&Stevens,A.(1982).The ory and practice of histological techniques. Churchill livingstone,London,2ndedn. : 662pp.
9. Maize,D.; Brewer,P.A. &Affert,M.(1953).The cytochemical staining &measurements of protein with mercuric bromophenol blue. Biol.Bull., 104:57-67.
10. Galigher,A.E. &Kozloff,E.N.(1964).Essentials of practical microtechnique. Lea &Febiger.Philadelphia:484 pp.
11. SAS.(2012).Statistical analysis system, User's Guide. Statistical. Version 9thedn.SAS.Inc.Cary.N.C.USA.
12. Baisakh,P.;Mohanty,B.;Agrawal,D.; Baisakh,M. & Dutta, K. (2014). Effect of Ibuprofen on kidneys of albino rats. RJPBCS.,5(5): 136-142.
13. El-Banhawy,M.A.;Mohallal, E.M.; Hamdy, M.H. &Attia, T.N.(1996). The toxic impacts of the narcotic drug(flunitrazepam) on the rat kidney tissues. Zag J.Med. Physiol.,1(3):233-39.
14. Robbins, S.L.& Kumar,V. (1987).Basic pathology. 4th edn. W.B. Saunders company. Philadelphia, London: 29-53pp.
15. Abdulrazak, M.H.(2012).Effect of Nitrofurantoin in the liver and kidney of male albino mice Mus musculus . MSc. Thesis, College of Science for Women. University of Baghdad.
16. Aydin,G.;ONCU,M.;Çiçek,E.;Karah an,N.&Goklap,O.(2003).Histopathol ogical changes in liver and renal tissues induced by different doses of diclofenac sodium in rats.Turk.J.Vet.Anim.Sci., 27:1131-1140.
17. Mahmoud, F.Y.;Abou-alghait,A.T.;Rateb, A.&Salah,E.(2010). Comparativestudy on the effect of long term administration of Non-Steroidal anti-inflammatory drugs meloxicam &ketoprofen on the structure of the kidney & gastric mucosa in the adult albino rats. Egypt. J. Histol., 33 (4) :722-734.
18. Kumar,V.;Abbas,A.K.;Fausto,N.&M itchell,R.(2007).Robbins basic pathology.8thedn.Saunders Elsevier: 632-634.
19. Stevens,A.&Lowe,J.(2005).Human histology 3rded.Elsevier.Mosby.Philadelphia ,: 296-298.
20. Ali, A.H.& Taha, H.A.(2008).Effect of sodium Diclofenate on albino rat kidney. El-minia med.Bull.,19(2):87-94.
21. Shaffie,N.M.; Morsy,F.A.; A.G.&Sharaf,H.A.(2010). Effect of Caraway, Coriander & fennel on the structure of kidney &islets of Langerhans in Alloxan-Induced Diabetic rats: Histological& Histochemical Study.,2(7): 27-40.
22. Olliges,A.;Wimmer,S. & Nusing,R.(2011).Defects in mouse nephrogenesis induced by selective &non-selective cyclooxygenase-2 inhibitors. British Journal of pharmacology, 163: 927-963.

23. Sheyda,A.;Lila,G.;Elhamy,R.K.;Hos sein,K.J.;Hamid,B.S.&Mohammed,F .(2013). Investigating antioxidant effect of cinnamon extract on elimination of toxicity of gelofen drug in kidney tissue of female rats. World Journal of Zoology,8(4): 401-406.

24. Safari,M.S.;Faghihi,M.;Parvis&colle agues.(1983).Effect of ischemia reperfusion of kidney on production of hydroxyl radical and changes in plasma copper and zinc. Physiology and Pharmacology, 8(1):61-70.

Design and Implementation of Patient Monitoring System for Medical Sign using GSM and Microcontroller

Reem Jamal Abbas* Rawaa Abdel Ridha kadhim* Siraj Qays Mahdi**

* Assist Lect. /Computer Engineering Techniques Department/ Electrical Engineering Technical College/ Middle Technical University.

** Lect. / Computer Engineering Techniques Department/ Electrical Engineering Technical College/ Middle Technical University.

reem84j@gmail. comrawaa84ha@gmail.comSiraj_qays@yahoo.com

Abstract:

The work presented in this paper concerned with the design of a new remote monitoring system for patients in An intensive care unit (ICU) , which can be used to read the medical signs such as (heart rate, temperature value and oxygen saturation percentage) from the patient's body beside checking the pacemaker device and send the values to the remote area. The proposed system deals with the patient vital signs as an input to send them to a computer in the nursing room by a transmitter-receiver system which composed of two Arduino kits connected with Bluetooth devices. The signal received by computer is processed and if there is an abnormal condition a message will be send to doctor mobile through Global System for Mobile Communications (GSM). The mechanism of the system is to send the medical signs to doctors in a remote area. The computer sends these values to doctor's mobile. Finally, visual basic language was used to implement the frame work of the system.

Keywords: *Arduino kit, medical sensors, Bluetooth, visual basic, GSM mobile, ICU.*

تصميم وتنفيذ نظام مراقبة الاشارات الطبية للمريض باستخدام تقنية ال GSM والمتحكم الدقيق

الخلاصة:

العمل في هذا البحث يتعامل مع تصميم نظام مراقبة المريض في وحدة العناية المركزة عن بعد، والذي يمكن ان يستخدم لقراءة الاشارات الطبية مثل (معدل سرعة دقات القلب ، درجة الحرارة، ونسبة الاوكسجين بالدم) من جسم المريض بالاضافة الى التحقق من عمل جهاز منظم ضربات القلب وارسال القيم الى النظام المقترح ، والذي بدوره يتعامل مع اشارات المريض الحيوية كاشارة ادخال لارسالها الى الحاسوب الموجود في غرفة الممرضات باستخدام منظومة الارسال والاستلام المكونة من بوردين اردوينو مربوطين عن طريق البلوتوث . الاشارة المستلمة من قبل الحاسوب يتم معالجتها وملاحظة ان كانت غير طبيعية ففي هذه الحالة يتم ارسال رسالة عن طريق نظام ال GSM الى موبايل الطبيب. ميكانيكة عمل النظام هو القيام بارسال الاشارات الطبية الى الاطباء عن بعد . اذ ان الحاسوب يقوم بعملية ارسال هذه الاشارات الطبية الى موبايل الطبيب. واخيرا لغة الفجوال بيسك تم استخدامها لتنفيذ هيكلية العمل بهذا النظام.

1. Introduction:

As a result of development in life, health monitoring becomes an important researched field. So researched in this field were developed through years for many applications such as military, homecare, hospital, sport training and activity emergency [1].

Telemedicine applications give a wide help in health monitoring field, where this technology is used to transmit medical information about the patient's status electronically, so it gives an easy way to monitor and diagnose the patient remotely, such as the ICU network [2]. ICU Networking means connecting the Intensive care unit (ICU) PC's (client) to the nursing room PC (server) with Local Area Unit (LAN),Metropolitan Area Network (MAN) or other network by providing a set of rules for communication called protocols, these protocols should be known by all participating hosts, which allows different computers with different operating characteristics to communicate with each other, and that in order to present whole information about the patient situation in nursing room so any abnormal condition can be recognized immediately by nurse without being in the ICU which could be then sent to doctor mobile[3].

Revolution in microcontrollers through years led to discover the Arduino, which is an open hardware board that rise in thoughts and projects of robotic control easily and simply by using an open hardware programmable language (Arduino c), the ability of using Arduino in projects that used a revolved engineering languages like matlab and java, beside the simplicity of dealing with and programming it, makes Arduino on the top of microcontrollers types [4]. Although there are a wide researches in this field but more efforts are required to prove clinical and cost effectiveness.

G.Virone, *et.al*.had been proposed system architecture for smart healthcare based on wireless sensor network (WSN). They suggested a strong potential for WSNs for low-cost and deployment of multimodal sensor for an improved quality of medical care [5].

Aartvan Halteren, *et.al*. had been developed a system allows the incorporation of diverse medical sensors via wireless connections and the live transmissions of the measured vital signs over public wireless networks to health care providers. The results documented the feasibility of using the system, but also demonstrated logistical problems with use of the BANs and the infrastructure for transmitting mobile healthcare data [6].

Dr. Deepack Choudhary, *et.al.* had been developed a portable real-time wireless health monitoring system. The system is used for remote monitoring of patient's heart rate and oxygen saturation in blood, the system was designed and implemented using ZigBee-wireless technology. They found that the system can successfully install for testing patient's home for health care monitoring and the wireless sensor network can operates on an area of 10-15 square meters [1].

This paper was implemented by developing a monitoring system to pursuing the patient's status immediately. The system was depending on microcontroller kit (Arduino) and using its Bluetooth network for sending the medical vital sign from the

patient's body to remote ICU (special computer) instead of the traditional computer network for reading and sending the important signs and avoids the connectionless problems.

2. Proposed Work.

The purpose of this work is to design a medical wireless monitoring system capable to sense the status of patient medical sign (the temperature, the heart rate through the Patient's blood pressure, in additionto regulate the abnormal beating of heart through the pacemakers shown in Fig. (1).

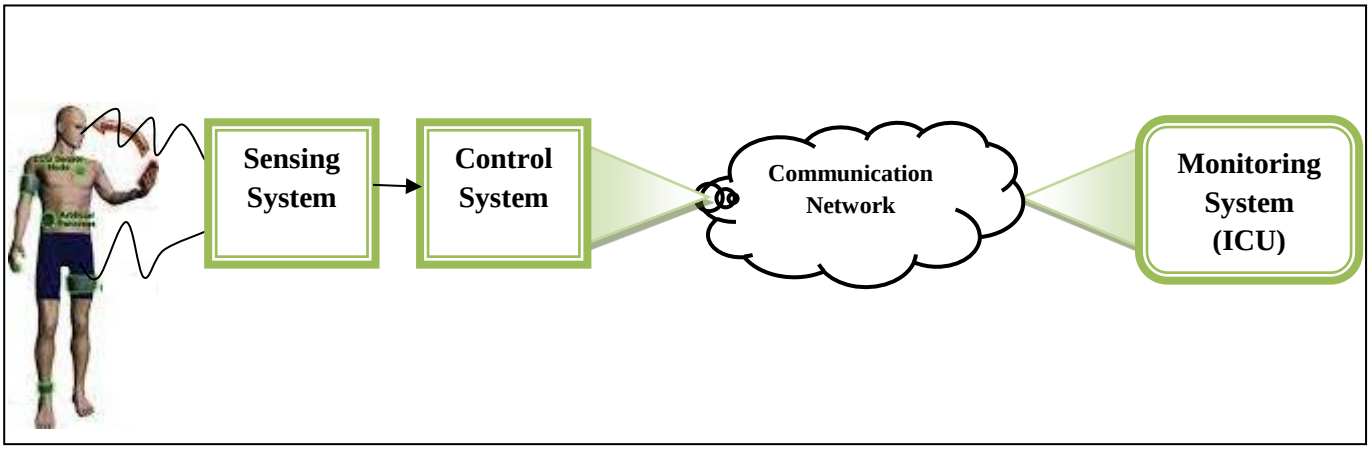

Fig (1): Shows The General Block Diagram Of The Monitoring System.

2.1 System Descriptions:
The system consist of many parts to satisfy the requirements of the idea as shown in fig (2)

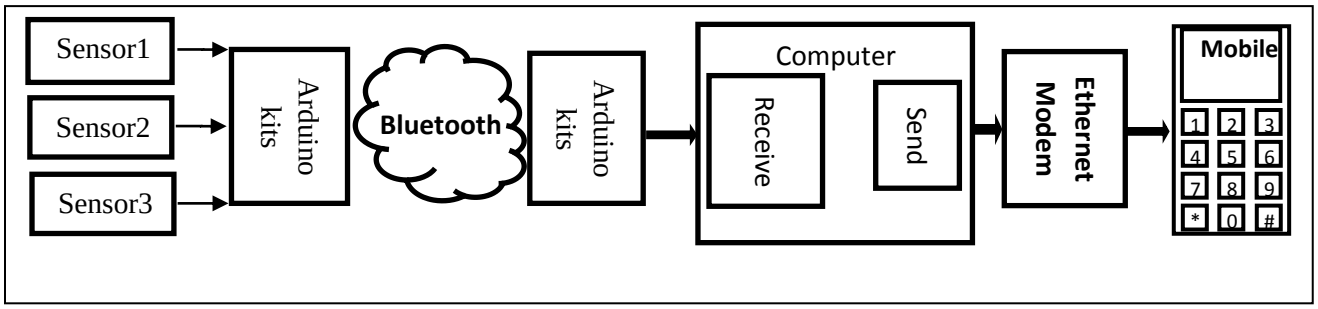

Fig. (2): Shows the Main Components of the Health Monitoring System.

2.1.1 Sensors: many of the medical sensors was connected to the Arduino ports to read the patient's status:

a. Temperature sensor: the responsibility of this sensor is to read the body's temperature and identify the status.

b. Heart rate: is the number of heart beat per minute; each beat represents the contract and relaxation of heart.

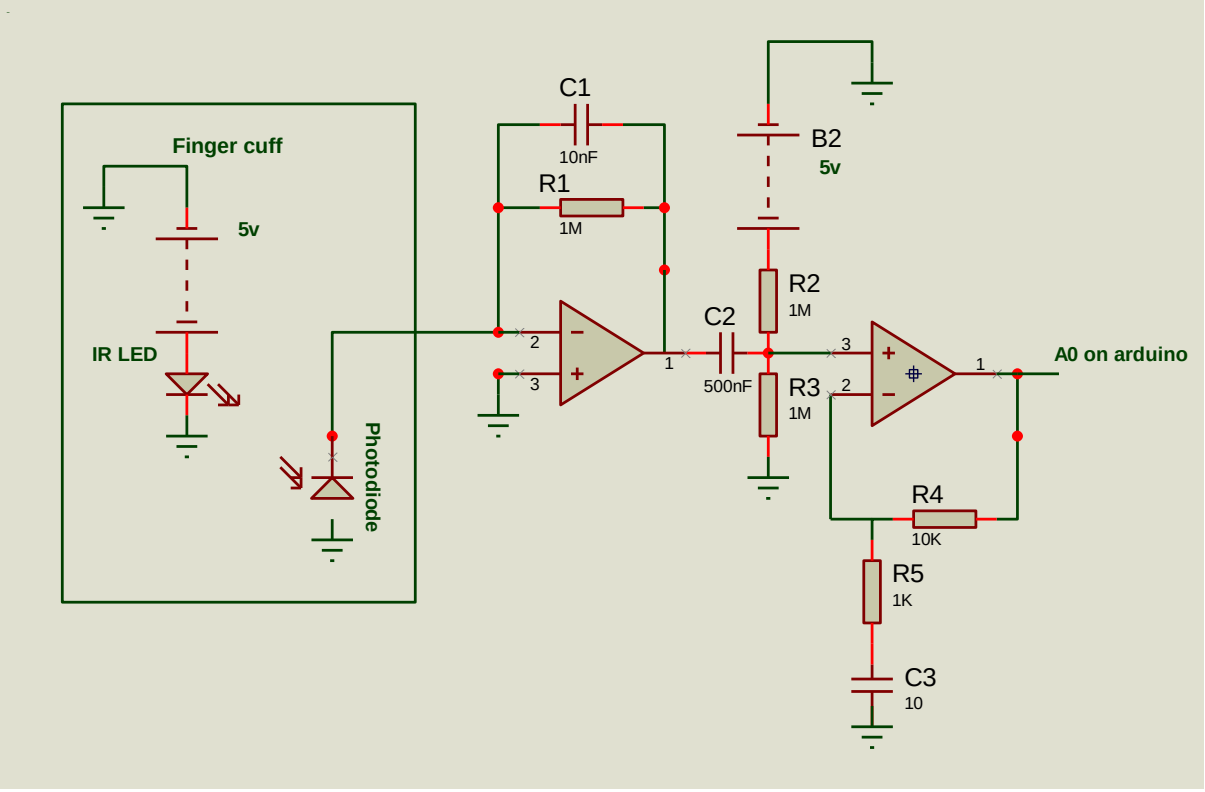

Fig (3): shows the circuit diagram of Heart Rate [7].

c. Pacemaker Sensor: is a device used to regulate the abnormal beating of heart; it is an internal device that transplanted within human body. It is composed of three parts_ input/output leads sensor circuit pulse generator the input/output leads are electrodes that connected to heart chambers taking the input signal from the heart to the pulse generator and transmit the output signal from the pacemaker back to the heart. Sensing circuit receives the heart input signal, processing it to a form acceptable to the pulse generator by using an oscillator triggering by the heart input wave and gives square wave as an output which goes to the pulse generator.

The pulse generator is the most important part of the pacemaker it is a preprogrammed microcontroller receives its input from the from the heart through the sensing circuit and responds to it with a stimuli that transmitted back to the heart the stimuli generate according to the program of the generator as shown in fig.(4). The pacing mode of the pacemaker should be only when it is needed so that there is no interference between the natural pacing and artificial pacing [8].

To understand the mechanism of artificial pacing more clearly we will take the R wave as an example which represents the ventricular contraction which in turn pumps the blood to the big arteries in the human body. In case of absence of R wave the pacemaker will pace by giving electrical activity to the heart while if the R wave is already exist there no need for artificial pacing .for a single chamber pacemaker which takes the input from one chamber only from the heart (one chamber needed to be regulated) the pacemaker has three paths to follow:RESET timer, WAIT, and PACE. after the R wave be sensed the generator will switch to WAIT stat for a time delay of 0.83 second which is the normal duration between two R waves, after this delay if another R wave sensed then the generator goes to RESET timer and start counting a delay of 0.83 second (WAIT state) if R wave doesn't sensed then the generator goes to PACE mode and give an electrical stimulus (pacing) delivered to the heart the leads and so on [8].

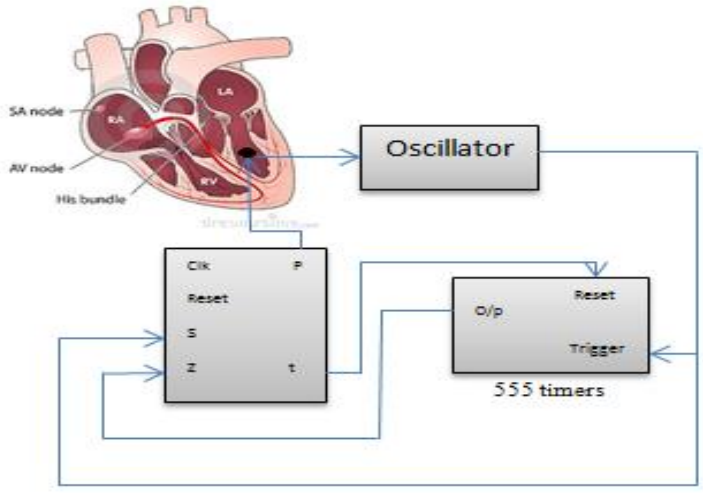

Fig. (4): shows the block diagram of Pacemaker.

d. Oximeter sensor : is a circuit that consist of red and infrared LEDs that generates red and infrared wavelengths respectively as shown in fig.(5), these wavelengths passed to a photo diode detector throughout the

finger where a portion of the two wavelengths absorbed by blood vessels in the finger (arterioles). The absorption ratio depends on oxygen saturation percentage(no of oxy hemoglobin molecules and the no of deoxy hemoglobin to the number of the total hemoglobin molecules) and the transmitted wavelengths of both LED s received by a single photodiode , after that the received light passed to a timing circuit that supplies a pulses with proper repetition rate to derive red and infrared wavelengths alternately so it acts as digital switch .after that both light wavelengths red and infrared amplified and convert to a voltage using current to voltage converter circuit operational amplifier (op_amp) . As the wavelengths received in photo diode in pulsed form because the blood in the artery is pulsed a sample and hold circuit is used to separate the wavelengths each with a single path. The timing circuit will used again to generate control pulses of the sample and hold circuit. The output voltage then passed to a band pass filter to remove low and high frequency noise after that the clear voltage signal passed to an Arduino to be converted to a digital signal and send to the computer by Bluetooth [9].

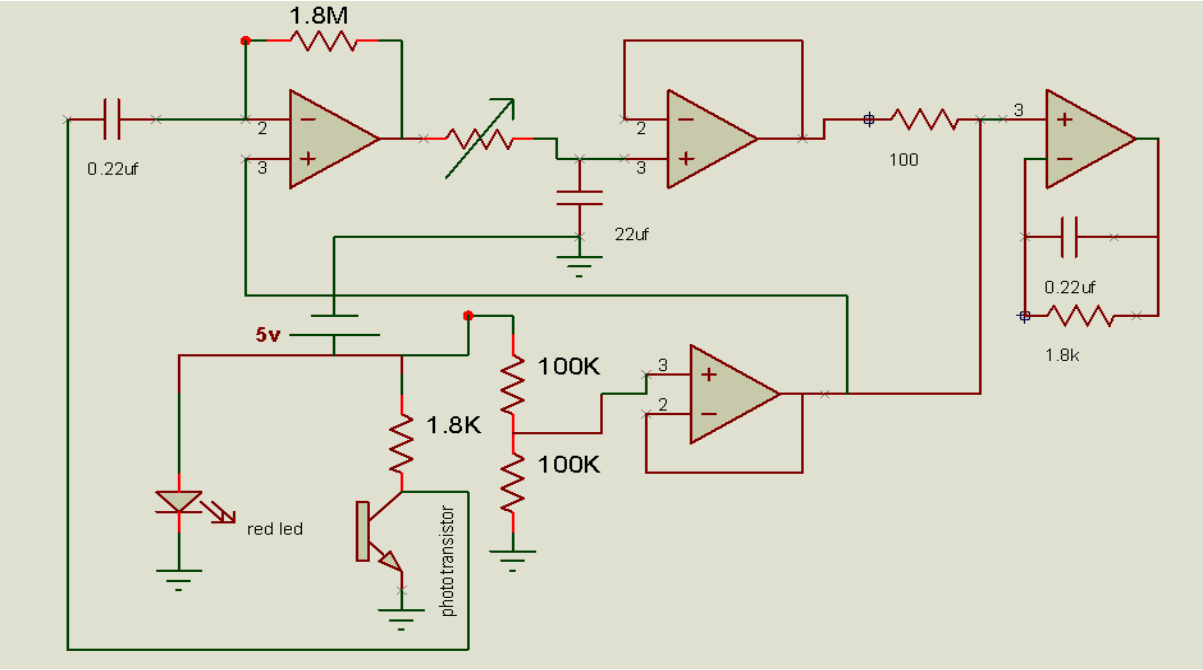

Fig. (5): shows the block diagram of Oximetry Sensor [9].

2.1.2 Connecting the Bluetooth with microcontrollerkit (Arduino):

Bluetooth is a wireless networking device that transmits data from point to point over a short distance using a communication protocol. In this work the Bluetooth is used to transmit data from medical sensors to computer by connecting it with the Arduino Uno microcontroller kit in both sides as shown in fig.(6). HC-05 Bluetooth module is

used for this purpose.The Bluetooth element connected wirelessly to Arduino kit in a serial module, it is easy to use a two pins chosen from Arduino kit to represent the connection of serial port between Bluetooth shield and Arduino where the Tx of Bluetooth side is connected to the Tx of Arduino side and the Rx of Arduino side is connected to the Tx of the Bluetooth side and with a suitable Arduino program the data transmission is achieves. Fig.(7) shows the overall system work to follow up on the patient's status.

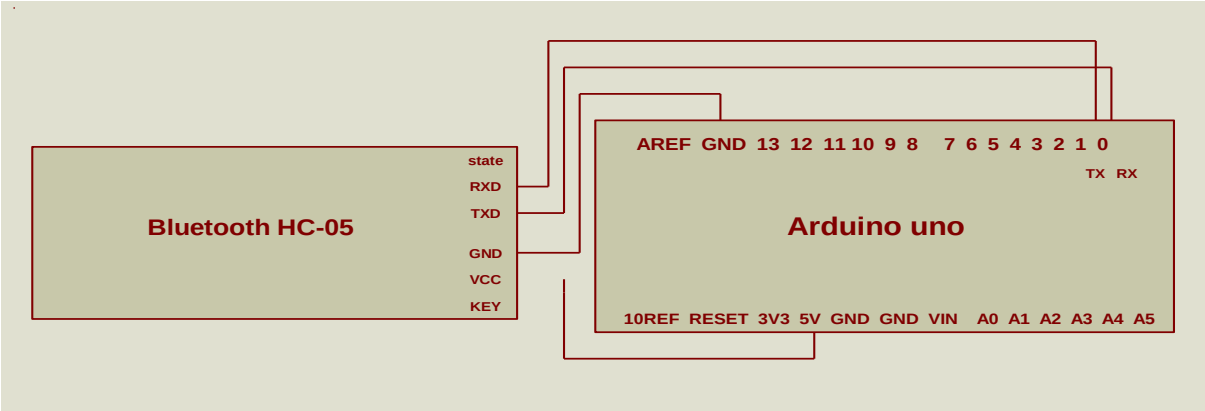

Fig. (6): shows the block diagram of Bluetooth connection with microcontroller kit (Arduino).

2.1.3 Connecting Mobile Phone with personal Computer:

Mobile phone technology has advanced in recent year. Many applications with mobile phones were implemented for sending short message service (SMS) from pc to mobile phone, where, when the system detect a (observe) a dangerous (risk) status or a threshold is reached. The monitoring system sends SMS through GSM to the doctor's mobile phone to inform him about the emergency case.**Fig.(7):** shows the modem device essentially consist of an internet modem and global system for mobile communication (GSM) modem / SMS gateway, the SMS sending is done through the SMS gateway. Patient information management system has knowledge about the number doctor. Hence the system basically will first query the database before sending SMS. SMS message to the corresponding doctor with respect to the patient ID as well as the message that has been sent to the doctor

.

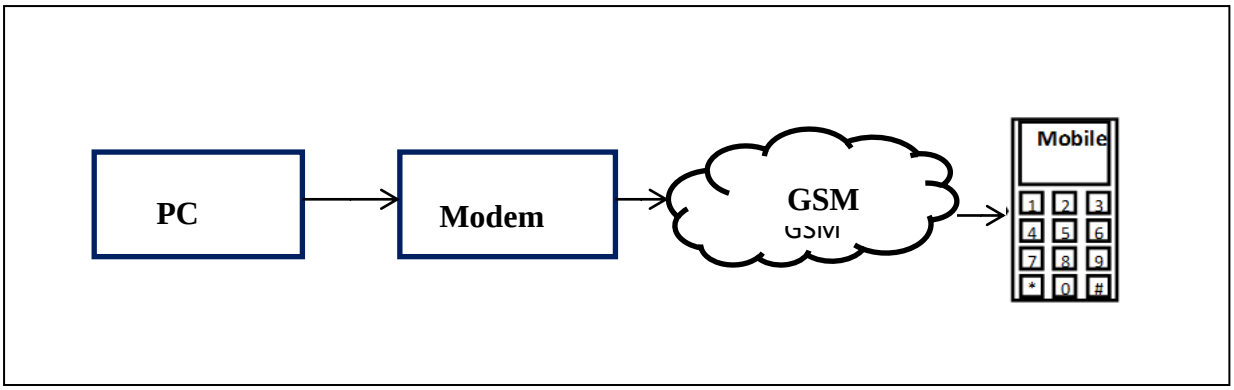

Fig.(7) : Shows the interface between personal computer and mobile phone through GSM modem.

3. **Working of the system**:

Fig.(8): shows the flowchart of the health monitoring system.

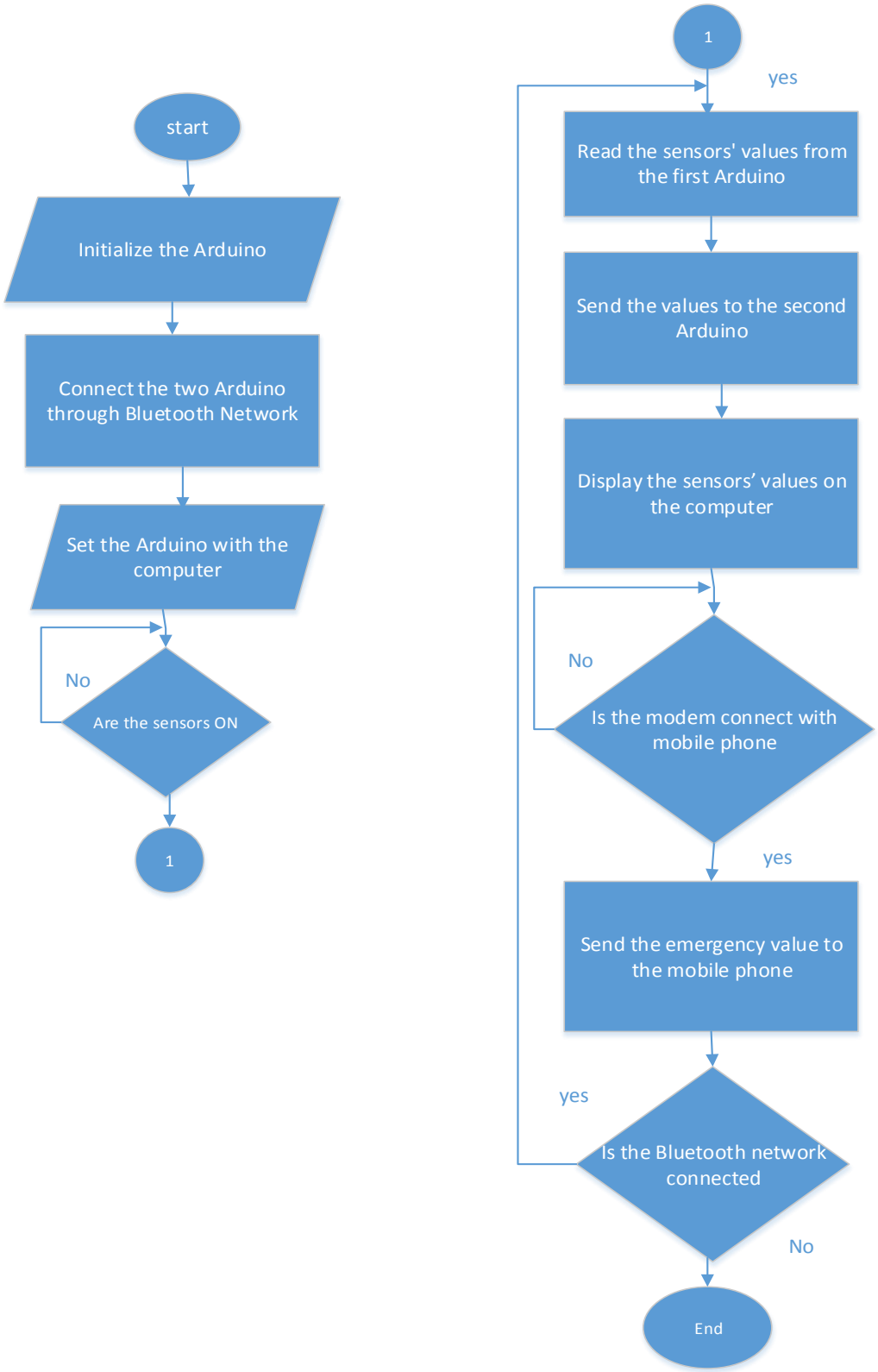

Fig.(8) : Flowchart illustrate the overall system mechanism.

4. Implementing the Proposed System.

The implementation of the monitoring system was achieved using hardware implementation from system's parts and visual basic language (ver.6) to programming the frame work as shown in Fig. 9 and Fig. 10.

Fig.(9): shows the hardware implementation of monitoring systems

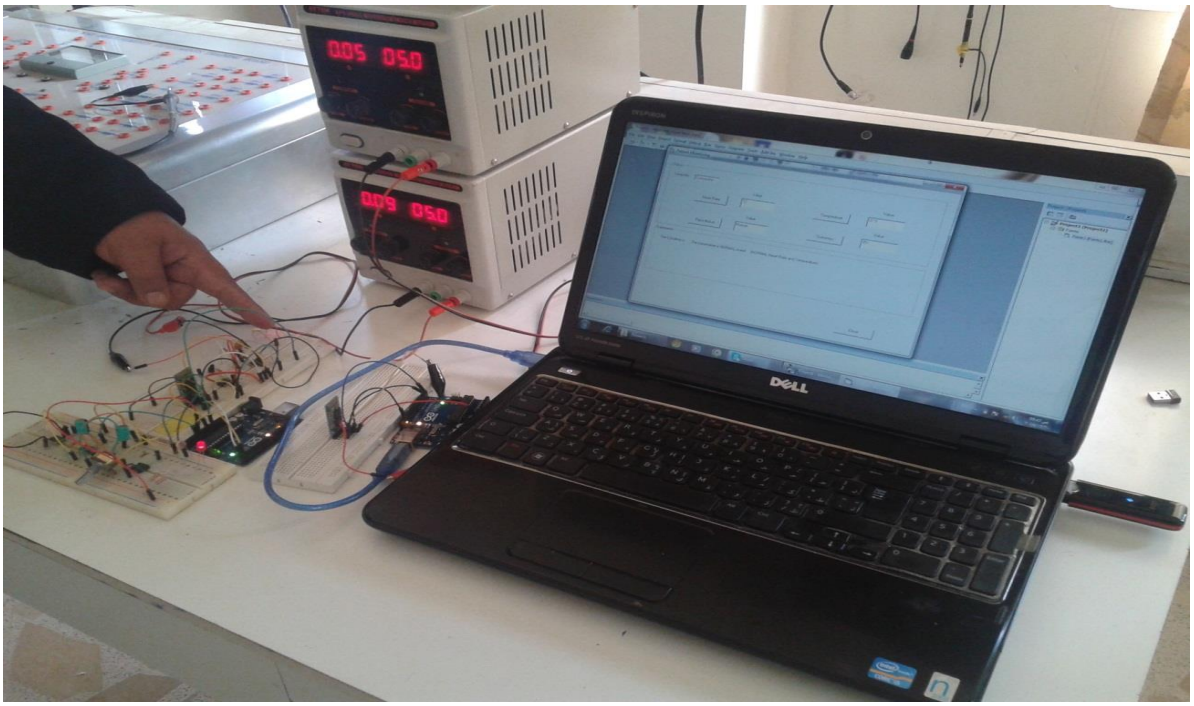

Fig.(10): shows the hardware implementati

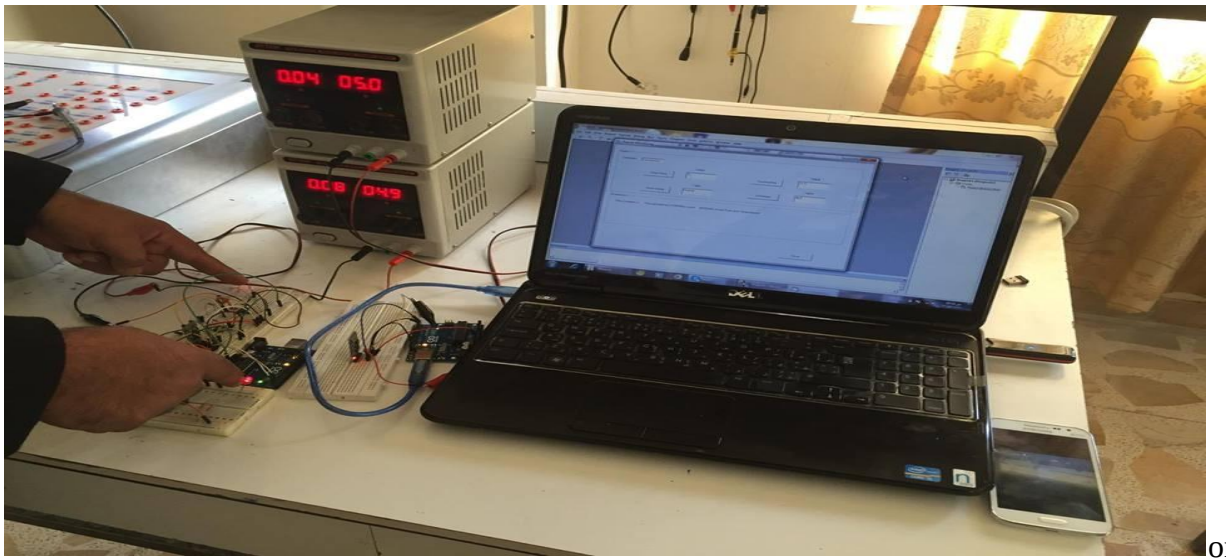

on of monitoring systems with GSM and mobile phone.

Conclusions:

The system is more flexible due to the usage of Bluetooth connection between

the first and second Arduino. Where, the vital signs and parameters data has been sent immediately to the server' PC in addition to alarm message to phone for directing the responsible about the patient's condition. At this meaning, the facility of data sending depend on the HC-05 Bluetooth which the range of Bluetooth is approximately (10 meters) that is capable to insure a large building. Moreover, Tx& Rx are separate pins for Bluetooth HC-05 instead of using microcontroller kit (Arduino) port's pins. Hence, this leads to reduced response time (sending and receiving) so as separate Pins are used instead of Arduino pins. The GSM network is higher baud rate that led to send all the sensors values to the mobile phone.

References:

1. (Sep/Oct 2012), network", IJAITI, vol. 1 No.5 ISSN:2277-1891, "Real-time health monitoring system on wireless sensor ,Dr. Deepak Choudhary *et.al*.,.
2. Hein,M.A. (2009). Telemedicine: An Important force in the transformation of healthcare.
3. Wesley, A. (1992). Wokingham, UK"Data communications, Computer networks and open systems", Third Edition, Halsall, F.
4. Mellis, D.A., *et.al*. (2007). conference on human factors in computing systems San Jose, California, USA "Arduino: An open electronics prototyping platform.
5. http://www.cs.virginia.edu/~adw5p/pubs/d2h206-health.pdf, "An advanced wireless sensor network for health monitoring".

Hulteren, A.*et.al*. (2004). 2(5): 365-373 , The journal on information technology in healthcare; "Mobile Patient monitoring: The mobile health system",

6. http://duino4projects.com/diy-arduino-pulse-sensor.
7. Panda, A. (2012), 108EI007, "VLSI Implementation of a demand mode dual chamber rate responsive cardiac pacemaker".
8. Lopez, S. (2012),Freescale semiconductor, Inc.," Pulse oximeter fundamentals and design",

Real-Time PCR detection of Ocular Toxoplasmosis in Iraqi patients.

Issra K. Al-AubaidiAli N. Yaseen*Waheeda R. Ali
Department of Biology, College of Education for pure science (Ibn al-Haitham), University of Baghdad, Baghdad, Iraq.
*Department of Science , College of Basic Education, AL- Mustansiriya University , Baghdad, Iraq.

Abstract

Current study was done to investigate ocular toxoplasmosis that caused by *Toxoplasma gondii* parasite in blood samples of patients that reviewers to retina unit in Ibn- al Haitham teaching Eye hospital in Baghdad , using real-time PCR technique. Initially the disease was diagnosed by ELISA method using specific IgG and IgM antibodies for *T. gondii*. According to its positive results the studied groups were divided to ocular toxoplasmosis group that contain 42 patients, their proportion 84%, 14 patients in positive uveitis group in 31.1% percentage and control group recorded 35 positive case for infection with *T. gondii* in 41.7% percentage this group named as Asymptomatic toxoplasmosis group with significant differences ($p<0.01$) between the three groups. The highest mean of IgG recorded in ocular toxoplasmosis group 1.661 ± 0.187 IU/ml and also for IgM 1.922 ± 0.510 IU/ml. when Real-time PCR applied 14 positive results in ocular toxoplasmosis group were registered with 33.3 percentage against 7 positive results only for uveitis and Asymptomatic toxoplasmosis groups with rates 50% and 20% respectively without any significant differences , this test was successes in diagnosing of *T.gondii* parasite in different groups, although most infections were chronic with low rates in comparison with ELISA technique that recorded high rates of positive diagnosis of infection.

Key words: Ocular toxoplasmosis, Diagnosis, IgG, IgM, Real-Time PCR.

التحري عن داء مقوسات العين في المرضى العراقيين باستعمال تفاعل انزيم البلمرة المتسلسل في الوقت الحقيقي

اسراء قاسم العبيدي*علي نزار ياسين وحيدة رشيد علي
قسم علوم الحياة، كلية التربية للعلوم الصرفة (ابن الهيثم)، جامعة بغداد، بغداد، العراق
*قسم العلوم، كلية التربية الاساسية، الجامعة المستنصرية، بغداد، العراق

المستخلص

اجريت الدراسة الحالية للتحري عن داء مقوسات العين Ocular toxoplasmosis الناجم عن طفيلي *Toxoplasma gondii*في عينات دم المرضى المراجعين لوحدة الشبكية في مستشفى ابن الهيثم للعيون في بغداد وباستعمال طريقة تفاعل إنزيم البلمرة المتسلسل في الوقت الحقيقي Real-Time PCR. شخص المرض مبدئيا بطريقة الاليزاELISAوللأضداد النوعية IgG وIgM للمقوسة الكوندية،واستنادا لنتائجه الموجبة قسمت المجاميع المدروسة الى مجموعة داء مقوسات العين عدد المرضى فيها 42 مريضا شكلوا نسبة 84% و14 مريضا من مجموعة التهابات العنبية Uveitis شكلوا نسبة 31.1% ومجموعة السيطرة التي سجلت 35 حالة موجبة للمقوسة الكوندية شكلت نسبة 41.7% وسميت بمجموعة داء المقوسات عديمة الاعراض Asymptomatic Toxoplasmosis وبفارق معنوي عند احتمالية ($p<0.01$)بين المجاميع الثلاثة ، بلغ اعلى معدل الضد IgGلدى مجموعة داء مقوسات العين 1.661 ± 0.187 وحدة عالمية /مل وكذلك الحال للضد IgMالذي بلغ معدله فيها1.922±0.510 وحدة عالمية /مل. وعند تطبيق تفاعل إنزيم البلمرة المتسلسل في الوقت الحقيقيسجلت 14نتيجة موجبة لمجموعة مرضى داء مقوسات العين وبنسبة 33.3 % مقابل 7 نتائج موجبة فقط لمجموعتي التهابات العنبية وداء المقوسات عديمة الاعراض شكلوا نسبتي 50 % و 20% على التوالي ، مع عدم تسجيل فروقات معنوية بينالمجاميع ($p<0.107$) ،نجح هذا الاختبار من تشخيص تواجد طفيلي المقوسة الكوندية لدى مختلف المجاميع بالرغم من اغلب الاصابات كانت مزمنة chronic وبنسب قليلة مقارنة مع اختبار الاليزا الذي سجل ايجابية عالية في تشخيص الاصابة.

الكلمات المفتاحية: داء مقوسات العين، التشخيص ، IgG،IgM،تفاعل انزيم البلمرة المتسلسل في الوقت الحقيقي

.

Introduction

Toxoplasmosis a disease resulting from infection by the protozoan *Toxoplasma gondii*, which infects, both humans and warm-blooded animals as a zoonotic pathogen a worldwide distribution (1,2). Approximately one-third of all humanity has been exposed to this parasite and this disease is listed as the third biggest cause of life threating food borne disease (3). *T. gondii* has a complex life cycle that includes an asexual and sexual cycles , the asexual cycle occurs in a wide range of intermediate hosts and the sexual cycleoccurs exclusively in feline hosts, which shed infectious oocysts in their feces(4).There are three major ways of transmission 1: consuming food or water containing oocyst 2: eating undercooked meats containing tissue cysts and 3: transmission via placenta (1).In humans, *Toxoplasma* infections are widespread and can lead to severe disease in individuals with an immature or suppressed immune system, (2,4).

Ocular toxoplasmosis (O.T.) or, more precisely, toxoplasmic retinochoroiditis is the most frequent cause of infectious blindness andvisual morbidityamongst young adults in developed countries and it's associated with both congenital and acquired infections (5,6). O.T. is characterized by necrotizing retinopathy, which is triggered by the activation of dormant organisms within the retina (5). Active lesions that are accompanied by a severe vitreous inflammatory reaction will have the classic "head light in the fog" appearance. It's the main cause of posterior uveitis and can cause serious sequelae including complete loss of vision (6,7).

Clinical ophthalmological findings together with positive anti – *T. gondii* serology provide sufficient information on which to base a diagnosis (8).Cell culture of intraocular fluids is particularly intensitive when any a small amount of materials is available but it may take days to weeks to obtain a result. PCR detects the DNAs of microorganisms and is a rapid method which has been used to detect *T. gondii* in different biological samples (9).The aim of the present work was to detect toxoplasmic DNA on peripheral blood of patients with ocular toxoplasmosis.

Materials and Methods

The current study was conductedon95 patients whose underwent to the retina unit at Ibn Al- Haitham hospital of eyes in Baghdad, Iraq, from March to September 2013. All patients were clinically diagnosed by physician using slit-lamp bio microscopy device and binocular ophthalmoscopy with the expansion of the iris maximum mydriasis. Healthy eighty four subjects were considering as control group. Age ranged from 10 to 70 in patients and control groups. Five ml of venous blood were drawn from patients and healthy individuals , each sample was divided in two tubes , the first one contain 3 ml of blood for immunological diagnosis (ELISA) and the second one contain 2 ml blood which placed in sterilized EDTA tube for molecular diagnosis.

The sera of all cases were tested for the presence of specific IgM and IgG anti- *Toxoplasma* antibodies via ELISA kits (Bio check diagnostics company, USA)according to the manufacturer's instructions.

Isolation of genomic DNA from whole blood / DNA was extracted from the whole blood samples of the study groups using a commercial purification system(*AccuPrep*® Genomic DNA Extraction Kit, Bioneer , Korea) following themanufacture's instruction for DNA purification from blood. For Real-Time PCR assay, commercial quality quantitative detection of DNA parasite *Toxoplasma gondii* (AccuPower® TG Real - Time PCR Kit) from the production of Korean company Bioneer was used (Table 1).

Table (1): Special components of Real-Time PCR kit.

Component	Quantity
TG PCR Premix (primers,probes , DNA polymerase, dNTPS, salts)	8- well strip x 12 ea
TG Positive Control (PC) DNA	15 µl / tube x 2 strips (Natural)
Internal Positive Control (IPC) DNA	15 µl / tube x 2 strips (Yellow)
DEPC DW (No Template Control,NTC)	15 µl / tube x 2 strips (Purple)
DEPC DW	1800 µl / tube x 4 ea

SL buffer	1800 µl / tube x 4 ea
Optical Sealing film	1 ea

The TG PCR Premix mix was prepared for each sample according to company instruction as following table (2).

Table (2): Components of TG PCR Premix mix.

Component	Volume
TG PCR Premix	Number of tubes
Internal Positive Control (IPC) DNA	1µl
DEPC DW	44µl
Genomic DNA template	5µl
Total volume	**50µl**

Then tubes placed Exispin vortex centrifuge at 2500 rpm for 5 minutes, after that transferred into Exicycler™ 96 Real-Time PCR and applied the following thermo cycler conditions as the following table (3).

Table (3): Thermo cycler conditions.

Step	Function	Temperature	Time (hh:mm:ss)	Repeat
1	INCUBATE	95.00	0:5:0	0
2	INCUBATE	95.00	0:0:5	0
3	INCUBATE	55.00	0:0:5	0
4	SCAN			0
5	GOTO	Step2		45
6	INCUBATE	25.00	0:1:0	0
7	End			

Statistical analyses were computer assisted using the Statistical Package Statistical Package for Science SPSS version 2010, and included the following statistical tests: Descriptive statistical tables: Mean, Standard Error, Standard Deviation, 95%Confidence Interval of the Mean and Contingency Coefficient (C.C.) by $P>0.05$ and $P<0.01$ was considered statistically significant.

Results

In the present study, 50 samples of sera from patients with ocular toxoplasmosis, 45 samples from uveitis and 84 samples was consider as a control group , were tested by ELISA specific IgM and IgG antibodies for T.gondii and by Real-Time PCR technique. As shown in table (1), positive and negative results were recorded, positive IgM and IgG in O.T. group was 42(84%) , while in uveitis 14(31.1%) and 35(41.7%) for control .Negative ELISA IgM and IgG, distributed as 8 (16%) for O.T. group, 31(68.9%) for uveitis and 49(58.3%) for control group. According to ELISA test the groups was renamed as shown in tables two and three. The cut – off value of positive IgM and IgG was 1.00 IU/ml., this point used to differentiate positive results from negative results.

Table (2) showed results of the level of IgG antibody in all studied groups. Higher results was recorded in O.T. group 1.661 ± 0.187 I.U./ml., followed by positive uveitisgroup1.596 ± 0.157 I.U./ml. and Asymptomatic toxoplasmosis group withvalue1.501 ± 0.257I.U./ml. while other groups presented low results of this antibody (Table 2), this table explained also the lower and upper limit of IgG level in all groups.

Levels of IgM antibody was detected in this study (Table 3). Patient of Ocular toxoplasmosis group recorded higher level of IgM in a value 1.922 ± 0.510 I.U./ml. followed by positive Uveitis group1.867 ± 0.061 I.U./ml., and finally Asymptomatic toxoplasmosis group which recorded 1.744 ± 0.070 I.U./ml., these patients were had acute toxoplasmosis,5.While negative results for all groups was represented in this table also. Table (3) shown lower and upper limit of IgM antibody in all studied groups. Some pathological effects of T. gondii infection in eyes of O.T. patients was documented in images (Figure 2,3).

Besides the serological diagnosis of O.T. Real-Time PCR technique was used to confirm the infection with T. gondii by detection of T. gondii DNA in the blood samples of patients and

control, the study revealed that out of 42 patients with O.T. only 14(33.3%) showed positive results by R.T.-PCR technique while 7(50%) and 7(20%) for positive uveitis and Asymptomatic toxoplasmosis respectively (Table 4, Fig.3). Statistically, there was no significant differences between them ($p<0.05$).

Discussion

Ocular Toxoplasmosis is a major cause of posterior uveitis worldwide but its incidence and prevalence are difficult to evaluate precisely (6).The diagnosis is usually based on ophthalmological examination showing unilateral, whitish, fuzzy-edged, round, and focal lesions surrounded by retinal edema (7). Laboratory diagnosis is based on the detected of antibody profiles in ocular fluid or in serum samples but it has many limitation(8,9,10).The results of the present study showed the presence of IgM and IgG antibodies in the sera of all studied groups with some variations (Table 1,2,3) but IgG antibody was detected in all groups with high percentages especially in patients with O.T. 83.33% and 85.71% in positive uveitis and Asymptomatic toxoplasmosis groups respectively, this finding referred that immunoglobulin G was the major class involved in the humoral immune response to against the T. gondii parasite, this is similar to the findings ofAl-Azawi et al.(11) and Al-Hakeem(12) which found the presence of IgG antibody was higher.

The detection of specific IgM antibodies has been the most frequently used serological marker for diagnosing recent toxoplasmosis (13). In current study the presence of specific IgM antibodies was low in all groups. Only 7 cases have positive results in O.T. group, 2 cases in positive uveitis group and 5 cases in control group. Other studies recorded this low rate also, Ronday et al.(14) detected only one case of IgM, Ongkosuwito *et al*.(15) diagnosed a rate 8% of positive IgM from 24 patients of ocular toxoplasmosis, Al-Azawi *et al.*(11) recorded a percentage 4.8% of positive IgM from 42patients of Toxoplasmicchorio retinitis, and this was similar to the results of the present study.

The real-time PCR, has grown considerably over recent years, the technique had proven to be useful for the early and accurate diagnosis of toxoplasmosis and for guiding pre-emptive therapy in patients at high

risk of developing invasive disease(16). Peripheral blood samples originated from patients that gave positive results for specific IgG and IgM toxoplasmosis were analyzed by rael-time PCR. The results showed few patients were positive for Toxoplasma parasitemia on blood samples (Table 4), only 33.3%, 50% and 28% percentages for O.T., uveitis and asymptomatic toxoplasmosis groups respectively. These results were in agreement with Cardona e t al. (17) that found 18.18% (4/22) of cases with cerebral toxoplasmosis were positive by R.T. PCR and concluded that, real-time PCR on peripheral blood samples was not useful for diagnosis of cerebral toxoplasmosis. In the study of Bouet al.(18) they found a positive PCR result was obtained with the blood from 8 of 15 (53.3%) patients with the diagnosis of ocular toxoplasmosis . Similar finding have been reported by Dupouy – Cametet al.(19). Moreover other studies (20,21,22,23) showed sensitivity values of tests with blood , 10 to 35% . Fekkar et al.(24) obtained only 8% of T. gondii detection on blood for diagnosis of ocular toxoplasmosis by PCR , and considered that PCR detection of T.gondii DNA in blood samples cannot be a sufficient tool for the diagnosis of ocular toxoplasmosis , and these similar to the results of this study. The low percentage of diagnosis may be explained that ocular toxoplasmosis is considered a local event in eye (25) and there is no in significant systematic parasitemia, instead most probably there exists a local reactivation (26), and most of patients were during the chronic phase of infection. In the present study *T.gondii* DNA in the blood of some patients of uveitis and asymptomatic toxoplasmosis groups were detected (Table 4). In order to explain this result, it is possible that a small number of parasites might be released from tissues into the blood at subclinical level, and their presence can be detected by PCR as low- level immunosuppressive states (18).

References

1- Robert- Gangenux, F. and Dardé, M. L. (2012). Epidemiology of and Diagnostic Strategies for Toxoplasmosis. Clin. Microbiol. Rev., 25(2):264-296.

2- Rosso, F.; Les, J.T.; Agudelo, A.; Villalobos, C.; Chaves, J.A.; Tunubala,G.A.; Messa, A.; Remington, J.S. and

Montoya, J.G. (2008). Prevalence of infection with *Toxoplasma gondii* among pregnant women in Cali, Colombia, South America. Am. J. Trop. Med. Hyg.,78(3):504–508.

3- Herrmann, D.C.; Pantchev, N.;GlobokarVrhovec, M.; Barutzki, D.; Wilking, H.; Frhlich, A.; Lüder, C.G.K.; Conraths, F.J. and Schares, G.(2010). Atypical*Toxoplasma gondii* genotypes identified in oocysts shed by cats in Germany. Int. J. Parasitol., 40: 285–292.

4- Sullivan Jr,W.J. and Jeffers,V. (2012). Mechanisms of *Toxoplasma gondii*persistence and latency. F.E.M.S. Microbiol. Rev. , 36: 717–733.

5- Holland, G. N. (2003). Ocular toxoplasmosis: a global reassessment. Part I: epidemiology and course of disease. Am. J. Ophthalmol., 136: 973-988.

6- Peterson, E.; Kiljsh, A. and Stanford, M. (2012). Epidemiology of ocular toxoplasmosis. Ocul. Immunol. Inflamm., 20(2): 68-75.

7- Butler, N. J.; Furtado, J. M.; Winthrop, K. L. and Smith, J. R. (2013). Ocular toxoplasmosis II: clinical features, pathology and management. Clin. Exp. Ophthalmol., 41(1): 95-108.

8- Weiss, L. M. and Kim, K. (2007). *Toxoplasma gondii* the model apicomplexan: perspectives and methods, Elsevier, Amsterdam: 777 pp.

9-Talabani, H.; Asseraf, M.; Year, H.; Delair, E.; Ancelle, T.; Thulliez, P.; Bre`zin, A. P. and Dupouy-Camet, J. (2009). Contributions of immunoblotting, real-time PCR, and the Goldmann-Witmer coefficient to diagnosis of atypical toxoplasmic retinochoroiditis. J. Clin. Microbiol., 47: 2131-2135.

10-Garweg, J. G.; De Groot-Mijnes, J. D. F. and Montoya, J. G. (2011). Diagnostic approach to ocular toxoplasmosis. Ocul. Immunol. Inflamm., 19(4): 255-261.

11-Al-Azawi, A. K. A.; Al-Rawe, I. H. A. and Al-Bayati, R. Y. J. (2013). Sero-prevalance of toxoplasmic chorioretinitis in

Baghdad province. Int. J. Sci. Nat., 4(1): 68-71.

12-Al-Hakeem, A.F.S. 2015).Prevalence of Ocular Toxoplasmosis and Evaluation of Some Immune Status Aspects in Samples of Iraqi Patients. M.Sc. Thesis, Coll.Edu. Pure Sci.(Ibn al- Haitham),Univ. Baghdad:146pp. (In Arabic).

13- Balsari, A.; Poli, G.; Molina, V.; Dovis, M.; Petruzzelli, E.; Boniolo, A. and Rolleri, E. (1980). ELISA for *Toxoplasma* antibody detection: a comparison with other serodiagnostic tests. J. Clin. Pathol., 33(7): 640-643.

14-Ronday, M.J.; Ongkosuwito, J.V.; Rothova, A. & Kijlstra, A. (1999). Intraocular anti-*Toxoplasma gondii* IgA antibody production in patients with ocular toxoplasmosis. Am. J. Ophthalmol., 127(3):294-300.

15-Ongkosuwito, J.V.; Bosch-Driessen, E.H.; Kijlstra, A. & Rothova, A. (1999).Serologic evaluation of patients with primary and recurrent ocular toxoplasmosis for evidence of recent infection. Am. J. Ophthalmol.,128:407-412.

16- Martino,R.; Bretagne, S.;Einsele, H. ; Maertens, J.; Ullmann, A. J. & Parody, R.(2005). Early detection of *Toxoplasma* infection by molecular monitoring of *Toxoplasma gondii* in peripheral blood samples after allogeneic stem cell transplantation. Clin. Infect.Dis., 40: 67–78.

17- Cardona,N.; Basto,N.; Parra,B.; Zea,A.F.; Pardo,C.A.; Bonelo,A. &G´omez-Marin, J.E.(2011).Detection of *Toxoplasma* DNA in the Peripheral Blood of HIV-Positive Patients with Neuro-opportunistic Infections by a Real-Time PCR Assay. J. Neuroparasitology. 2: 1-6.

18-Bou,G. ; Figueroa,M.S. ; Marti´-Belda, P. ;Navas,E.and Guerrero, A.(1999).Value of PCR for Detection of *Toxoplasma gondii*in AqueouHumor and Blood Samples from Immunocompetent Patientswith Ocular Toxoplasmosis. J. Clin. Microbiol.,37: 3465-68.

19- Dupouy-Camet, J. ; de Souza, S. L.;Maslo, C.;Paugam, A. ;Saimot, A.;Benarous, R. ;Tourte-Schaefer,

C.&Derouin, F.(1993). Detection of *Toxoplasma gondii* in venous blood from AIDS patients by polymerase chain reaction. J. Clin. Microbiol.,31:1866-1869.

20-Dupon, M. ; Cazenave, J.; Pellegrin, J. L.;Ragnaud, J. M. ;Cheyrou, A. ; Fischer, I.; Leng, B. & Lacut, J. Y.(1995). Detection of *Toxoplasma gondii* by PCR and tissue culture in cerebrospinal fluid and blood of human immunodeficiency virus-seropositive patients. J. Clin. Microbiol., 33:2421-2426.

21-Filice, G. A. ;Hitt, J. A. ; Mitchell, C. D. ;Blackstad, M. & Sorensen, S. W.(1993). Diagnosis of toxoplasma parasitemia in patients with AIDS by gene detection after amplification with polymerase chain reaction. J.Clin.Microbiol.,31:2327-2331.

22- Franzen, C. ;Altfeld, M.;Hegener, P.; Hartmann, P.; Arendt, G. ;Jablonowski, H.;Rockstroh, J.; Diehl, V.; Salzberger, B. & Fatkenheuer, G.(1997). Limited value of PCR for detection of *Toxoplasma gondii* in blood from human immunodeficiency virus-infected patients. J. Clin.Microbiol. ,35:2639-2641.

23-Guy, E. C. &Joynson, D. H.(1995). Potential of the polymerase chain reaction in the diagnosis of active Toxoplasma infection by detection of parasite in blood. J. Infect. Dis.,*172:319*-322.

24-Fekkar, A.; Bodaghi, B.; Touafek, F.; Le Hoang, P.; Mazier, D. & Paris, L.(2008). Comparison of immunoblotting, calculation of the Goldmann-Witmer coefficient, and real-time PCR using aqueous humor samples for diagnosis of ocular toxoplasmosis. J. Clin. Microbiol., 46: 1965-1967.

25-Contini, C.; Seraceni, S. ;Cultrera, R.; Incorvaia, C.; Sebastiani, A. & Picot, S. (2005). Evaluation of a Real-time PCR-based assay using the light cycler system for detection of *Toxoplasma gondii* bradyzoite genes in blood specimens from patients with toxoplasmic retinochoroiditis. Int. J. Parasitol., 35:275-283.

26-Silveira, C.;Vallochi, A. L. ; Rodrigues da Silva, U.; Muccioli, C.; Holland, G. N. ; Nussenblatt, R. B. ; Belfort, R. & Rizzo, L. V. (2011). *Toxoplasma gondii* in the peripheral blood of patients with acute and chronic toxoplasmosis. Br. J. Ophthalmol., 95:396-400.

Table: (1) The ELISA assay and percentages for all the study groups.

Groups	No. and Percent	ELISA Result		Total	C.C.& P-value
		Positive	Negative		
O.T.	No.	42	8	50	C.C. = 0.389 P=0.000 H.S.
	%	84	16	100	
Uveitis	No.	14	31	45	
	%	31.1	68.9	100	
Control	No.	35	49	84	
	%	41.7	58.3	100	
Total	No.	91	88	179	
	%	50.8	49.2	100	

H.S.: Highly Significant at P< 0.01

Table(2): Levels of IgG antibody by IU/ml for all study groups.

Groups	The Total No. of Samples	No. of Positive Samples	Mean	Standard Deviation	Standard Error	%95Confidence Interval for Mean		Lower Value	Upper Value
						Lower Bound	Upper Bound		
O.T.	42	35	1.661	0.187	0.032	1.597	1.7	1.319	2.143
Uveitis +	14	12	1.596	0.157	0.045	1.496	1.7	1.344	1.831
Uveitis -	31	-	0.389	0.19	0.034	0.319	0.5	0.123	0.702
Asymptomatic Toxoplasmosis	35	30	1.501	0.257	0.047	1.405	1.6	1.184	1.897
Control	49	-	0.35	0.167	0.024	0.302	0.4	0.122	0.712

Table(3): Levels ofIgMantibody by IU/ml for all studygroups.

Groups	The Total No. of Samples	No. of Positive Samples	Mean	Std. Dev.	Std. Error	%95 Confidence Interval forMean		Lower Value	Upper Value
						Lower Bound	UpperBound		
O.T.	42	7	1.922	0.51	0.193	1.45	2.4	1.472	2.658
Uveitis +	14	2	1.867	0.061	0.043	1.321	2.4	1.824	1.91
Uveitis -	31	-	0.632	0.166	0.03	0.571	0.5	0.306	0.768
Asymptomatic Toxoplasmosis	35	5	1.744	0.07	0.031	1.657	1.8	1.679	1.858
Control	49	-	0.618	0.236	0.034	0.55	0.7	0.238	0.762

Table(4): Results of Real - time PCR test and percentagesforpositiveELISAstudy groups.

Groups	No. and Percent	Real-timePCRResult		Total	C.C.& P-value
		Positive	Negative		
O.T.	No.	14	28	42	C.C. = 0.216 P=0.107 NS
	%	33.3	66.7	100	
Uveitis +	No.	7	7	14	
	%	50	50	100	
Asymptomatic Toxoplasmosis	No.	7	28	35	
	%	20	80	100	
Total	No.	28	63	91	
	%	30.8	69.2	100	

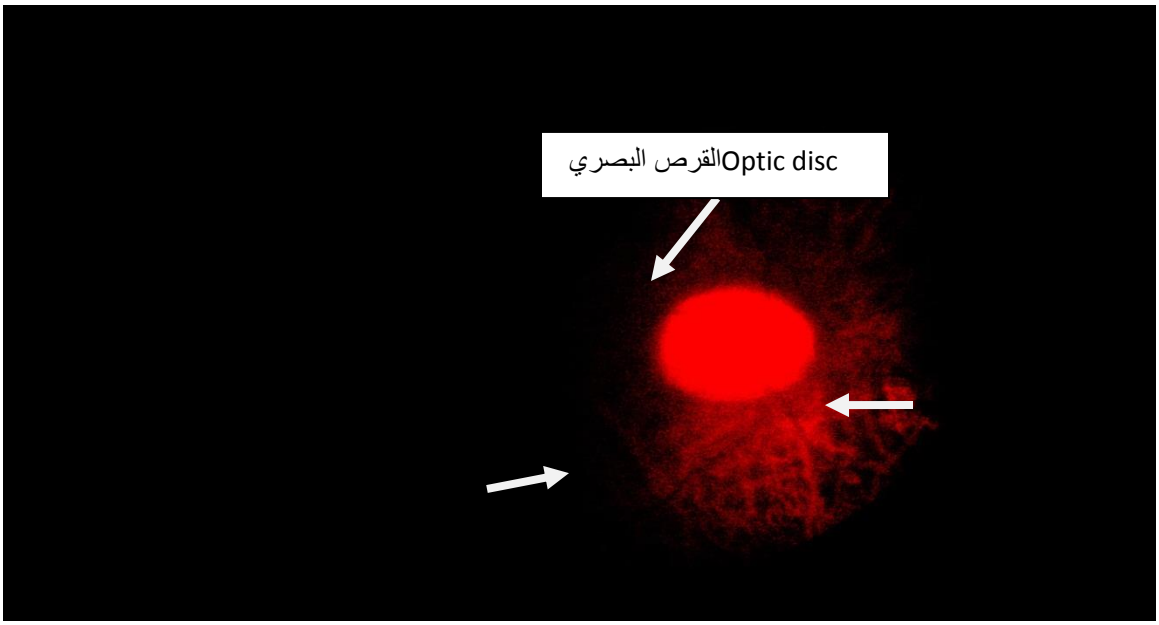

Figure(1): Scar diffused in the retinaas a result of OcularToxoplasmosisinfection.

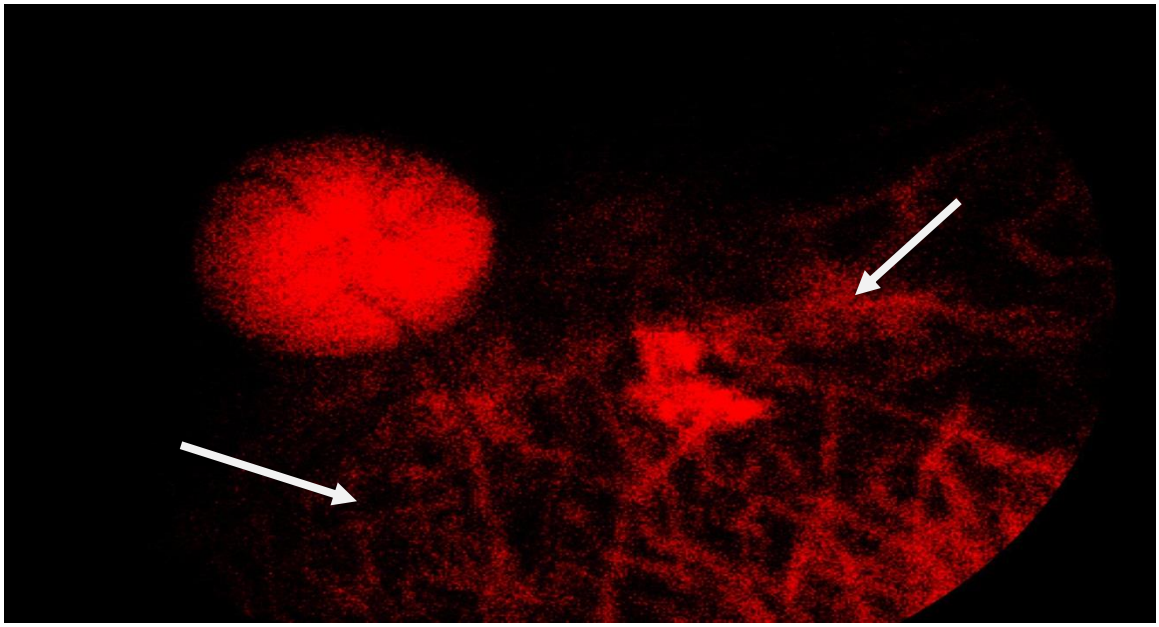

Figure(2): The spread ofmanyscares inthe retinadue tochronicOcular Toxoplasmosisinfection.

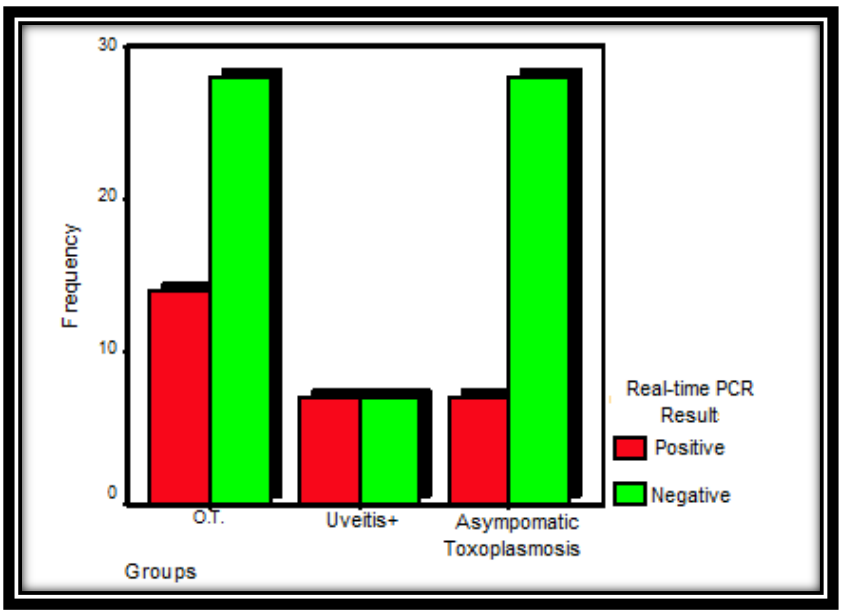

Figure(3): graphictapesfor the distribution offrequencies in accordance with thepercentageReal-time PCRtest for positiveELISAstudy groups.

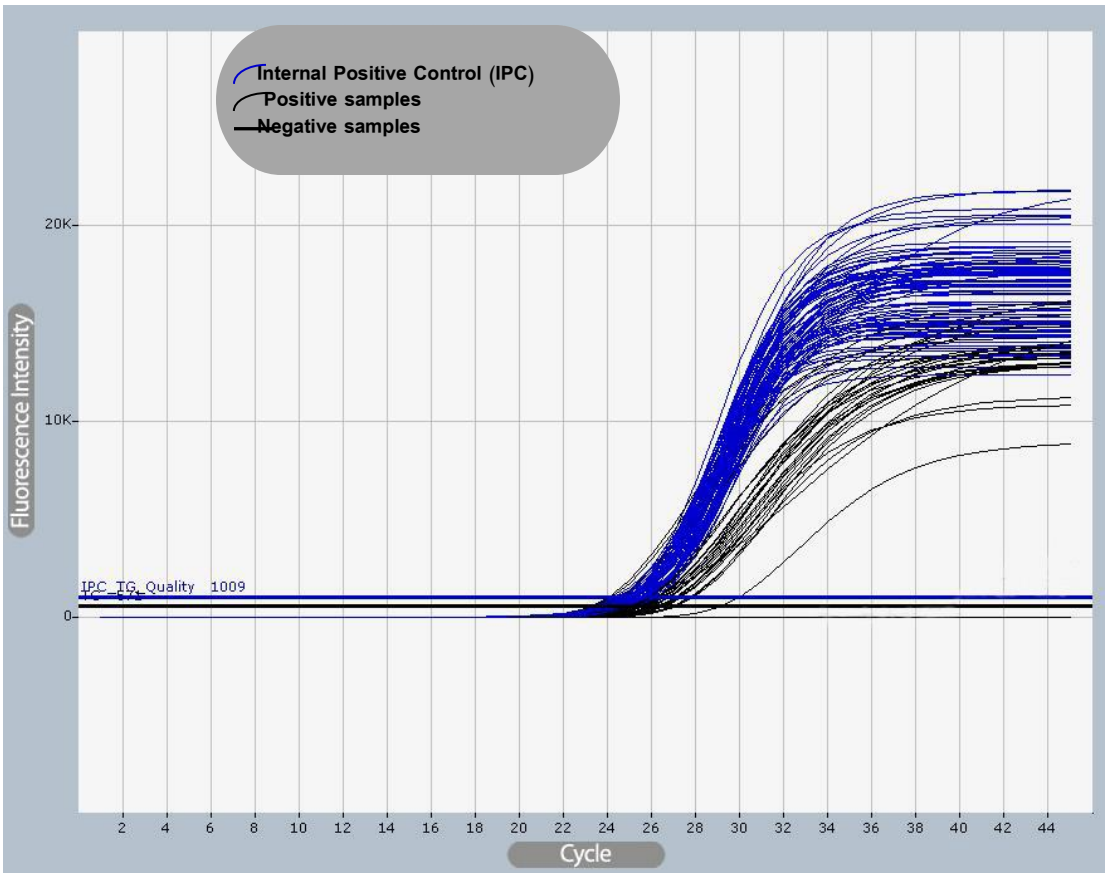

Figure (4): The results of Real time PCR reaction for positive ELISA study groups.

Efficient Text Message Hidden Technique Using YIQ Model

Ali Nasser Hussain[a, #], Entidhar Mhawes Zghair[b, *]

[a]*College of Electrical Engineering Techniques, Middle Technical University, Baghdad, Iraq*
[b]*Technical Instructors Training Institute, Middle Technical University, Baghdad, Iraq*

[#]*E-mail:* alinasser1974@yahoo.com, [*]*E-mail*: ent_mz2005@yahoo.com

Abstract

This paper produces and investigates the steganography technique of information hiding in communication system by using other information to provide major security. Nowadays, the security in the information transferring plays a vital role due to data protection importance. Therefore, the traditional techniques by using invisible ink or hidden tattoos need to developed and compensate under digital processing. Hence, Red (R), Green (G) and Blue (B) plans (RGB) approach is activated to improve the proposed scheme. By this technique, the text message converted to binary code as first stage. Then, the binary code is arranged as an image and converted to (YIQ) model as second stage. The final stage is to save the picture and converted to color image to minimize the distortion. Results show high Peak Signal to Noise Ratio (PSNR) and minimum Mean Square Error (MSE) in the extracted picture. The suggested algorithm is a promising technique to enhance the current and future communication security and open new widow to develop this issue.

Keywords: Steganography, Data Hiding, Image Stages, YIQ**.**

فاعلية تقنية اخفاء رسالة نصية يستخدام بنموذج YIQ

الخلاصة:
تقدم هذه الدراسة، البحث في تقنية إخفاء المعلومات بواسطة معلومات أخرى في نظام الاتصالات لتوفير أمن كبير. في الوقت الحاضر،أمن نقل المعلومات يلعب دورا حيوياً بسبب أهمية حماية البيانات. لذلك، التقنيات التقليدية باستخدام حبر غير مرئي أو الوشوم المخفية تحتاج إلى تطويرها والاستعاضة عنها بالطرق الحديثة او ما تدعى بطريقة (B) والأزرق (G)، الأخضر (R)من المعالجات الرقمية. وبالتالي خطط، الأحمر تفعل لتحسين المخطط المقترح. بواسطة هذه التقنية، الرسالة النصية تحول إلى شفرة ثنائية كمرحلة (RGB) كمرحلة ثانية. المرحلة الأخيرة هي (YIQ)أولى. ثم، يتم ترتيب الشفرة الثنائية كصورة وتحويلها الى موديل والنتائج أظهرت أشارة القمة العالية الى نسبة معدل .لحفظ الصورة وتحويلها إلى صورة ملونة لتقليل التشوية في الصورة المستخرجة. الخوارزمية المقترحة هي تقنية (MSE)مع نسبة خطأ طفيفة (PSNR)الضوضاء واعدة لتعزيز أمن الاتصالات الحالية والمستقبلية وفتح نافذة جديدة لتطوير هذه المسألة.

1. Introduction

The digitalization of data transmission in the modern communication processing gave the researchers new open window to develop the security in the send information. Interfere information via internet suffer from unlawfully copy, tamper and intercept. Hence, fast growth in the data security technique was needed to overcome this phenomenon. One of the most important techniques is by using a steganography to hiding the data in the communication channels. The objective of this method is to increase the capacity and security enhancement for traditional message. The Steganographyapproach is typically containing a media conversion into secret data in term of such called storage media [1]. The cryptography, watermarking, and steganography is a different methods which is used to hidden the information via internet channels. Many researchers are contributing in this field as in [2-5]. This paper introduces and investigated a steganography technique only as a major goal. However, the hiding secret data is changed the Least Significant Bit (LSB) of each pixel in the image cover by the bits in the secret information resulting in low distortion. The idea contributed by [6] considers a simple and traditional compared with used demand in current communication complexity.

2. Bit Insertion Strategy

Today, the LSB insertion strategy is the most important method in the steganography data encryption way[7]. In the below message hidden example, one could hide the letter (A) in the first 8-bytes of three pixels in 24-bits image pixel.

(00100111 11101001 11001000)
(00100111 11001000 11101001)
(11001000 00100111 11101001)

A:01000001

Result:

(00100110 11101001 11001000)
(00100110 11001000 11101000)
(11001000 00100111 11101001)

The transformed bits is show as three underlined bit which represent the half message bit in the LSB insertion bit were required. Insignificant difference in the suggested approach permit to insert the message in more LSB for each byte resulting in big information capacity as well. Due to slight change, one could avoid the pixel change too [8,9]. In the case of 24-bit image, every color bit of the red, green and blue components could be used. Subsequently, each color represented by a byte. In this case one could store 3 bits in each pixel. Thus, a 800×600 pixel

image could store a total amount of 1,440,000 bits or 180,000 bytes of fixed information as illustrated in the below example.
The 3 pixels of 24-bit image could be represented as:

(00101101 00011100 11011100)

(10100110 11000100 00001100)

(11010010 10101101 01100011)

The binary representation of (11001000) for the number 200 is embedded into LSB, then the resulting grid written as:

(00101101 00011101 11011100)

(10100110 11000101 00001100)

(11010010 10101100 01100011)

While the first 8 byte in the grid need to change only 3 underlined bits according to fixed message. Then, by using the maximum cover size one can use only half bits from the image for this duty. Subsequently, the 256 possible intensity of each color will change the LSB of pixel to introduce a small change in the colors intensity. Hence, the human eye can't distinguish this changes and the hidden process is successfully established [5].

$R, G, B, Y \in [0, 1][-0.5957, 0.5957]$

$I \in [-0.5957, 0.5957]$

$Q \in [-0.5226, 0.5226]$

$$\begin{bmatrix} R \\ G \\ B \end{bmatrix} = \begin{bmatrix} 1 & 0.9563 & 0.6210 \\ 1 & -0.2721 & -0.6474 \\ 1 & -1.1070 & 1.7046 \end{bmatrix} \begin{bmatrix} Y \\ I \\ Q \end{bmatrix}$$

$$\begin{bmatrix} Y \\ I \\ Q \end{bmatrix} = \begin{bmatrix} 0.299 & 0.587 & 0.114 \\ 0.595716 & -0.274453 & -0.321263 \\ 0.211456 & -0.522591 & 0.311135 \end{bmatrix} \begin{bmatrix} R \\ G \\ B \end{bmatrix}$$

3. YIQ Color

The National Television Systems Committee (NTSC) in United States used YIQ color space due to a great advantage of gray scale information could separate from color data; therefore it's used for both black/white and colors signals. The three components of NTSC color space include Luminance Y, hue I and saturation Q which represent gray and chrominance respectively. The approximation of given formulation between RGB and YIQ as in [11]:

4. Suggested Model

The suggested technique depends on psycho visual redundancy and pixel dependency.
In general, the color image contains 3 different bands in its formed. This color like red, green and blue represent the color coordinate systems. The proposed flow chart of suggested algorithms for basing text message is illustrated in Figure 1.

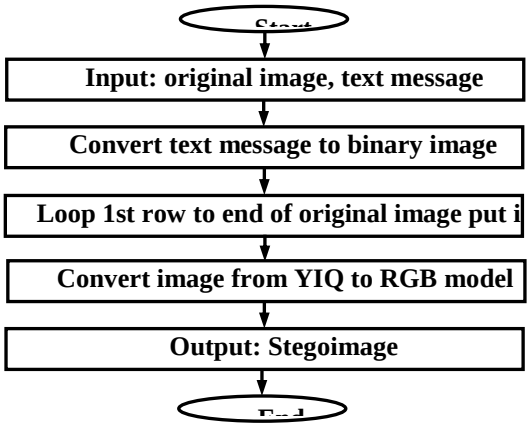

Figure 1: Suggest algorithms flowchart.

The information hiding process in suggested algorithms achieved in R, G and B band. Hence, theMATLAB program version (7.1) has been used to design the proposed algorithms. The first stage is to data hidden passing to Graphical User Interface(GUI) in MATLAB to implement the LSB algorithms. The second stage in this approach is to return back the reverse data in the cover RGB image cover by using GUI interface tool as illustrated below:

Input: RGB color cover image, text message to recover.

Output: Stego RGB color image.

Step 1: Decompose the color image into R, G, and B bands.

Step 2: Decompose each of the R, G, and B band data into binary bit planes.

Step 3: Transfer the covert information into the binary bit stream.

Step 4: Scan each binary bit in first binary image
1^{st}Red band of cover image bit = current pixel in the first binary image.

Step 5: Scan each binary bit in second binary image
1^{st}Green band of cover image bit = current pixel in second binary image.

Step 6: Scan each binary bit in third binary image
1^{st}Blue band of cover image bit = current pixel in third binary image.

Step 7: Save those information generated in steps 4, 5 and 6.

5. Hidden Data Extraction

The extraction of hidden data from original host image could be recreated without data losses as shown below:

Input: Embedded image.

Output: Original RGB color image, 3 Hidden Binary images.

Step 1: Decompose the Embedded image into R, G, and B bands.

Step 2: Decompose each of the R, G, and B band data into binary bit planes.

Step 3: Design temple zeroes matrix:
Temple (size) =original (size)
For each pixel in temple =1st Red band bit of Embedded image.

Step 4: Save temple matrix a first binary image.

Step 5: Implement step3 to step4 for Green band and Blue band.

Step 6: Save this information generated in steps 3, 4 and 5.

6. Results

Different image in size, application and field has been chosen to implement the suggested algorithms as illustrated in Table 1. Figures 2, 3 and Figure 4 show the different steps of implementation process in the suggested model.

Table 1: Groups original cover images size.

Class	Size
A	512×512
B	288×237
C	332×400

Figure 2: Class A covers images.

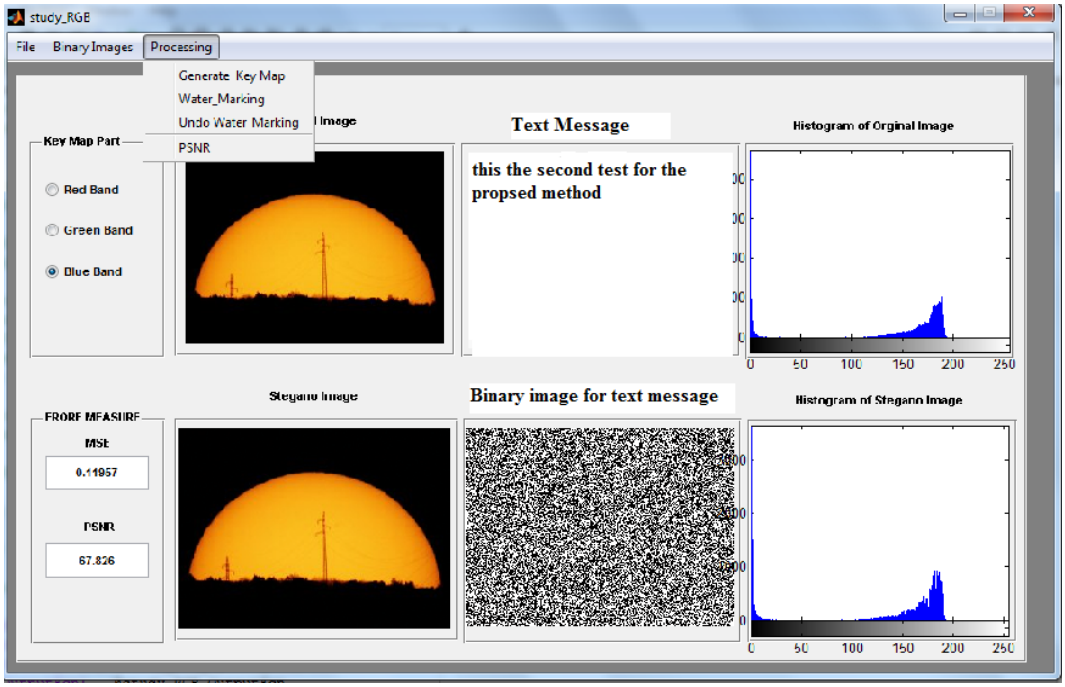

Figure 3: Class B covers images.

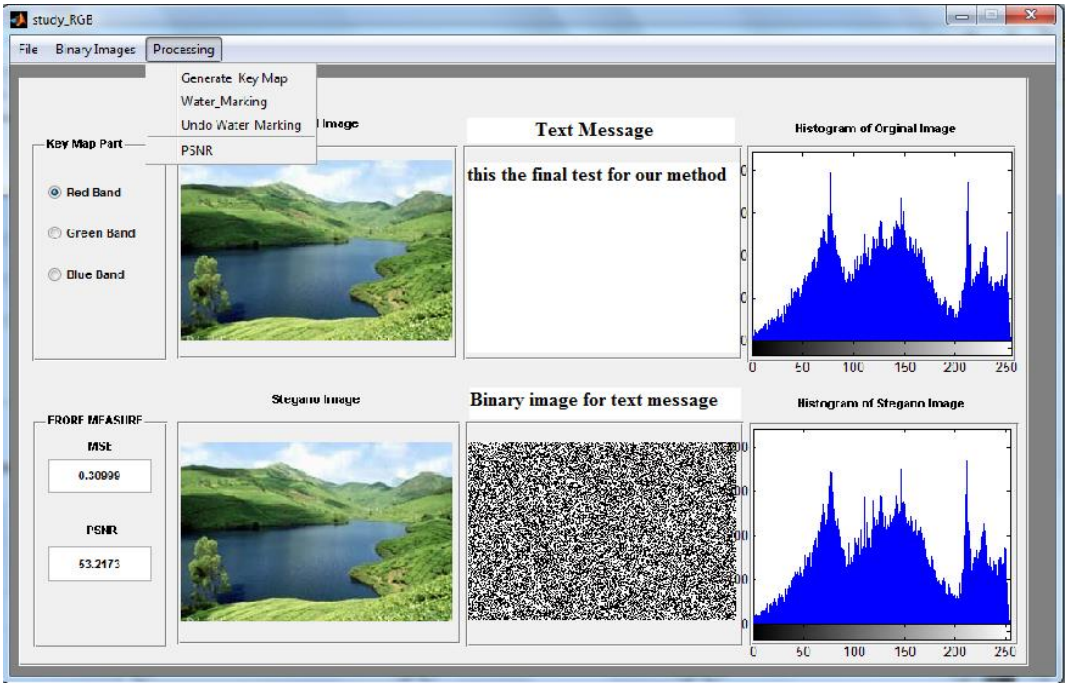

Figure 4: Class C covers images.

To create secret message, the MATLAB is used to implement the hidden image. The measurement of 3 stages image quality has been done using PSNR level. Hence, alarge PSNR level represents small possibility of visual attack in human eyes. The three standard gray scale images in Figure 1, 2 and Figure 3 named Lena, Medical and Famous picture is illustrated as well. The exhibition of all images show the amount of smooth area and complicated area in the image effect which depend on the PSNR capacity inserting. The spreading in all images stage is highlight due to big secret message affected by use LSB in the RGB band techniques which is hidden for human eyes. As clear in all images, the medical image is more complicated than other image due to more edge area and frequent variation. Hence, the capacity is affected more than Lena image as shows in Figure 5, 6 and Figure 7.

The image imperceptibility is shown by PSNR values [3].

$$MSE = \frac{1}{MN}\sum_{i=0}^{M}\sum_{j=0}^{N}(X_{ij} - y_{ij}) \quad (1)$$

$$PSNR(dB) = 10\ log_{10}\left(\frac{1^2}{MSE}\right) \quad (2)$$

Where$X_{ij}$is the i^{th} rows and j^{th} columns of original imagewhiley_{ij} is the i^{th} row and j^{th} column of transformed image. Higher the PSNR value means more difficult to perceive that any hidden message is hidden. In our experimental work we have found that by increasing the payload, the PSNR value drops down. We have to make a compromise between payload and PSNR.

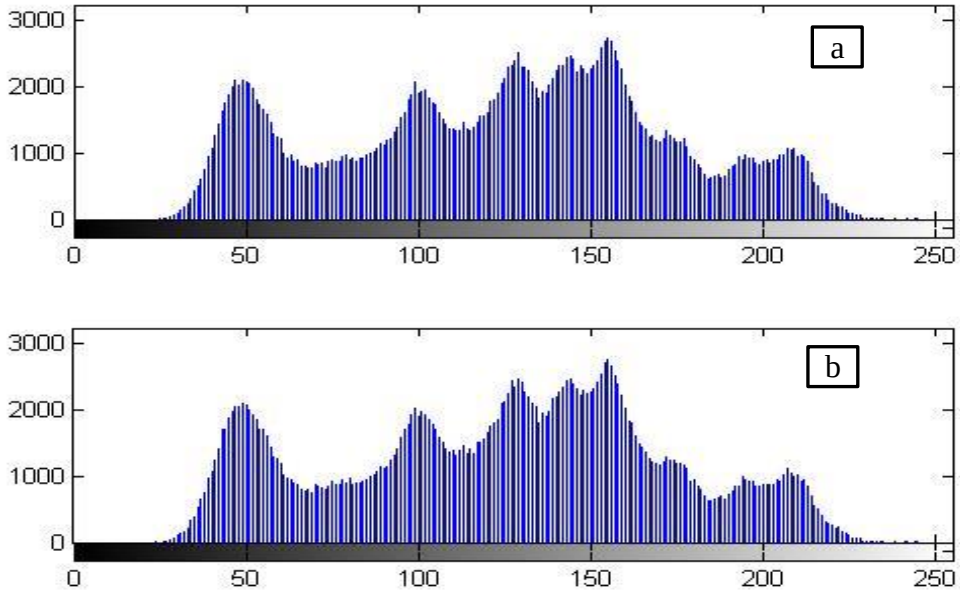

Figure 5: Histogram embedded image of original (a) and hidden (b) forclassA.

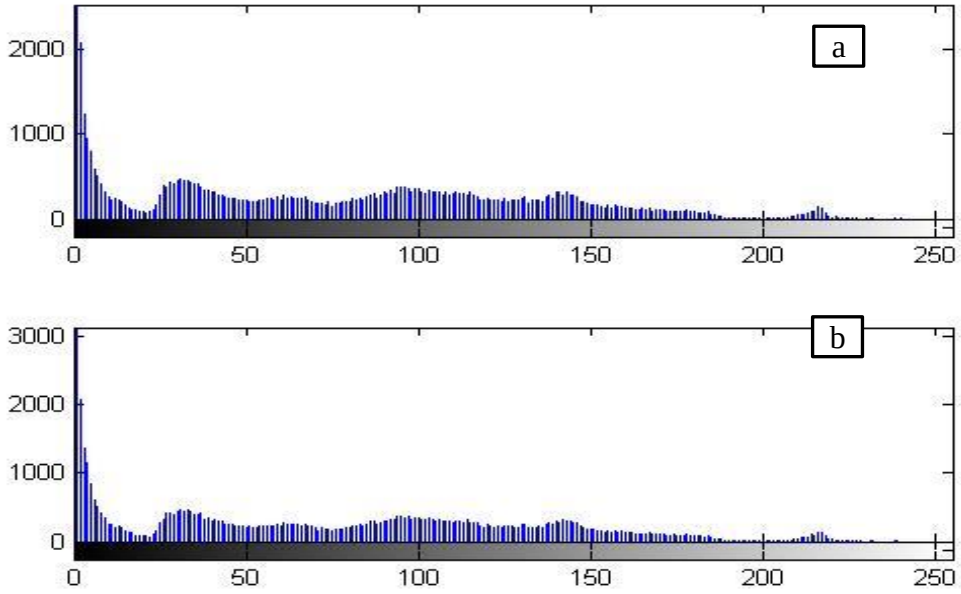

Figure 6: Histogram embedded image of original (a) and hidden (b) forclass B.

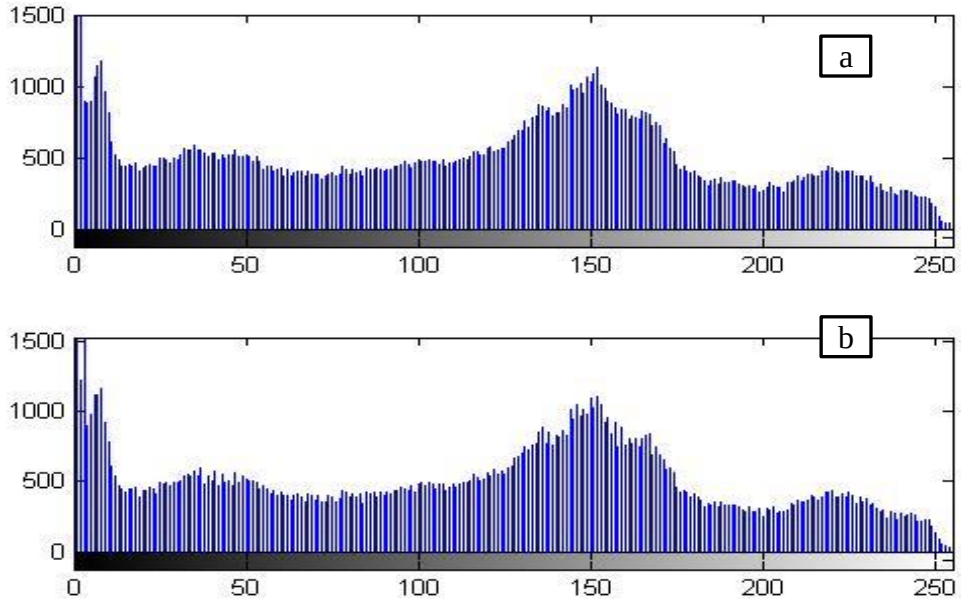

Figure 7: Histogram embedded image of original (a) and hidden (b) forclass C.

Table 2: The average results for each group of colored images.

Class	PSNR(dB)	Maximum Hiding Capacity in (bits)
A	41.1468	786432
B	36.5154	204768
C	41.0449	398400

Figures 5– 7show the results of each group for colored images in graph to help study the results more easily. Table 2shows the average results of each group for colored images. If we change our set of images, the results will change accordingly. The payload values can also be changed by using a different information or content to be Stephen by the proposed method**.**

7. Conclusions

The new technique of watermarking using RGB bandfor all images size is implemented in this paper. The suggested methods provide randomize key map hidden in single channel and two channels in binary and copyright image embedded into original image for more protection and improve the system security. The suggested technique is promising in attack the JPEG compression and noise. The more attractive feature for this proposed method is the ability to use either symmetric key or public key and the verification of original message could be done without hash. This work will support and accelerate the researcher developments in the communication security field.

References

1-Schaathun, H. G. (2012). Machine Learning in Image Steganalysis", *A John Wiley & Sons, Ltd., Publication*, pp. 279.

2-Provos and P. Honeyman, "Hide and Seek: an Introduction to Steganography", *IEEE Security Privacy Magazine*,Vol. 1, No. 3, 2003. pp. 32–42.

3-Rubab, S., Younus,M. (2012). Improved Image Steganography Technique for Colored Images Using Wavelet Transform. *Int. J. Computer Applic.* 39(14): 29–32.

4-Petitcolas, F.A.P., Anderson, R.J., Kuhn, M.G. (2004). Information Hiding a Survey, *Proceedings IEEE*. 87(7): 1062–1078.

5-Kumar, M., Kumar, S., Gupta, N. (2011). Image Steganography Tool Using Adaptive Encoding Approach to Maximize Image Hiding Capacity, *Int. J. Soft Computing Eng*, 1(2): 7–11.

6-Chan, C.K., Chen, L.M. (2004). Hiding Data in Images by Simple LSB

Substitution, *Pattern Recognition*, 37(3): 469–474.

7-Juneja, M., Sandhu, P. (2009). Implementation of Improved Steganographic Technique for 24-bit Bitmap Images in Communication, *Marshland Press J. Am. Sci.*, 5(2): 36–42.

8-Al-Taani ,T. A. and AL-Issa, A. M. (200(). A Novel Steganographic Method for Gray-Level Images, *World Acad. Sci. Eng. Technol.* 27: 613– 618.

9-Johnson, N.F. and Katzenbeisser, S.C." A survey of Steganographic techniques", in S. Katzenbeisser and F. Peticolas (Eds.): Information Hiding, Artech House, Norwood, MA, pp.43–78.

10-Lou,D. C. and Liu,J. L. (2002). Steganography Method for Secure Communications, Elsevier Science on Computers& Security, 21 (5): 449–460.

11-Gonzalez,R.C., Woods,R.E. (2009). Digital Image Processing Using MATLAB", Second Edition.

Optimization of PAPR Reduction Technique for OFDM Signal Based Discrete Multiwavelet Critical-Sampling Transformin MC-CDMA using Selected Mapping with Phase Modification Method

Dr. Mohammed Aboud Kadhim

Middle Technical University,Institute of Technology Baghdad, Iraq

Email: makaboud@gmail.com

Abstract

Multi-carrier code-division multiple access (MC-CDMA) is anextensively known transmission technique for high speed data communication. In MC-CDMA, transmission is performed in parallel on various frequencies. This technique is widely sought after for the transmission of digital data via the media offadding channels. This paper showcases original contribution to the field of “peak-to-average power ratio (PAPR)” reductioneffect by using “Multiwavelet Critical-Sampling Transform (DMWCST)” in the developmental “MC-CDMA systems”. In this study, primarily oriented towards the selected mapping techniques and phase modification was used. As well showcase how selected mapping with phase modification can be applied to mitigate PAPR since they are signal distortionless and their complexity is lesser compared to other techniques.

Keywords: MC-CDMA, OFDM, PAPR, CCDF, DMWCST.

تحسين تقنية تقليل نسبة القدرة العظمى الى القدرة المعدلة لاشارة مقسم التردد العامودي المبني على التحويل المنفصل لمتعدد المويجات العينة الحرجة في تقسيم الرموز لعدة حوامل بتعدد الدخولباستخدام طرق اختيارتقنيات التضمين و تحسين الطور

مدرس دكتور محمد عبود كاظم

الجامعة التقنية الوسطى معهد التكنلوجيا بغداد ـ العراق

الخلاصة

تقسيم الرموز لعدة حوامل بتعدد الدخول (MC-CDMA) هواسلوب معروف على نطاق واسع لنقل البيانات بسرعةعالية. فى MC-CDMA يتم الارسال على التوازى فى مختلف الترددات. هذاالاسلوب على نطاق واسع لنقل البيانات الرقمية عن طريق وسائط نقل وقنوات تلاشي ضعيفة. هذا العمل يعرض اسهامه الاصلى فى مجال تقليل نسبة القدرة العظمى الى القدرة المعدلة لاشارة مقسم التردد العامودىباستخدام نظام التحويل المنفصل لمتعددالمويجات العينة الحرجة في تطوير نظام MC-CDMA .فـهذا العمل، فى المقام الاول الاتجاه نحومرحلة اختيار تقنيات التضمين و تحسين الطور وكيفية تطبيقه لتخفيف PAPRلانتشويه الاشارة اقل و درجة التعقيداقل مقارنة بتقنيات اخرى.

Introduction

Mobile radio communication schemes are required to render high-character multimedia services to mobile users. To cater for same, modern mobile systems are required to strengthen high capacity and changeable bit rate transmission with bandwidth efficiency to safeguard the restricted spectrum resource. Generally, MC-CDMA accumulated a considerable measure of consideration towards future creation of wireless communication. MC-CDMA is a cross breed gathering of two access techniques, "frequency division multiplexing (OFDM)" and "Code Division Multiple Access (CDMA)" which consider advantage of two strategies. Recently, CDMA strategy has been considering as a hopeful that requirements quick and capable information exchange to bolster interactive media administrations, video conferencing and promote applications[1-3]. MC-CDMA and OFDM frameworks are generally utilized as a part of the current third and fourth generation wireless networks. They are excessively perceived candidates for the future era systems for broadband and individual correspondences. In that capacity,"Discrete Multiwavelet Transform (DMWT)" is intended to meet the previously stated need. So this anticipate shows DMWT subordinate orthogonal modulator. But, "Discrete Wavelet Transform (DWT)" have the great properties however it doesn't satisfy the future needs. By actualizing DMWT, it can accomplish sound ghastly proficiency and increases great "bit error rate (BER)" when contrasted with "Fast Fourier Transform (FFT)" and DWT[4]. MC-CDMA system is extensively used for "Long Term Evaluation (LTE)","Worldwide Interoperability for Microwave Access (WiMAX)", and Digital TV transmission [5].It MC-CDMA schemes have inbuilt issue of a high PAPR and also the reason for serious performance degradation in the transmitted signal. One of the key downsides of an OFDM plan is that it has a high crest factor. Brought about by the nonlinearity of a powerful enhancer "high power amplifier (HPA)", the high crest factor component acquires on sign twisting the nonlinear HPA. These further results in the debasement of "bit error rate (BER)".Numerous topic[6-16] has been considered to mitigate the crest factor of the OFDM signals. The alignment for the crest factor reduction can be categorized into two types. First, there are deterministic approaches that keep the limit forthe crest factor of the OFDM signals under a limit level. Clipping and block coding have a place with this write. The second sort is reliant on probabilistic technique. These methodologies factually propel the run of the mill of the crest factor appropriation of the OFDM signals without sign bending. "Selected mapping (SLM)" and "partial transmit sequence (PTS)"[17-20]form part of this type. In the SLM with OFDM system, an arrangement of comparable symbol sequences is delivered from a given information symbol sequence by having the capacity to duplicate with the stage successions. At that point, the one with the crest factor variable in the set is decided for transmission. It is recognized from the reproduction results in various writing[21, 22] that the randomly produced phase sequence set outperforms any other applicants in SLM OFDM scheme. The search issystematized as follows. Section two briefly showcases the proposed modified "MC-CDMA transceiver". Simulation results are rendered in Section three. At last, conclusions are drawn in Section four.

Proposed of Modified MC-CDMA Transceiver

Block diagram of Modified MC-CDMA Transceiver as shown Figure 1.In selective

mapping, parallel data symbols are multiplied by the phase sequences before the procedure computation of "Invers Multiwavelet Critical-Sampling Transform (IDMWCST)" in [23]. Thereafter, symbol sequence with the lesser PAPR is picked upand transmitted. The multiwavelet two scale equations mirrors those for scalar wavelets [24]:

$$\Phi(t) = \sqrt{2} \sum_{k=-\infty}^{\infty} \mathrm{H_k}\, \Phi(2\mathrm{t} - \mathrm{k}), \qquad (1)$$

$$\psi(t) = \sqrt{2} \sum_{k=-\infty}^{\infty} \mathrm{G_k}\, \Phi(2\mathrm{t} - \mathrm{k}) \qquad (2)$$

Albiet,$H_k$andG_k, and are *matrix* filters (i.e.,$H_k$and G_k *are* $n \times n$ matrices in place of scalars).
In order to pull back the source data at the receiver, information is needed forchannel exemplification of the block of source data to be transmitted. Alongside, this information is transmitted apart, and is called out as side information.
Figure 1 showcases the functional block diagram of MC-CDMA scheme with phase modification. The complex-valued data symbol$S(k)$ is multiplied alongwith user specific spreading code $C^{(k)} = \left(C_0^{(k)}, C_0^{(k)}, \dots C_{V-1}^{(k)}\right)^T$ of spreading factor *V*. The complex-valued sequence sought after spreading is rendered in vector notations as,$n(k) = S(k)C(k) = \left(N_0^{(k)}, N_0^{(k)}, \dots N_{V-1}^{(k)}\right)^T$.A multi-carrier spread spectrum signal is considered after modulating the components$N_v^{(k)}, v = 0, \dots, V-1$, in parallel onto *V* sub-carriers. Let us consider for now that *K* users are supremely transmitting data. The spread data symbols of *K* users are summed, and then input to the IDMWCST of size *Z=1xV*. The signal for MC-CDMA symbol, $0 \le t \le T$is showcased as

$$m(t) = \frac{1}{\sqrt{2D_r}} \sum_{d=0}^{2^D-1} \sum_{t=1}^{T} \sum_{k=1}^{K} S(k)\, C_v(k) \phi_{d,t} \qquad 0 \le t \le T \qquad (3)$$

Hereby,*m*[*n*] relies on the selected phase-shifted signal. The optimization problem which we are intending to resolve is to minimize the PAPR. The PAPR is used as the objective phase modification of the optimization problem; so;where: *T* is the data duration, the PAPR of the transmitted signal in (1) can be written as:

$$PAPR = \frac{max|m(t)|^2}{E[|m(t)|^2]} (4)$$

Where $max|m(t)|^2$signifies the peak power and $E[|m(t)|^2]$ means the average power. Further, E [.] denotes expectation and complementary cumulative distribution function for MC-CDMA signal can be written as "Complementary Cumulative Distribution Function (CCDF)" = probability (PAPR> P0), where P0 is the Threshold [12]. PAPR of MC-CDMA signal is mathematically definite as

$$PAPR = 10log_{10} \frac{max|m(t)|^2}{\frac{1}{T}\int_0^T |m(t)|^2\, dt} \quad dB \qquad (5)$$

It further guides the above equation by decreasing the numerator $max|m(t)|^2$ or increasing the denominator $E|m(t)|^2$or both.If the number of subcarriers becomes large, the PAPR of transmitted signal becomes large and as such the signal is distorted by the nonlinear amplifer. To decrease the nonlinear distortion of nonlinear amplifer, we need to decrease the PAPR of transmit signal. When $0 \leq \Theta_i \leq 2\pi$, the resultant baseband transmission is stated as:

$$S^{(n)}[p] = m(t)e^{j\Theta_i} (6)$$

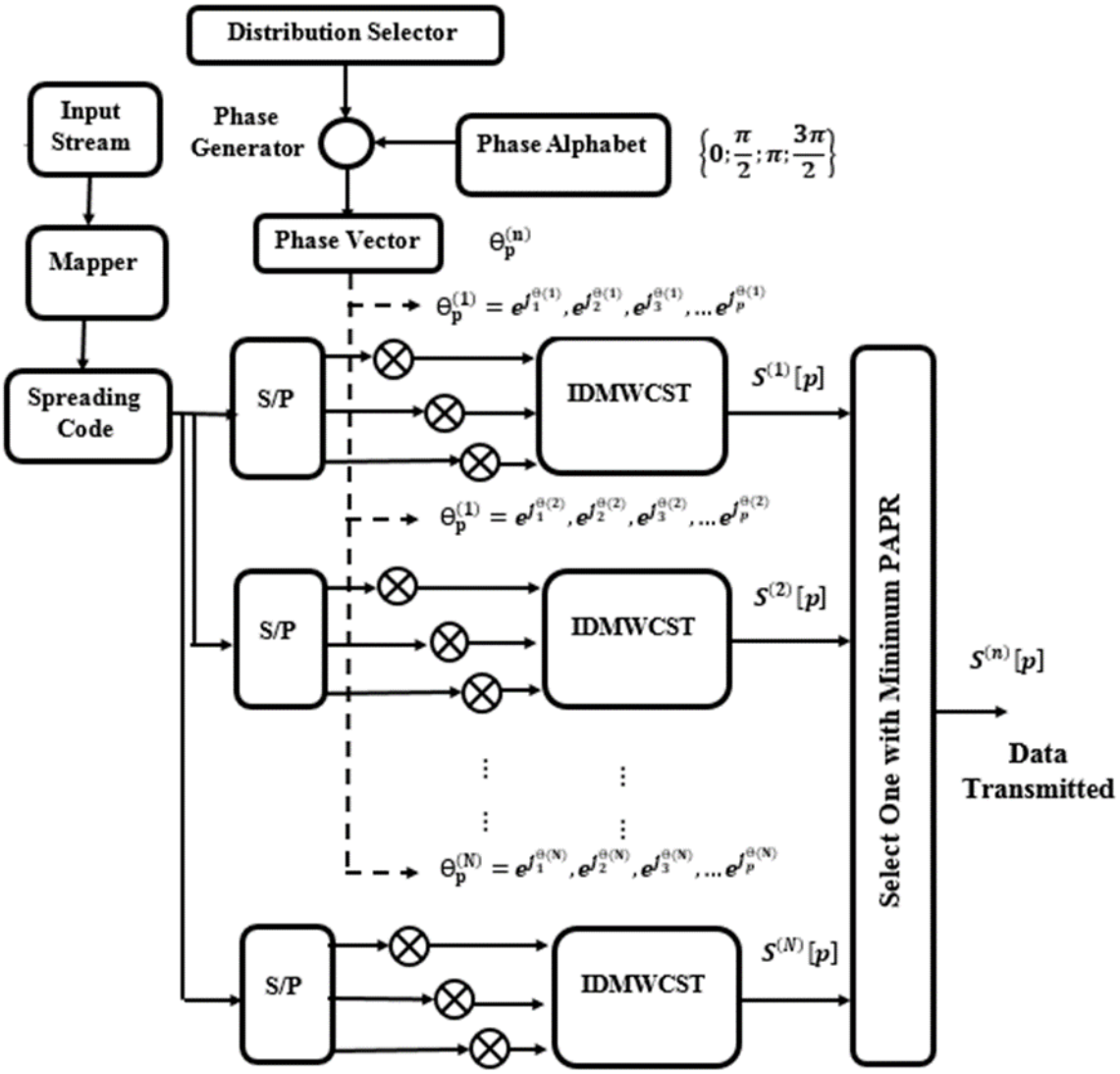

Figure 1: *Block diagram of MC-CDMA System Based OFDM Discrete "Multiwavelet Critical-Sampling Transform" using "Selected Mapping with Phase Modification"*

Simulation Results

In this section, we reconfirm results of the studies and assess the performance of MC-CDMA dependentDMWCST signals with the PAPR reduction method. The examination are carried out using "MATLAB R2015a" simulations and the performance metric of select is the "Complementary Cumulative Distribution Function (CCDF)". In "Orthogonal Frequency Division Multiplexing (OFDM)" the PAPR is commonly calculated per symbol. This is not possible in DMWCSTdue toDMWCST symbols overlap in the time-domain while the PAPR has to be computed per frame. The DMWCST system is recognized using a filter bank structure with many levels of decomposition. The modulation structure used is "4-QAM". The phase alphabet is taken to be $\phi \in (0, \pi/2, \pi, 3\pi/2)$ which is randomly selectedthoughproducing the phase vector.

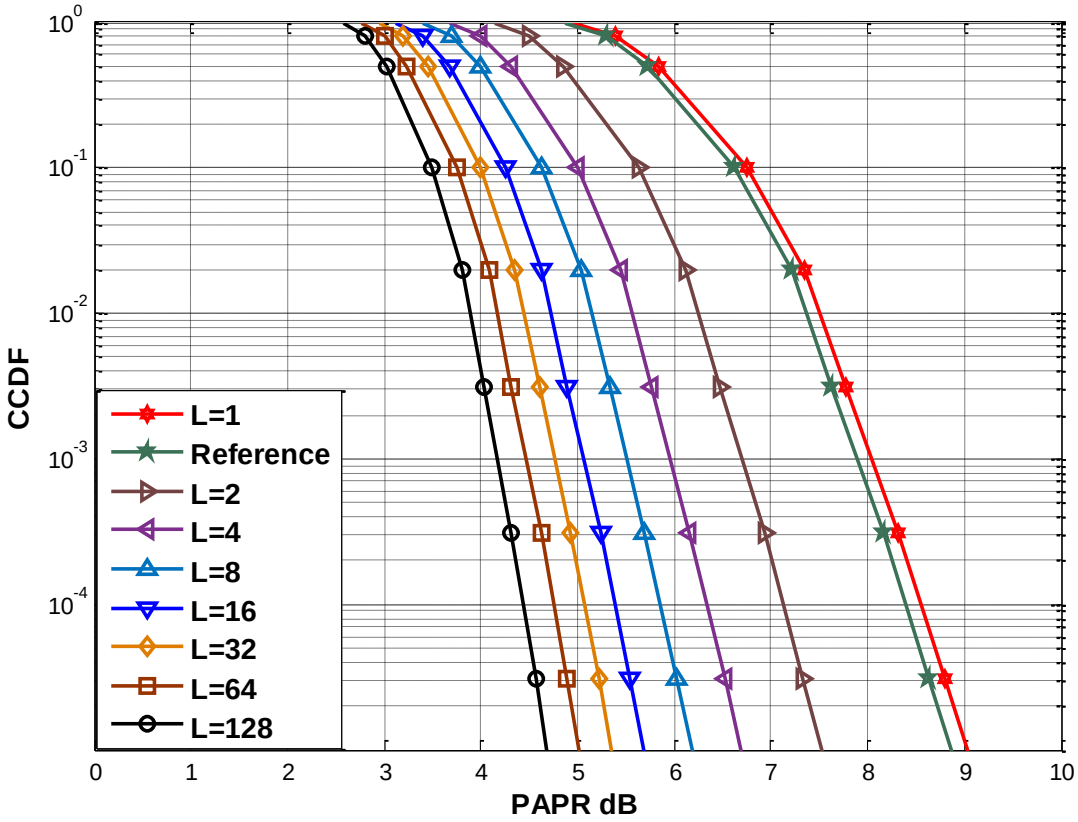

Figure 2*: CCDF of the PAPR of the MC-CDMA System based DMWCST signals for different values of L. A reference curve with no PAPR reduction is also plotted.*

To suitably scrutinize the enhancements due to the PAPR reduction method, a reference PAPR-CCDF curve achieved for DMWCST for the case without PAPR reduction (i.e. no phase modification) will too be rendered. Figure 2 showcases the CCDF curves for the difference of

PAPR under the PAPR reduction method for different number of replications, *L*. It is vivid from the plots that the enhancements are crucial and bring in up to 3.5dB reduction in PAPR in comparison to the case when no PAPR reduction method is used.

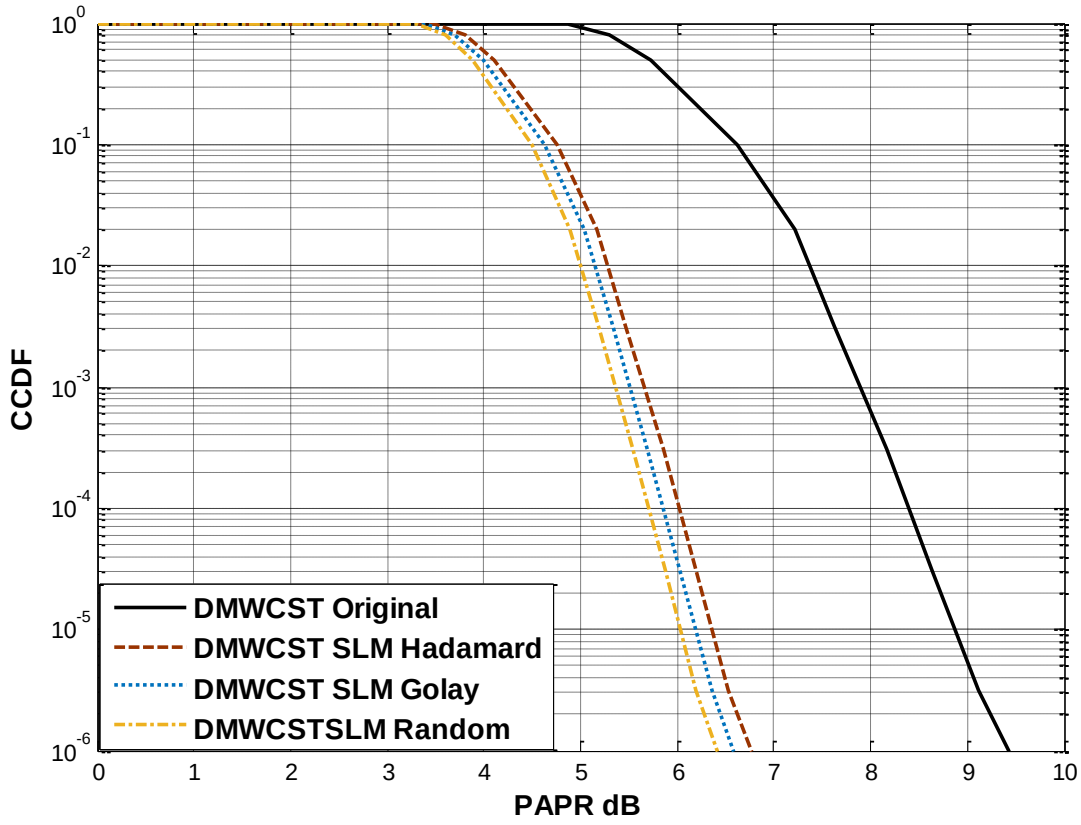

Figure 3: *Complementary cumulative distribution function (CCDF) of the PAPR of MC-CDMA System based DMWCST signals for different distributions of the phase sequences.*

Figure 3 displays the respective plots and it can be inferred from the figures that all the distributions result insignificant improvements. Also, there are no notable differences in their performances. These results are crucial because the imperceptible difference in the performances when using pseudo-random and random sequences. This also means that the former can be used in place of the later. Thus the receiver end only needs to know the key used to generate the pseudo-random phase sequences used at the transmitter (and not the entirephase sequence). This guides the way for a notable mitigation in the transfer of side information.

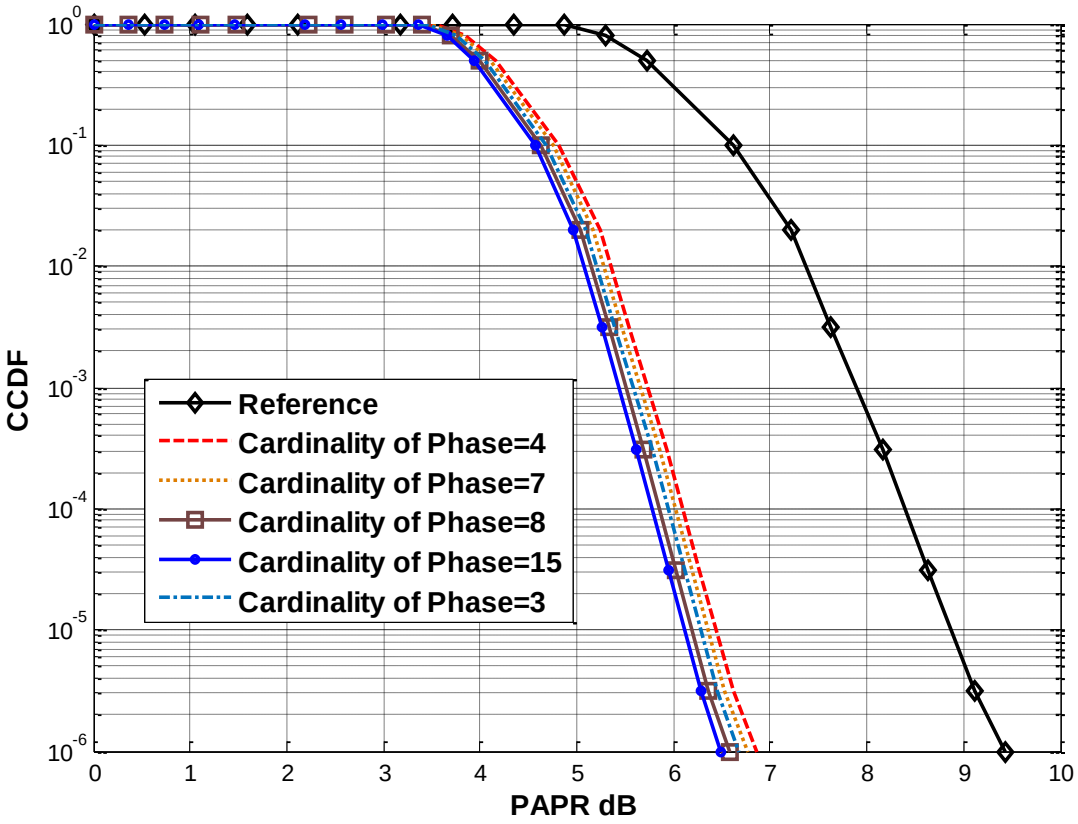

Figure 4: *CCDF of the PAPR of MC-CDMA System based DMWCST signals using the PAPR reduction method for different phase sequences.*

We presently scrutinize the impact of the phase alphabet on the PAPR reduction technique. The results are displayed in Figure 4where a range of cardinalities for the phases are referred back. The results showcased based on the select of the phase alphabet does not affect the performance of the PAPR reduction method.

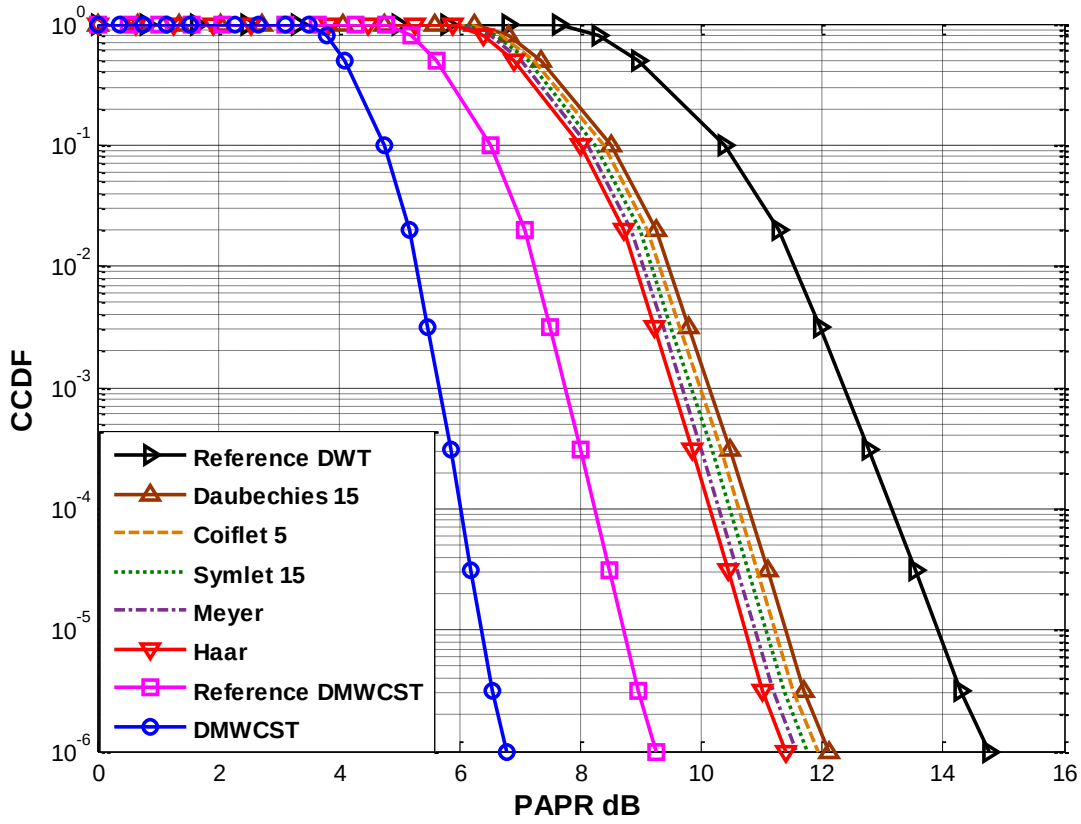

Figure 5*: CCDF comparison of the PAPR for MC-CDMA System based DMWCST signals and several DWT family.*

In Figure 5 where a comparison between DWT family and DMWCST for the phases are referred back, we can infer that all the wavelets follow a similar CCDF pattern for their PAPR performances. Also show the PAPR performance curves for various wavelet families and various filter lengths, respectively. Simulations analyzed also verified that suggested design using DMWCST achieves much lower PAPR and enhanced performance over other DWT family.

Conclusion

In this work, we suggested a technique to mitigate the PAPR in the progressive"MC-CDMA" System based DMWCST signals. The method revealed the postulate that by modifying the phase of the DMWCST sub-carriers one can amend the PAPR of the transmitted signal. By randomly changing the phases of the sub-carriers that modulate the information, one can get different DMWCST frames with different PAPRs. In addition, by transmitting the DMWCST frame with least PAPR than other DWT family, the probability of the DMWCST system slipping into non-linear region is significantly lowered

References

1. Fazel, K. and Kaiser, S. (2008). Multi-Carrier and Spread Spectrum Systems from OFDM and MC-CDMA to LTE and WiMAX, John Wiley & Sons Ltd, Second Edition, pp. 1-8.
2. Hara,R. P. S. (1997). Overviewof Multi-carrier CDMA", IEEE Communication Magazine, 35 (12): 126-133.
3. Molisch,A.F. (2011). Wireless Communications", John Wiley & Sons Ltd, Second Edition, pp.429-432.
4. Anusuya, PA., Anitha, K., Varughese, D.K. (2013). Design of multiwavelet filter bank for 4G wireless communications,Communications and Signal Processing (ICCSP), International Conference.
5. Fu, I.K. et al. (2010). Multicarrier technology for 4G WIMAX system, IEEE Comm. Mag.48 (8).
6. Breiling,S.H.M.M. and Huber,J.B. (2001). SLM peak power reduction without explicit side information, IEEE Commun. Lett. 5 (6): 239–241.
7. Davis,J.A. and Jedwab,J. (1999). Peak-to-mean power control in OFDM, Golay complementary sequences, and Reed–Muller codes," IEEE Trans. Inf. Theory, 45(7): 2397–2417.
8. Eetvelt,G.W.P.V. and Tomlinson, M. (1996). Peak to average power reducing for OFDMschemes by selective scrambling, Electron. Lett. 32(21): 1963–1964.
9. Kang,S. G. and Kim,J. G. (1999). A novel subblock partition scheme for partial transmit sequence OFDM," IEEE Trans. Broadcast.45 (3): 333–338.
10. R. W. B. S. H. Muller, R. F. H. Fischer, and J. B. Huber, "OFDM with reduced peak-to-average power ratio by multiple signal representation," Ann. Telecommun., vol. 52, no. 1–2, pp. 58–67, 1997.
11. H. Nikookar and K. S. Lidsheim"Random phase updating algorithm for OFDM transmission with low PAPR," IEEE Trans. Broadcast., vol. 48, no. 2, pp. 123–128, Jun. , 2002.
12. H. Nikookar and R. Prasad, "Weighted OFDM for wireless multipath channels," IEICE Trans. Commun., vol. E83-B, no. 8, pp. 1864–1872, 2000.
13. H. Ochiai and H. Imai, "Performance of the deliberate clipping with adaptive symbol selection for strictly band-limited OFDM systems," IEEE J. Sel. Areas Commun., vol. 18, no. 11, pp. 2270–2277. , 2000.
14. N. Ohkubo and T. Ohtsuki, "A peak to average power ratio reduction of multicarrier CDMA using selected mapping," in Proc. IEEE Vehicular Technology Conf, pp. 24–28., 2002.
15. V. Tarokh and H. Jafarkhani, "On the computation and reduction of the peak-to-average power ratio in multicarrier communications," IEEE Trans. Commun., vol. 48, no. 1, pp. 37–44, 2000.
16. J. Tellado and J. Cioffi, "PAR reduction in multicarrier transmission systems,"ANSI Document, T1E1.4 Technical Subcommittee, 97–367, 1997.
17. H. Tiwari, Roshan, R. ; Singh, R.K,, "PAPR reduction in MIMO-OFDM using combined methodology of selected mapping (SLM) and partial transmit sequence (PTS)," Industrial and Information Systems (ICIIS), International Conference on 2014 9th, 2014.

18. V. Sudha, Sriram Kumar, D, "PAPR reduction of OFDM system using PTS method with different modulation techniques," Electronics and Communication Systems (ICECS), International Conference on 2014, 2014.

19. T. Sravanti, Vasantha, N, "A combined PTS & SLM approach with dummy signal insertion for PAPR reduction in OFDM systems," Computer and Communications Technologies (ICCCT), International Conference on 2014, 2014.

20. B. Somasekhar, Visakhapatnam, India; Mallikarjunaprasad, A, "Modified SLM and PTS approach to reduce PAPR in MIMO OFDM," Electronics,Communication and Computational Engineering (ICECCE), International Conference on 2014, 2014.

21. U. P. K. Kavita Mhatrea, "Efficient Selective Mapping PAPR Reduction Technique"International Conference on Advanced Computing Technologies and Applications (ICACTA),Volume 45, 2015, Pages 620–627, 2015.

22. S. G. M. Saheed A. Adegbite, Brian G. Stewart, "Time-Domain SI Estimation for SLM Based OFDM Systems Without SI Transmission," Wireless Personal Communications, 2015.

23. W. A. M. Abbas Hasan Kattoush a, S. Nihadc,"The performance of multiwavelets based OFDM system under different channel conditions," Digital Signal Processing: p. YDSPR: 943.2009.

24. A. E. B. M.B. Martin, "New image compression techniques using multiwavelets and multiwavelet packets." IEEE Trans. Image Process, 10: p. 500–510., 2001.

Energy Stopping Power of Electrons in the Energy Range (0.01- 1000 MeV) In Some Human Body Tissues and Water

Saeed S.Kamoon, Shaker M.Murbatand Fatima H.Fakhri
Madenat Al-Elem University Collage

E-Mail- Kamoonsaeed@yahoo.com

Abstract

Electron accelerator is considered as an important tool in cancer radio-therapy and it providing unique choice in treatment of superficial tumor. In this paper, the mass stopping power of electrons has been calculated in biomedical human substances such as bones, soft-tissues and water with energy range of (10 keV-1000 MeV)using two methods. The first methodis done by calculating the energy loss of electrons in the tissue as one compound. The second method is by calculating the collision energy loss of electrons for each element of the compositions of bone, soft-tissue and water, and then calculates the collision energy loss of the tissue, where the tissue was considered to be made up of thin layers of pure elements (H, C, N, O, Na, Mg, P, S, Cl, K, Ca, Fe and Zn). The present results of the mass stopping power (dE/ρdX) for bone, tissue(soft) and waterwere compared for the two methods with the standard published results (ESTAR PROGRAM). The results are found in excellent agreement with the standard published data, where the error doesn't exceeds 0.3% when the first method was used. But it was found that the error is high when the second method is used. Therefore, werecommended using the first method and treating the tissue as one compound instead of it is composed of thin layers of pure elements.

Keywords: stopping power, human body tissues, electron therapy, bone, biomedical human substances.

حساب الفقدان لطاقة الالكتروناتفي بعض الانسجة البشرية ضمن مدى طاقة الالكترونات (0.01 – 1000 مليون الكترون فولت)

د.سعيد سلمان كمون ود.شاكر محمود مربط وفاطمة حسن فخري

كلية مدينة العلم الجامعة

الخلاصة :

يعتبر معجل الالكترونات احد الوسائل المهمة في العلاج الاشعاعي للأورام السرطانية وقد تكون هي الوسيلة الوحيدة في معالجة بعض حالات الاورام السرطانية مثل معالجة الاورام السرطانية تحت السطحية والجلدية.تم في هذا البحث حساب قدرة الايقاف للالكترونات خلال مرورها فيالانسجة الرخوة والعظام وبعض مكونات الجسم البشري(الماء) في مدىالطاقة من (10 keV) الى (1000MeV) باستخدام طريقتين ، الاولى هيحساب الفقدان في طاقة الالكترونات خلال مرورها في النسيج واعتبار النسيج كمركب واحد. والطريقة الثانيةحساب الفقدان في طاقة الالكترونات خلال مرورها في النسيج واعتبار النسيج مكونا من عدة طبقات كل طبقة تمثل عنصرا من العناصر الكيميائية المكونة له (H،Na،Mg،P،S،Cl،K،Ca،Fe،Zn).وقد تبين بان النتائج الحالية متطابقة بشكل كبير مع اهم النتائج العالمية المنشورة ولا تتعدى نسبة الخطأ 0.3% كأقصى حد عند استخدام الطريقة الاولى ويمكن اعتمادها كنتائج قياسية لحساب الجرعات المكافئة للالكترونات عند مرورها في تلك الانسجة.وفي حالة استخدام الطريقة الثانية وجد ان نسبة الخطأ عالية على النتائج،وبناء عليه توصي الدراسة الحالية بعدم اعتماد الطريقة الثانية في حساب الفقدان في طاقة الالكترونات خلال مرورها فيالانسجة .

1. Introduction

When charged particles pass through matter they interact with atomic electrons by several ways. The charge particles may interact with atoms through inelastic collision and resulting in excitation and ionization of atoms, this is known as collision loss. The charged particles may suffer another type of interaction which is known as elastic collision in which it doesn't loss any energy. In addition, the particle can interact with atoms through bremsstrahlung production and it known as radiative loss. The current knowledge, both experiment and theoretical, is far from being complete, and is often inadequate for the determination of stopping power values of a variety of materials and fora wide range of particle energies. [1].

Information about interaction of radiation with matter especially with the tissue of human body and water is very important from the point of dosimetry and radiation protection, radiotherapy and calibration of computed tomography scanners.

Since the human body contains mostly water, the knowledge of depth doseprofile of charged particles in this stopping medium is also of great importance for anaccurate treatment planning.

Electron linear accelerator becomes one of the effective equipment in cancer radiotherapy and treatment of many tumors [2, 3], so that the radiation dose should be accurate to obtain therapeutic success, when a significant under dose can cause failure to control the disease and overdose increases the risk of damage to normal tissues. Therefore the knowledge of mean free path and continuous slowing down approximation range (CSDA) for biological materials are also important, so that many authors made several studies on biological compounds [4-9].

Tissues and water equivalent materials (TEMs) can be used in quality assurance in radiotherapy[10], dosimetry measurements, CT-Scanner calibration[11], such materiel was consider to be equivalent to a tissue has the same radiation characteristics as the real human tissues ,accordingly many (TEMs) have been studied and developed [12-22].

Phantoms are physical or virtual representations of the human body to be used for the determination of absorbed dose to radiosensitive organs and tissues. In radiation protection a widely used physical model is the ALDERSON-RANDO phantom (Alderson [23], Fisher and Snyder [24,25] introduced this type of phantom for an adult male which also contains ovaries and a uterus .the phantom has been further developed by Snyder et al [26,27]. Since then it is known as "MIRD-5 phantom" (*M*edical *I*nternal *R*adiation *D*ose Committee (MIRD) Pamphlet No.5).and many other phantoms for children of various age [28], and a pregnant female adult phantom Stabin et al [29].

The International Commission on Radiological Protection (ICRP) has created a task group on dose calculations, which, among other objectives, should replace the currently used mathematical MIRD phantoms by voxel phantoms [30].

2-Mass Stopping Power of the Electrons

The electron loses their energy by ionization and excitation of the orbital electrons in the medium.Mass stopping Power ($dE/\rho dX$) can be defined as the rate of energy loss per unit path length of an electron or positron by excitation and ionization which was known as "collisional energy loss."The mass collision stopping powers for electrons and positrons are given by [31]:

$$\left(\frac{dE}{\rho dX}\right)_c = K\left[Ln\left\{\frac{\tau^2(\tau+2)}{2\left(\frac{I}{m_oc^2}\right)^2}\right\} + F^{\mp}(\tau) - \delta(\beta\gamma) - \frac{2C}{Z}\right] \ldots\ldots\ldots(1)$$

Where,

$$C = \pi\left(\frac{N_A Z}{A}\right)\left(\frac{e^2}{m_oc^2}\right)^2$$

$$K = \frac{2Cm_oc^2}{\beta^2} = \frac{0.1535\ Z}{A\beta^2}(Mev.cm^2.g^{-1}) \quad I\ and\ m_oc^2\ in\ eV$$

$\tau = \frac{T}{m_oc^2}$ T is the kinetic energy of the electrons in unites ofm_oc^2

$$F^-(\tau) = 1 - \beta^2 + \frac{1}{(\tau+1)^2}\left[\frac{\tau^2}{8} - (2\tau+1)Ln2\right]$$ is used for electrons ….(2)

and

$$F^+(\tau) = 2Ln2 - \frac{\beta^2}{12}\left[23 + \frac{14}{(\tau+2)} + \frac{10}{(\tau+2)^2} + \frac{4}{(\tau+2)^3}\right]$$ for positrons …(3)

where

$\frac{C}{Z}$ is for shell correctionaccounting for non-participation of K-shell electrons at low energies and;

δ is for the polarization or density effect correction in condensed media[31,32,33]

δ(X) =

4.6052X+ C		X >X_1
4.6052X + a(X1- X)^m + C		X_0< X < X_1
0	for non - conducting materials	X < X_o
$\delta(X_o)10^{2(x-xo)}$	for conducting materials	X < Xo.

The parameters X_o, Xi, *a*, ***m,*** and C Parameters for elements and many compounds and mixtures were published [34, 35].

In this equation, X= $\log_{10}(\tau(\tau+2))^{\frac{1}{2}}\tau$ is the electron kinetic energy in units of the rest mass, and

$$C = -2ln\left(\frac{I}{\hbar\omega_0}\right) - 1$$

Where,

$\hbar\omega_o$: is the Plasma energy = $\sqrt{4\pi N_e r_e^3}m_oc^2/\alpha$ = $28.816\sqrt{\rho\langle Z/A\rangle}eV$

N_e: is the electron density (electron /cm^3)of the medium.

α: is the Fine structure constant = 1/137

ρ : is the density of the medium (g/cm^3)

2.1 Stopping Power In Compound

The mass stopping power can be well approximated for a mixture of elements or chemical compounds through the assumption of Bragg's additive Rule [36, 37].

It states "that atoms contribute nearly independently to the stopping power, and hence their effects are additive "in terms of the weight fractions $w_i$of elements of atomic number Z_i Present in a compound or mixture. The mass stopping power $\left(\frac{dE}{\rho dX}\right)_{mix}$ can be written according to Bragg's additive Rule as:

$$\left(\frac{dE}{\rho dX}\right)_{mix} = \sum_i w_i \left(\frac{dE}{\rho dX}\right)_{Z_i} \quad \ldots\ldots\ldots\ldots(4)$$

Where, $w_i$is the fraction byweight of the ith element.

The rule can also be applied for mass collision and radiative stopping power as well, and the mean excitation energy for compound or mixture can also be calculated using the same rule by the following relation [38];

$$\ln I = \frac{\sum_j w_j (Z_j/A_j)\, lnI_j}{\sum_j w_j (Z_j/A_j)}$$

Where: $Z_j$is the atomic weight of the jth element in the compound
A_j is the atomic mass of the jth element in the compound
I_j is the excitation energy of the jth element in the compound

3. Calculation of Energy Loss of Electrons

Following the ESTAR program [39] which is a PC package used for calculating stopping power and ranges of electrons in any element and the results of about (180) compounds and mixture were published. In the present study we use two methods to calculate the energy loss of electronsin the energy range of electrons from 10 keV up to 1000MeV for tissues and water. The first oneis by calculating the energy loss of electrons in the tissue as one compound using equation (1).The results are compared with published results and given in Table(1).

The second method is by calculating the collision energy loss of electronsfor each element of the compositions of bone, soft-tissue and water using Eq. (1), where the tissue was considered to be made up of thin layers of pure elements.The composition of tissue (soft), bone (compact) and water (liquid) are given in Table (2).Accordingly we calculate the stopping power in H, C, N, O, Na, Mg, P, S, Cl, K, Ca, Fe and Zn, which are the elemental compositions of the tissues and waterusing Eq.(1). The excitation energy and the density effect parameters used in this study were taken from NIST program .[39].The results are compared with the standard and presented in Table (3) and Table (4),and then using Eq. (4) to calculate the collision energy loss in the tissues and water.

The present results of the mass stopping power (dE/ρdX) for bone, tissue(soft) and water which are calculated by this methodare compared with other published results and presented in Table (5).

3.1 calculation of Z_{eff},A_{eff} and $(Z/A)_{eff}$

In the calculation of stopping power of electrons in the tissues, the values of Z_{eff},A_{eff} and $(Z/A)_{eff}$ have been used and can be calculated using the following formulas [40]:

$$Z_{eff} = \frac{\sum(w_i Z_i^2/A_i)}{\sum(w_i Z_i/A_i)} \quad \ldots\ldots\ldots \quad (5)$$

$$A_{eff} = \frac{Z_{eff}}{(Z/A)_{eff}} \quad \ldots\ldots\ldots\ldots\ldots (6)$$

Where $(Z/A)_{eff}$ is given by:

$$(Z/A)_{eff} = \sum(w_i Z_i/A_i) \quad \ldots\ldots\ldots\ldots (7)$$

4. Discussion and Conclusion

The results of the present work of stopping power are in excellent agreement with the standard results published by reference [39], where the error on the present study doesn't exceeds 0.3% as a maximum when the tissues and water was considered as one compound as shown in Table (1). The present study provides good information about the stopping power of electrons in some human substances when the electron accelerator is used in tumors and cancer therapy. The present study also provided excellent and accurate results about the stopping power of electron in 14 elements as showing in Table (3) and Table (4).

It can be noticed that from Table (5), when the second methodis used to calculate the collision energy loss of electrons in bone, soft-tissue and water in which the tissue was considered to be composed of a thin layer of pure elements of the tissue′s composition, the error on the results is high and reached to about 25% in some cases, so we recommended to use the first method and treating the tissue as one compound instead of composed of thin layers of pure elements.

References

1. G. Tanır,M. H. B¨ol¨ukdemir, S. Kele¸s, and ˙I. G¨oker, On the Stopping Power for Low Energy Positrons, **Chinese Journal Of Physics Vol. 50, No. 3 June 2012**
2. Sam Beddar A., Peter J. Biggs, Sha Chang, Gary A. Ezzell, Bruce A. Faddegon, Frank W. Hensley, and Michael D., Mills, Intraoperative radiation therapy using mobile electron linear accelerators: Report of AAPM Radiation Therapy Committee Task Group No. 72 , Medical Physics 33, 1476 (2006).
3. A.Wambersie and R.A. Gahbauer, Medical Applications Of Electron Linear Accelerators http://linac96.web.cern.ch/Linac96/Proceedings/Thursday/TH202/Paper.html (26-30 August 1996)
4. Anshu Saxena , Rathi S.K. and Verma A.S., Continuous Slowing Down Approximation (CSDA) ranges of electrons for biomedical materials, Elixir Bio. Phys. 37 (2011) 3860-3863
5. Verne, J., Pimblott, M.S., Electron energy-loss distributions in solid, Dry DNA. Radiat. Res. Vol.141, (1995) p. 208–215.
6. Akkerman A. and Akkerman E., Characteristics of electron inelastic interactions in organic compounds and water over the energy range 20–10 000 eV. J. Appl. Phys. Vol. 86, (1999) p.p.5809–5816.

7. Tan, Z., Xia, Y., Zhao, M., Liu, X., Li, F., Huang, B., Ji, Y.,electron stopping power and mean free path in organic compounds over the energy range of 20–10 000 eV. Nucl. Instrum. Meth. B Vol. 222, (2004) p.p.27–43.
8. Sandeep Gupta, Calculation of the Range of Electrons for parts of Human Body over the Energy Range of 30 – 1000 keV, International Journal of Engineering Technology, Management and Applied Sciences ,(IJETMAS) Volume 3, Special Issue, ISSN 2349-4476, September 2015
9. Singh Hemlata, Rathi S.K. and Verma A.S., Ranges of Electrons for Human Body Substances, Research Journal of Chemical Sciences (Res. J. Chem. Sci.) Vol. 3(3), 4-8, March (2013).
10. S. Belletti,A. Dutreix TM, G. Garavaglia, H. Gfirtner ,J. Haywood , K.A. Jessen I.-L. Lamm , B. Mijnheer, A. Noel, F. Ntisslin, U. Rosenow, P. Schneider,W. Seelentag, S. Sheriff, H. Svensson,D. Thwaites , Quality staffing assurance in radiotherapy: the levels. Recommendations from Group importance of medical physics an ESTRO/EFOMP joint task group. Radiotherapy and Oncology 41 (1996) 89-94.
11. Indra Yohannes, Daniel Kolditz, Oliver Langner and Willi A. Kalender A., formulation of tissue- and water-equivalent materials using the stoichiometric analysis method for CT-number calibration in radiotherapy treatment Planning, Phys. Med. Biol. 57 (2012) 1173–1190
12. White D.R. ,The formulation of tissue substitute materials using basic interaction data Phys. Med. Biol. 22(1977) 889–99
13. Constantinou C., Attix F. H. and Paliwal B.R., A solid water phantom material for radiotherapy x-ray and γ –ray beam calibrations, Med. Phys. 9(1982) 436–41
14. Goodsitt M.M., Johnson R.H. and Chesnut C.H. A new set of calibration standards for estimating the fat and mineral content of vertebrae via dual energy QCT, Bone Miner.13 (1991) 217–33
15. Jones A.K., Hintenlang D.E. and Bolch W.E., Tissue-equivalent materials for construction of tomographic dosimetry phantoms in pediatric radiology, Med. Phys. 30(2003) 2072–81
16. Burmeister J., Kota C., Maughan R.L., Spokas J.J., Coderre J.A., Ma R. and Wielopolski L., A conducting plastic simulating brain tissue, Med. Phys. 27(2000) 2560–4
17. Iwashita Y., Basic study of the measurement of bone mineral content of cortical and cancellous bone of the mandible by computed tomography Dentomaxillofac, Radiol. 29(2000) 209–15
18. Homolka P. and Nowotny R., Production of phantom materials using polymer powder sintering under vacuum ,Phys. Med. Biol. 47(2002) 47–52
19. Homolka P., Gahleitner A. and Nowotny R., Temperature dependence of HU values for various water equivalent phantom materials Phys. Med. Biol. 47(2002) 2917–23
20. Homolka P., Gahleitner A., Prokop M. and Nowotny R., Optimization of the composition of phantom materials for computed tomography Phys. Med. Biol. 47(2002) 2907–16
21. ICRU ,Tissue substitutes in radiation dosimetry and measurement Report 44 (Bethesda, MD: International Commission on Radiation Units and Measurements) (1989)
22. Schneider U., Pedroni E. and Lomax A., The calibration of CT Hounsfield units for radiotherapy treatment planning Phys. Med. Biol. 41(1996) 111–24
23. Alderson S.W., Lanzl L.H., Rollins M. and Spira J., An instrumented phantom system for analog computation of treatment plans. Am. J. Roentg. 87(1962) 185
24. Fisher H.L. and Snyder W.S., Distribution of dose in the body from a source of gamma rays distributed uniformly in an organ. Report No. ORNL-4168, Oak Ridge National Laboratory, Oak Ridge, Tenn., USA (1967)
25. Fisher H.L. and Snyder W.S., Distribution of dose in the body from a source of gamma rays distributed uniformly in an organ. In: Proceedings of the First International Congress on Radiation Protection, Pergamon Press, Oxford, pp 1473-1486 (1968)
26. Snyder W.S., Ford M R, Warner G.G. and Watson G.G., Revision of MIRD Pamphlet No. 5 Entitled “Estimates of absorbed fractions for monoenergetic photon sources uniformly distributed in various organs of a heterogeneous phantom”. ORNL-4979,

Oak Ridge National Laboratory, Oak Ridge, Tenn. (1974)
27. Snyder W.S., Ford M.R. and Warner G.G., Estimates of absorbed fractions for monoenergetic photon sources uniformly distributed in various organs of a heterogeneous phantom. MIRD Pamphlet No.5, revised, Society of Nuclear Medicine, New York N. Y. (1978)
28. Cristy M., Mathematical phantoms representing children at various ages for use in estimates of internal dose. Report ORNL/NUREG/TM-367, Oak Ridge National Laboratory, Oak Ridge, Tenn., USA(1980)
29. Stabin M., Watson E., Cristy M., Ryman J., Eckerman K., Davis J., Marshall D. And Gehlen K., Mathematical models and specific absorbed fractions of photon energy in the non-pregnant adult female and at the end of each trimester of pregnancy. Report No. ORNL/TM-12907, Oak Ridge National Laboratory, Oak Ridge, Tenn., USA(1995)
30. Kramer R., Khoury H.J.,Vieira J.W., Loureiro E.C.M., Lima V.J.M., A Lima F.R. and Hoff G., All about FAX: a Female Adult voXel phantom for Monte Carlo calculation in radiation protection dosimetry Physics in Medicine and Biology, Volume 49, Number 23(2004)
31. Attix F. H., Introduction to radiological physics and radiation dosimetry, Wiley & Son, New York,(1986)
32. Berger M. J. and S. M. Seltzer: Stopping powers and ranges of electrons and positrons (2nd ed.). NBSIR 82-2550-A (1983).
33. Sternheimer R. M., Seltzer S. M. and Berger M. J., Density effect for the ionization loss of charged particles in various substances, Phys. Rev. B 26, 6067, 1982
34. Sternheimer R.M.,Seltzer S.M. and Berger M.J., The Density Effect for the Ionization Loss of Charged Particles in Various Substances," Atomic Data & Nucl. Data Tables 30, 261 (1984).
35. Sternheimer R.M. and Peierls R.F., Phys. Rev. B3, 3681 (1971).
36. ICRU, Report No. 37, Stopping powers for electrons and positrons. (International Commission on Radiation Units and Measurements, Bethesda, MD,(1984).
37. Brian J. Mcparland, “medical radiation dosimetry”, **chapter 14**, collision energy loss in compound media, (2013) pp 483-492.
38. Martin, Berger M.J. and Seltzer S. M., National Bureau of Standards, Washington ,D. C. (1964).
39. Berger M.J., Coursey, J. S., Zucker, M. A., Chang, J., ESTAR, PSTAR and ASTAR , “ computer programs for calculating stopping powers and range tables for electrons, protons and helium ions,” Available online as: http://physics.nist.gov/Star, NIST, Gaithersburg, MD, (2005).
40. Tatsuo Tabata, Pedro Andre,Kunihiko Shinoda,An analytic formula for the extrapolated range of electrons in condensed materials, Nuclear Instruments and Methods in Physics Research B 119 (1996) 463-470
41. International Commission on Radiological Protection. Report of the Task Group on Reference Man. Oxford: Pergamon Press; ICRP Publication 23; (1975)

Table (1): Comparison of the mass collision stopping power of electrons with the standard results in Bone, Tissue (soft) and Water, where all tissues was considered to be as one compound

dE/ρdX (MeV.cm^2/g)									
ENERGY (MeV)	**BONE**			**TISSUE (soft)**			**WATER**		
	ESTAR(std)[39]	present study	ERROR%	ESTAR (std)[39]	present study	ERROR %	ESTAR(std)[39]	present study	ERROR%
0.010	20.680	20.671	0.043	22.570	22.511	0.264	22.560	22.509	0.224
0.020	12.130	12.134	-0.032	13.170	13.137	0.249	13.170	13.148	0.170
0.040	7.191	7.192	-0.008	7.767	7.751	0.202	7.777	7.763	0.186
0.060	5.370	5.371	-0.016	5.787	5.776	0.185	5.797	5.787	0.181
0.080	4.412	4.413	-0.032	4.749	4.740	0.191	4.757	4.749	0.162
0.100	3.820	3.821	-0.031	4.107	4.100	0.176	4.115	4.108	0.158
0.200	2.599	2.600	-0.037	2.786	2.782	0.155	2.793	2.789	0.153
0.400	1.996	1.997	-0.026	2.142	2.139	0.158	2.148	2.145	0.147
0.600	1.815	1.816	-0.033	1.955	1.952	0.146	1.963	1.961	0.117
0.800	1.740	1.741	-0.053	1.876	1.873	0.146	1.886	1.883	0.147
1.000	1.705	1.706	-0.071	1.839	1.836	0.164	1.849	1.847	0.124
2.000	1.684	1.685	-0.088	1.812	1.810	0.123	1.824	1.821	0.141
4.000	1.735	1.736	-0.077	1.859	1.857	0.116	1.870	1.868	0.102
6.000	1.778	1.779	-0.063	1.901	1.898	0.144	1.911	1.909	0.102
8.000	1.810	1.811	-0.074	1.932	1.930	0.102	1.943	1.941	0.122
10.000	1.835	1.836	-0.074	1.958	1.955	0.139	1.968	1.966	0.112
20.000	1.909	1.911	-0.084	2.035	2.032	0.139	2.046	2.044	0.118
40.000	1.976	1.977	-0.054	2.105	2.102	0.131	2.118	2.116	0.117
60.000	2.012	2.013	-0.069	2.142	2.140	0.100	2.156	2.154	0.093
80.000	2.037	2.038	-0.068	2.168	2.166	0.110	2.182	2.180	0.083
100.000	2.056	2.058	-0.077	2.188	2.185	0.127	2.202	2.200	0.090
200.000	2.114	2.116	-0.084	2.247	2.245	0.091	2.263	2.260	0.118
400.000	2.171	2.173	-0.091	2.306	2.304	0.087	2.322	2.320	0.091
600.000	2.204	2.206	-0.102	2.341	2.339	0.098	2.357	2.354	0.117
800.000	2.228	2.230	-0.096	2.365	2.363	0.099	2.381	2.379	0.075
1000.000	2.246	2.248	-0.090	2.384	2.382	0.082	2.400	2.398	0.088

Table (2): Composition of Tissues (Soft)ICRP [41] **, Bone** (Compact)ICRU**[**36**]** and **Water** (Liquid) **[**39**]**

composition of TISSUE, SOFT (ICRP): [41] **Density (g/cm3)= 1.00000E+00** **Mean Excitation potential(eV)= 72.300000**					**Composition of BONE, COMPACT (ICRU) [36]** **Density (g/cm3) =1.85000E+00** **Mean Excitation potential(eV) =**				**Composition of WATER, LIQUID [39]:** **Density (g/cm3) =1.00000E+00** **Mean Excitation potential(eV) =75.0000**			
No.	**Element**	**Density ρ (gm/cm3)**	**Fraction by weight**	**Mean ionization potential (I (eV)**	**Element**	**Density ρ (gm/cm3)**	**Fraction by weight**	**Mean ionization potential (I (eV)**	**Element**	**Density ρ (gm/cm3)**	**Fraction by weight**	**Mean ionization potential (I (eV)**
1	H	0.0899×10-3	0.104472	19.2	H	0.0899×10-3	0.063984	19.2	H	0.0899×10-3	0.111894	19.2
2	C	2.26	0.232190	81	C	2.26	0.278000	81	O	1.429×10-3	0.888106	95
3	N	1.25×10-3	0.024880	82	N	1.25×10-3	0.027000	82				
4	O	1.429×10-3	0.630238	95	O	1.429×10-3	0.410016	95				
5	Na	0.97	0.001130	149	Mg	1.74	0.002000	156				
6	Mg	1.74	0.000130	156	P	1.82	0.070000	173				
7	P	1.82	0.001330	173	S	2.07	0.002000	180				
8	S	2.07	0.001990	180	Ca	1.55	0.147000	191				
9	Cl	3.21	0.001340	174								
10	K	1.78	0.001990	190								
11	Ca	1.55	0.000230	191								
12	Fe	7.87	0.000050	286								
13	Zn	7.13	0.000030	330								

Table (3): Values of mass collision stopping power (MeV.cm^2/g) for electrons in pure elements of the tissues composition

Elements	H		C		N		O		Na		Mg		P	
Energy (MeV)	*dE/ρdX*		*dE/ρdX*		*dE/ρdX*		*dE/ρdX*		*dE/ρdX*		*dE/ρdX*		*dE/ρdX*	
	std.	calc.	std.	calc.	std.	calc.	std.	calc.	std.	calc.	std.	calc.	std.	calc.
0.010	51.24	51.22	19.99	19.93	19.95	19.90	19.37	19.33	16.79	16.77	17.15	17.12	16.41	16.39
0.020	29.16	29.15	11.69	11.66	11.68	11.65	11.38	11.35	9.99	9.98	10.22	10.20	9.81	9.80
0.040	16.87	16.86	6.91	6.89	6.90	6.89	6.75	6.73	5.98	5.97	6.12	6.11	5.89	5.89
0.060	12.45	12.44	5.15	5.14	5.15	5.14	5.04	5.03	4.49	4.48	4.60	4.59	4.43	4.42
0.080	10.15	10.14	4.23	4.22	4.23	4.22	4.14	4.13	3.70	3.70	3.79	3.78	3.65	3.65
0.100	8.74	8.73	3.65	3.65	3.66	3.65	3.59	3.58	3.21	3.21	3.29	3.28	3.17	3.17
0.200	5.85	5.85	2.47	2.47	2.49	2.48	2.44	2.44	2.20	2.19	2.25	2.25	2.17	2.17
0.400	4.45	4.44	1.89	1.88	1.91	1.91	1.88	1.88	1.70	1.70	1.74	1.74	1.68	1.68
0.600	4.04	4.04	1.71	1.71	1.75	1.75	1.73	1.72	1.56	1.56	1.60	1.59	1.54	1.54
0.800	3.88	3.88	1.64	1.64	1.69	1.69	1.67	1.67	1.51	1.51	1.54	1.54	1.48	1.48
1.000	3.82	3.81	1.61	1.61	1.67	1.67	1.65	1.64	1.49	1.49	1.52	1.52	1.46	1.46
2.000	3.82	3.82	1.59	1.59	1.69	1.69	1.67	1.67	1.51	1.51	1.53	1.53	1.47	1.47
4.000	4.02	4.02	1.64	1.64	1.80	1.80	1.78	1.78	1.58	1.58	1.60	1.60	1.54	1.54
6.000	4.18	4.17	1.68	1.68	1.88	1.88	1.86	1.86	1.63	1.63	1.65	1.65	1.59	1.59
8.000	4.30	4.29	1.71	1.71	1.94	1.94	1.92	1.92	1.66	1.66	1.68	1.68	1.63	1.62
9.000	4.35	4.34	1.72	1.72	1.97	1.96	1.94	1.94	1.67	1.67	1.69	1.69	1.64	1.64
10.000	4.39	4.39	1.74	1.73	1.99	1.99	1.97	1.96	1.68	1.68	1.70	1.70	1.65	1.65
20.000	4.70	4.70	1.80	1.80	2.14	2.14	2.12	2.12	1.76	1.75	1.77	1.77	1.72	1.72
40.000	5.01	5.01	1.87	1.86	2.29	2.29	2.27	2.27	1.82	1.82	1.84	1.84	1.79	1.79
60.000	5.14	5.14	1.90	1.90	2.36	2.35	2.34	2.34	1.86	1.86	1.88	1.88	1.83	1.82
80.000	5.21	5.21	1.92	1.92	2.40	2.39	2.38	2.38	1.89	1.89	1.90	1.90	1.85	1.85
100.000	5.26	5.26	1.94	1.94	2.42	2.42	2.41	2.41	1.91	1.91	1.92	1.92	1.87	1.87
200.000	5.38	5.38	1.99	1.99	2.51	2.51	2.49	2.49	1.96	1.96	1.98	1.98	1.92	1.92
400.000	5.49	5.49	2.05	2.04	2.59	2.59	2.57	2.57	2.01	2.01	2.03	2.03	1.98	1.98
600.000	5.55	5.55	2.08	2.07	2.63	2.63	2.62	2.61	2.04	2.04	2.06	2.06	2.01	2.01
800.000	5.60	5.60	2.10	2.10	2.66	2.66	2.65	2.64	2.07	2.06	2.09	2.08	2.03	2.03
1000.000	5.63	5.63	2.12	2.11	2.68	2.68	2.67	2.67	2.08	2.08	2.10	2.10	2.05	2.04

Table (4): Values of mass collision stopping power (MeV.cm^2/g) for electrons in pure elements of the tissues composition

Elements	P		S		Cl		K		Ca		Fe		Zn	
Energy (MeV)	$dE/\rho dX$		$dE/\rho dX$		$dE/\rho dX$		$dE/\rho dX$		$dE/\rho dX$		$dE/\rho dX$		$dE/\rho dX$	
	Std.	cal.	Std.	cal.	Std.	cal.	Std.	cal.	Std.	cal.	Std.	cal.	Std.	cal.
0.010	16.41	16.389	16.75	16.73	16.23	16.21	16.10	16.08	16.51	16.50	13.88	13.87	13.15	13.14
0.020	9.81	9.798	10.03	10.01	9.70	9.69	9.66	9.65	9.91	9.89	8.46	8.45	8.06	8.06
0.040	5.894	5.887	6.029	6.02	5.83	5.83	5.82	5.81	5.97	5.96	5.15	5.14	4.93	4.93
0.060	4.429	4.425	4.533	4.53	4.39	4.38	4.38	4.37	4.49	4.49	3.89	3.89	3.74	3.74
0.080	3.654	3.650	3.741	3.74	3.62	3.62	3.61	3.61	3.71	3.70	3.22	3.22	3.10	3.10
0.100	3.172	3.169	3.248	3.24	3.14	3.14	3.14	3.14	3.22	3.22	2.80	2.80	2.70	2.70
0.200	2.171	2.169	2.224	2.22	2.16	2.15	2.16	2.15	2.21	2.21	1.93	1.93	1.87	1.87
0.400	1.677	1.676	1.719	1.72	1.68	1.67	1.67	1.67	1.71	1.71	1.50	1.50	1.45	1.45
0.600	1.537	1.535	1.574	1.57	1.54	1.54	1.54	1.54	1.58	1.57	1.37	1.37	1.33	1.33
0.800	1.483	1.481	1.519	1.52	1.49	1.49	1.49	1.49	1.52	1.52	1.33	1.33	1.29	1.29
1.000	1.461	1.460	1.496	1.49	1.48	1.48	1.47	1.47	1.50	1.50	1.31	1.31	1.27	1.27
2.000	1.47	1.469	1.505	1.50	1.51	1.51	1.49	1.49	1.51	1.51	1.32	1.32	1.28	1.28
4.000	1.541	1.540	1.579	1.58	1.61	1.61	1.56	1.56	1.59	1.58	1.38	1.38	1.35	1.34
6.000	1.591	1.590	1.633	1.63	1.69	1.69	1.62	1.61	1.64	1.64	1.42	1.42	1.39	1.39
8.000	1.625	1.624	1.67	1.67	1.75	1.75	1.66	1.65	1.68	1.67	1.46	1.46	1.42	1.42
10.000	1.651	1.649	1.698	1.70	1.80	1.80	1.69	1.69	1.71	1.70	1.48	1.48	1.45	1.45
20.000	1.723	1.722	1.776	1.77	1.95	1.94	1.78	1.78	1.79	1.79	1.56	1.56	1.53	1.53
40.000	1.789	1.788	1.846	1.84	2.08	2.08	1.85	1.85	1.86	1.86	1.63	1.63	1.60	1.60
60.000	1.826	1.825	1.884	1.88	2.14	2.15	1.89	1.89	1.90	1.90	1.66	1.66	1.64	1.64
80.000	1.851	1.850	1.91	1.91	2.19	2.20	1.92	1.92	1.93	1.93	1.69	1.69	1.67	1.66
100.000	1.869	1.868	1.93	1.93	2.23	2.23	1.94	1.94	1.95	1.95	1.71	1.70	1.68	1.68
200.000	1.924	1.923	1.987	1.99	2.33	2.34	2.00	2.00	2.01	2.00	1.76	1.76	1.74	1.74
400.000	1.977	1.976	2.042	2.04	2.41	2.42	2.05	2.05	2.06	2.06	1.81	1.81	1.79	1.79
600.000	2.008	2.006	2.073	2.07	2.45	2.46	2.08	2.08	2.09	2.09	1.84	1.84	1.82	1.82
800.000	2.029	2.028	2.096	2.09	2.47	2.49	2.11	2.10	2.12	2.11	1.86	1.86	1.84	1.84
1000.000	2.046	2.044	2.113	2.11	2.50	2.51	2.12	2.12	2.13	2.13	1.88	1.88	1.86	1.86

Table (5): Comparison of the mass stopping power of electrons in bone, tissue (soft) and water, where the tissue was considered to be made up of thin layers of pure elements with the standard results

dE/ρdX (MeV.cm^2/g)									
ENERGY (MeV)	BONE			TISSUE (soft)			WATER		
	ESTAR(std)[39]	present study	ERROR%	ESTAR (std)[39]	present study	ERROR %	ESTAR(std)[39]	present study	ERROR %
0.010	20.680	20.943	-1.273	22.570	22.790	-0.974	22.560	22.895	-1.485
0.020	12.130	12.273	-1.181	13.170	13.280	-0.837	13.170	13.346	-1.336
0.040	7.191	7.264	-1.016	7.767	7.826	-0.760	7.777	7.867	-1.161
0.060	5.370	5.421	-0.945	5.787	5.828	-0.709	5.797	5.860	-1.088
0.080	4.412	4.452	-0.901	4.749	4.780	-0.654	4.757	4.807	-1.058
0.100	3.820	3.852	-0.849	4.107	4.133	-0.630	4.115	4.157	-1.026
0.200	2.599	2.616	-0.642	2.786	2.800	-0.495	2.793	2.819	-0.932
0.400	1.996	2.009	-0.636	2.142	2.147	-0.244	2.148	2.166	-0.848
0.600	1.815	1.835	-1.124	1.955	1.961	-0.332	1.963	1.982	-0.991
0.800	1.740	1.768	-1.621	1.876	1.890	-0.740	1.886	1.913	-1.443
1.000	1.705	1.741	-2.086	1.839	1.861	-1.188	1.849	1.887	-2.033
2.000	1.684	1.749	-3.851	1.812	1.874	-3.400	1.824	1.910	-4.701
4.000	1.735	1.838	-5.915	1.859	1.976	-6.289	1.870	2.026	-8.353
6.000	1.778	1.906	-7.190	1.901	2.055	-8.088	1.911	2.115	-10.660
8.000	1.810	1.957	-8.133	1.932	2.115	-9.455	1.943	2.182	-12.306
10.000	1.835	1.998	-8.865	1.958	2.162	-10.439	1.968	2.236	-13.618
20.000	1.909	2.123	-11.197	2.035	2.313	-13.671	2.046	2.408	-17.712
40.000	1.976	2.240	-13.384	2.105	2.458	-16.787	2.118	2.576	-21.630
60.000	2.012	2.296	-14.104	2.142	2.524	-17.833	2.156	2.650	-22.930
80.000	2.037	2.330	-14.397	2.168	2.564	-18.249	2.182	2.695	-23.492
100.000	2.056	2.355	-14.559	2.188	2.592	-18.466	2.202	2.726	-23.797
200.000	2.114	2.428	-14.858	2.247	2.673	-18.975	2.263	2.815	-24.390
400.000	2.171	2.497	-15.006	2.306	2.750	-19.236	2.322	2.898	-24.785
600.000	2.204	2.535	-15.039	2.341	2.792	-19.274	2.357	2.943	-24.875
800.000	2.228	2.562	-14.989	2.365	2.821	-19.288	2.381	2.974	-24.915
1000.000	2.246	2.582	-14.972	2.384	2.843	-19.257	2.400	2.997	-24.884